OPTIMIZATION OF AIR TO AIR CROSS FLOW HEAT EXCHANGER

A THESIS SUBMITTED TO
THE GRADUATE SCHOOL OF NATURAL AND APPLIED SCIENCES
OF
MIDDLE EAST TECHNICAL UNIVERSITY

BY

İSMAİL ÇAĞATAY KOYUNCUOĞLU

IN PARTIAL FULFILLMENT OF THE REQUIREMENTS
FOR
THE DEGREE OF MASTER OF SCIENCE
IN
MECHANICAL ENGINEERING

OCTOBER 2018

Approval of the thesis:

OPTIMIZATION OF AIR TO AIR CROSS FLOW HEAT EXCHANGER

submitted by **İSMAİL ÇAĞATAY KOYUNCUOĞLU** in partial fulfillment of the requirements for the degree of **Master of Science in Mechanical Engineering Department, Middle East Technical University** by,

Prof. Dr. Halil Kalıpçılar
Dean, Graduate School of **Natural and Applied Sciences** _____

Prof. Dr. M. A. Sahir Arıkan
Head of Department**, Mechanical Engineering** _____

Prof. Dr. Abdullah Ulaş
Supervisor, **Mechanical Engineering, METU** _____

Examining Committee Members:

Prof. Dr. Hüseyin Vural
Mechanical Engineering, METU _____

Prof. Dr. Abdullah Ulaş
Mechanical Engineering, METU _____

Prof. Dr. Zafer Dursunkaya
Mechanical Engineering, METU _____

Assoc. Prof. Dr. Cüneyt Sert
Mechanical Engineering, METU _____

Assist. Prof. Dr. Özgür Ekici
Mechanical Engineering, Hacettepe University _____

Date: 10.10.2018

I hereby declare that all information in this document has been obtained and presented in accordance with academic rules and ethical conduct. I also declare that, as required by these rules and conduct, I have fully cited and referenced all material and results that are not original to this work.

Name, Surname: İsmail Çağatay Koyuncuoğlu

Signature:

ABSTRACT

OPTIMIZATION OF AIR TO AIR CROSS FLOW HEAT EXCHANGER

Koyuncuoğlu, İsmail Çağatay
Master of Science, Mechanical Engineering
Supervisor: Prof. Dr. Abdullah Ulaş

October 2018, 137 pages

An air to air cross flow heat exchanger for a jet fighter air conditioning system is optimized and analyzed in this work. Conditioned air should be supplied continuously in order to provide a safe and comfortable environment for passengers and crew. For this purpose, a small amount of highly pressurized and heated air is extracted from different stages of engine compressor, which is called 'bleed air'. Bleed air temperature can be decreased by heat exchangers. Therefore, design of high performance, lightweight and small volume (compact) heat exchangers for aircrafts is very important. In the present study, optimum air to air cross flow heat exchangers are designed for generic supersonic aircrafts by using genetic algorithm optimization method. Firstly, parametric thermal and hydrodynamic performance formulae are created for offset-strip fin and wavy fin heat exchanger by using computational fluid dynamics (CFD). Ansys Fluent 16.0 software is used for all CFD analyses. This study allows designing unavailable fin shapes in literature for heat exchangers. Several geometrical and flow parameters such as fin height, fin spacing, wavelength, and the Reynolds number are selected for optimization. Then, multi-objective genetic algorithm is applied by choosing maximum heat transfer, minimum volume, and minimum ram air mass flow rate as three objective functions. Optimization is achieved by using Matlab commercial software. Finally, optimized design is validated by full scale CFD analysis using porous media approach instead of modelling full details of the heat exchanger in order to decrease computational effort.

Keywords: Genetic Algorithm, Optimization, Computational Fluid Dynamics, Porous Media, Compact Heat Exchangers

ÖZ

HAVA HAVA ENİNE AKIM ISI EŞANJÖRÜ OPTİMİZASYONU

Koyuncuoğlu, İsmail Çağatay
Yüksek Lisans, Makina Mühendisliği
Tez Danışmanı: Prof. Dr. Abdullah Ulaş

Ekim 2018, 137 pages

Bu çalışmada savaş uçağı iklimlendirme sistemi için enine akım hava hava ısı eşanjörü optimize ve analiz edilmiştir. Yolculara ve mürettebata güvenli ve konforlu bir ortam sağlamak için iklimlendirilmiş hava sürekli olarak sağlanmalıdır. Bu amaçla az miktarda yüksek sıcaklık ve basınçtaki hava, motor kompresörünün çeşitli kademelerinden çekilir ve 'hava tahliyesi' olarak adlandırılır. Hava tahliyesi sıcaklığı ısı eşanjörleri kullanılarak düşürülebilir. Bu nedenle hava araçları için yüksek performanslı, hafif ve küçük boyutlu (kompakt) ısı eşanjörü tasarımı çok önemlidir. Bu çalışmada, genetik algoritma optimizasyon metodu kullanılarak jenerik süpersonik uçaklar için optimum hava hava enine akım ısı eşanjörü tasarımı yapılmıştır. İlk olarak hesaplamalı akışkanlar dinamiği (HAD) kullanılarak, şaşırtmalı ve dalgalı kanatlar için parametrik termal ve hidrodinamik performans formülleri yaratılmıştır. Bütün HAD analizleri Ansys Fluent 16.0 yazılımı kullanılarak yapılmıştır. Bu çalışma ısı eşanjörleri için literatürde var olmayan kanat şekilleri tasarımına izin vermektedir. Kanat yüksekliği, kanat aralığı, dalga boyu ve Reynolds Numarası gibi bazı geometrik ve akış parametreleri optimizasyon için seçilmiştir. Sonrasında ise çok amaçlı genetik algoritma; maksimum ısı transferi, minimum hacim ve minimum ram havası objektif fonksiyonları için uygulanmıştır. Optimizasyon için Matlab yazılımı kullanılmıştır. Son olarak; optimize tasarım, hesaplama yükünü düşürmek amacıyla, detaylı ısı eşanjörü modeli yerine tam ölçek gözenekli ortam HAD yaklaşımı ile doğrulanmıştır.

Anahtar Kelimeler: Genetik Algoritma, Optimizasyon, Hesaplamalı Akışkanlar Dinamiği, Gözenekli Ortam, Kompakt Isı Eşanjörleri

To My Family

ACKNOWLEDGEMENTS

Firstly, I would like to express my gratitude to Prof. Dr. Abdullah Ulaş for his contributions, guidance, and encouragement throughout my graduate studies. It is an honor to be his student.

Secondly, I am very thankful to Dr. Mehmet Umut Haliloğlu and Dr. Ender Özden for sharing their guidance. Being influenced by their perspective is a great chance for me.

Thirdly, I would like also to specially thank my colleagues Serdar Hiçdurmaz, Görkem Demir, Kadir Gökhan Güler and Oğuzhan Çabuk for helpful discussions about my thesis.

Lastly, I would like to thank my family for their great support, understanding and encouragement.

TABLE OF CONTENTS

LIST OF TABLES

TABLES

LIST OF FIGURES

FIGURES

LIST OF ABBREVIATIONS

ABBREVIATIONS

A	Total Heat Transfer Area
Af	Fin Heat Transfer Area
Aff	Free Flow Area
AFS	Average Flow Spacing
Amp	Amplitude
Ap	Primary Heat Transfer Area
C	Heat Capacity
C^*	Heat Capacity Ratio
CCD	Central Composite Design
CFD	Computational Fluid Dynamics
CP	Crossover probability
Cp	Specific Heat
D_h	Hydraulic Diameter
DOE	Design of Experiments
DPs	Design Points
e	Effectiveness
ECS	Environmental Control Systems
f	Fanning Friction Factor
FA	Fin Area
FIA	Fin Inclination Angle
Fl	Fin Length
FS	Maximum Flow Spacing
G	Mass Flux
GA	Genetic Algorithm
h	Convection Heat Transfer Coefficient

HT	Heat Transfer
IAD	Interfacial Area Density
j	Colburn j Factor
kf	Fin Metal Conductivity
L	Flow Length
l	Fin Heat Conduction Length
Ma	Mach Number
MFR	Mass Flow Rate
MFS	Minimum Flow Spacing
MP	Mutation probability
n	Number of fin per meter
N	Number of Plates
n_o	Overall Fin Efficiency
NTU	Number of Transfer Units
OSF	Offset- Strip Fin
P	Fin Pitch
PHX	Primary Heat Exchanger
Pr	Prandtl Number
PS	Plate Spacing
pt	Plate Thickness
r	Recovery Factor
s	Plate Spacing
t	Fin Metal Thickness
TA	Total Area
T_o	Outside Ambient Temperature
T_r	Air Recovery Temperature
U	Overall Heat Transfer Coefficient
Vol	Volume
WF	Wavy Fin
Wl	Wavelength
y^+	Dimensionless Wall Distance

LIST OF SYMBOLS

SUBSCRIPTS

ave	Average
c	Cold Side
f	Fin
h	Hot Side
i	Inlet
max	Maximum
min	Minimum
o	Overall
p	Plate
p	Primary
tot	Total

SYMBOLS

ρ	Density
μ	Dynamic Viscosity
γ	Specific Heat Ratio
δ	Thickness
ε	Heat Exchanger Effectiveness

CHAPTER 1

INTRODUCTION

1.1. General

Aircraft air conditioning system has become one of the most important systems since this system is not only responsible for air conditioning as in the case of automotive industry but also for cabin pressurization, defogging, smoke removal, air filtering, fuel tank pressurization, supplying conditioned air for oxygen system, anti-g pressurization, and avionics bay cooling. In general, this system is responsible for maintaining a comfortable environment for a given payload by keeping some parameters (temperature, pressure, air flow rate etc.) within acceptable limits. Air conditioning system in aircraft industry can also be called as 'environmental control systems (ECS)'.

Cooling for air conditioning system in aircrafts can be accomplished by using air cycle cooling, vapor cycle cooling or even liquid cycle cooling. Sometimes, combinations of these systems may be used as hybrid systems. All of them require an air source to provide conditioned air for passengers and crew. Since ambient air pressure is quite low at high altitudes, it cannot be used as an air conditioning source for pressurized aircraft cabins. Therefore, pressurized air, which is extracted from engine compressor and called "engine bleed air", is utilized for air conditioning purposes of an aircraft. The bleed air is extracted from one or more compressor stages of jet engines. As bleed air pressure increases, temperature also increases. Bleed air temperatures can reach up to 1250 °F (675 °C) [1]. Consequently, this air needs to be cooled down in order to be used for air conditioning. Appropriately sized and designed heat exchangers should be used for this purpose. Type of the heat exchanger depends on the type of heat sink used. Several heat sinks are available in aircraft thermal management systems. Ambient air is one of the widely-used fluid as heat sink. Additionally, fuels, expendables, liquid coolants, and thermal storage heat sinks can also be used for this

purpose. Ambient air can be used in two ways: ducted into the aircraft as 'Ram air' or used to transfer heat directly from the fuselage [1]. The second option is generally preferred on commercial aircrafts and requires big noisy fans due to cooling requirement of the large heat transfer areas. It is not suitable for jet fighters because of aerodynamic heating effect on high-speed flights. Ram air is the ambient air which is sucked by special type inlets in flight or sucked by a fan or ejector discharge in low speed operations in order to decrease bleed air temperature.

Several air cycle cooling systems have been used in aircraft industry. Simple air cycle, two-wheel bootstrap air cycle, and three-wheel bootstrap air cycle are well-known ones. Only first two systems will be explained in this section in order not to get into too much detail. Simple air cycle schematic can be found in Figure 1.

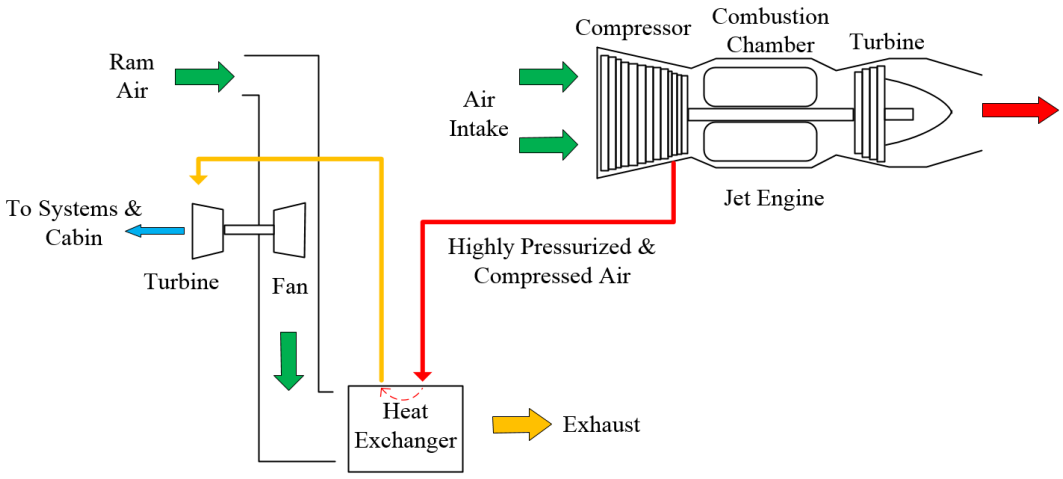

Figure 1: Simple Air Cycle Schematic [2]

Simple air cycle is the simplest version of the air cycle cooling schemes. It has one heat exchanger and one turbine-fan component which is called air cycle machine. Firstly, high pressure bleed air is cooled by the heat exchanger. Then, cooled air

expands in the turbine to drive the turbine fan and to further decrease its temperature. Lastly, expanded air can be supplied to the cabin and other systems.

The bootstrap air cycle is the advanced form of the simple air cycle (Figure 2). It has a compressor impeller instead of fan and an additional secondary heat exchanger compared to the simple air cycle. Firstly, bleed air is cooled in the primary heat exchanger and compressed again before the secondary heat exchanger. At the exit of the secondary heat exchanger, twice cooled bleed air is directed to the air cycle machine turbine for further cooling. Later, air is directed to the cabin and systems. In these processes, ram air is used in both the primary and the secondary heat exchangers as a heat sink. The bootstrap air cycle has lower turbine outlet temperature than the simple air cycle. Moreover, some upgrades can be implemented on it such as a high-pressure water separator which makes the bootstrap air cycle more beneficial. Additionally, this air cycle is widely used among well-known jet fighters such as F-15 and F-18 [3] [4]. A more detailed version of the bootstrap air cycle for jet fighters is shown in Figure 3.

Aircraft air conditioning system is a mission-critical system which means if the system fails, mission is aborted due to insufficient avionics cooling or cabin pressurization. In this case, the aircraft must land as practicable as possible. In other words, extended flight is not recommended and the pilot must decide the landing site and flight duration. In Figure 3, there are four heat exchangers, one water separator, one air-cycle machine and numerous pneumatic valves and ducts. Consequently, heat exchangers have important roles in aircraft air conditioning systems.

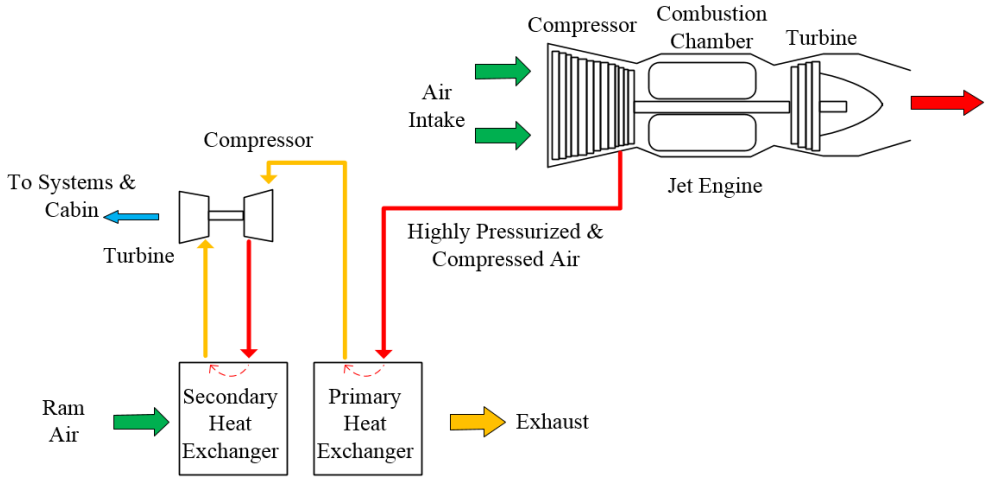

Figure 2: Bootstrap Air Cycle Schematic [2]

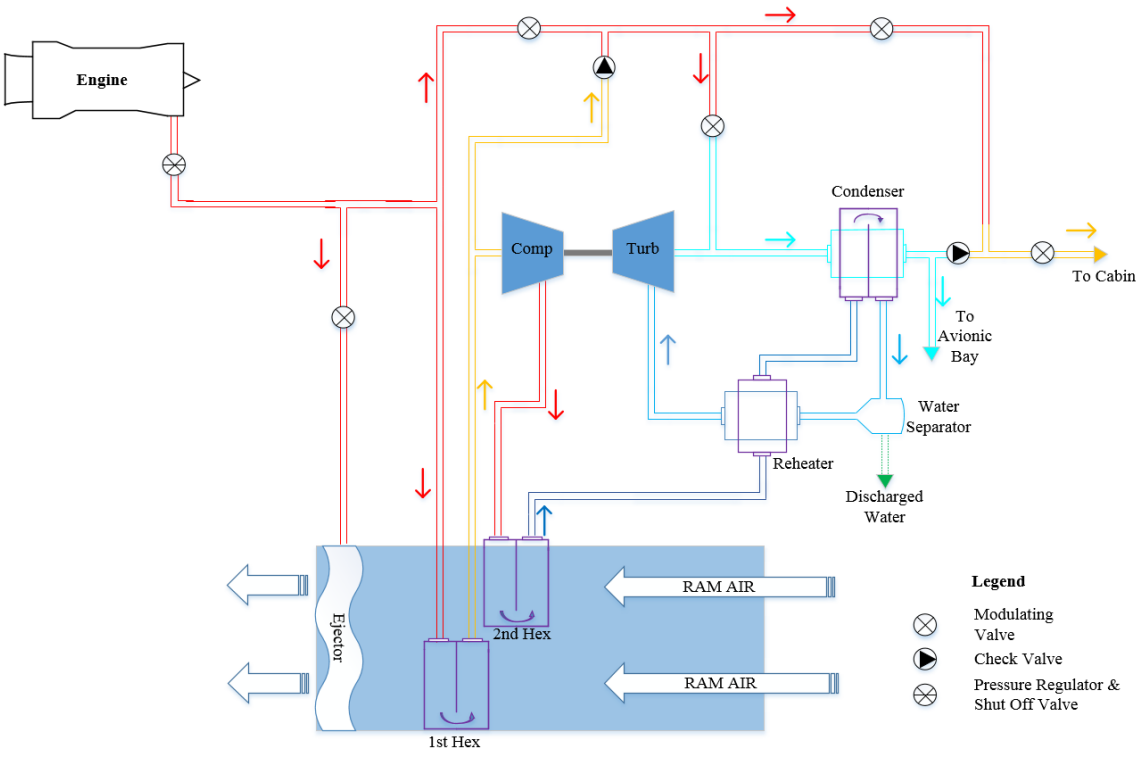

Figure 3: Typical Jet Fighter Air Conditioning System

Following requirements should be considered in order to make a good aircraft heat exchanger design:

- ✓ Small
- ✓ Having High Effectiveness
- ✓ Lightweight
- ✓ Fireproof
- ✓ Requires Less Maintenance
- ✓ Resistant to Clogging

1.2. Objectives of the Thesis

Heat exchanger design and optimization is a challenging process. It has several geometric parameters and flow parameters such as fin pitch, fin height, fin type, and Reynolds number. In aircrafts, heat exchangers generally work with one highly pressurized hot side and one unpressurized cold side which can be pressurized by aircraft speed, ejectors or fans. As a result, optimizing all these parameters for different working conditions of heat exchanger hot and cold streams requires a significant amount of computational effort.

In this study, the primary heat exchanger (or precooler) of the two-wheel bootstrap air cycle is modelled and optimized for a generic fighter aircraft according to three objective functions, which are the maximization of the heat transfer, the minimization of the volume and the ram air flow rate. The flowchart of the thesis is given in Figure 4.

The main objectives of this thesis can be summarized as:

- Determination of the operating conditions of the heat exchanger and performing preliminary calculations for the heat exchanger
- Predicting f and j factors by using Computational Fluid Dynamics (CFD) for two different heat exchanger fin configurations and obtaining correlations which relate f and j factors to the Reynolds number and the characteristic

geometrical parameters of the heat exchanger by using Design of Experiments (DOE)

- Optimizing cross flow heat exchangers with a suitable algorithm for a given set of conditions
- Performing full scale CFD analysis for the optimized model by using porous media approach to validate the final optimized design

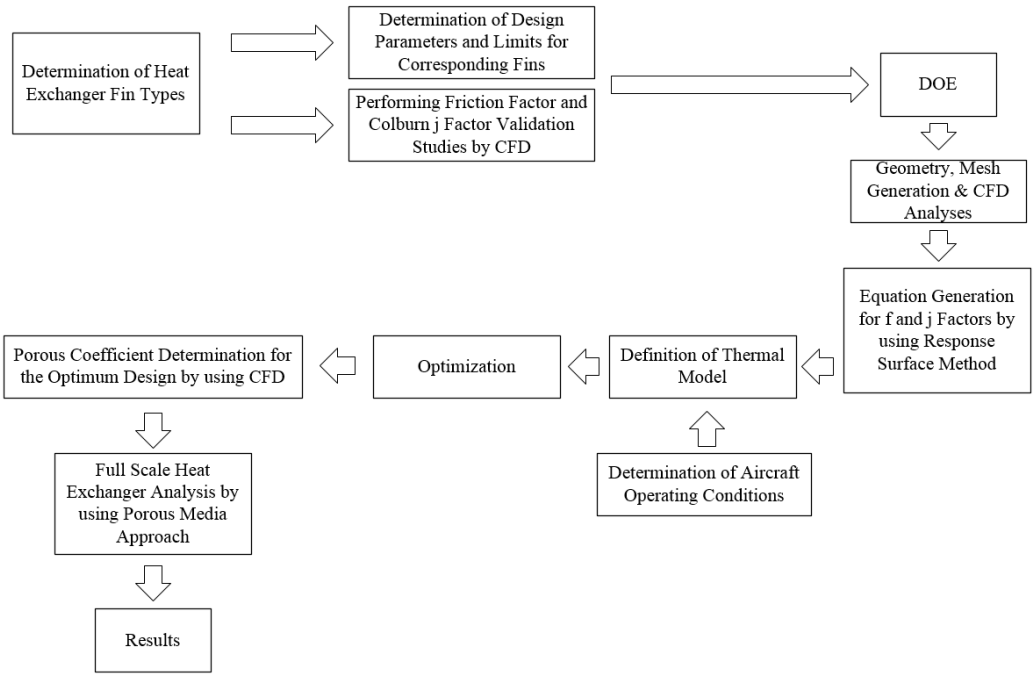

Figure 4: Flowchart of the Thesis

1.3. Outline of the Thesis

This chapter provides a short introduction to the aircraft environmental control systems with the definition of the main parts, the working principle, and different types. The importance of the heat exchangers is also emphasized. After describing the objectives of the study, Chapter 2 is introduced.

In Chapter 2, a literature survey on the heat exchangers is provided. Several heat exchanger types for aircraft applications are introduced and corresponding literature studies are presented. Moreover, computational fluid dynamics (CFD) applications on heat exchangers are provided with a couple of literature studies. Additionally, widely-used heat exchanger optimization methods are introduced. Lastly, design of experiments (DOE) studies on heat exchangers are given with the response surface methodology.

Chapter 3 includes the method of approach for the thermal design of the plate-fin heat exchanger, optimization studies, and porous media applications. Compact heat exchanger fin selection is presented first. Governing equations of CFD and porous media are also introduced. Then, the heat exchanger optimization methodology is explained with DOE and response surface method.

In Chapter 4, validation studies are conducted for the works in Chapter 5. Dimensionless pressure drop for internal flow (fanning friction factor) and dimensionless heat transfer coefficient (Colburn j factor) validation studies are done by using experimental data from the literature. Additionally, Genetic Algorithm is also validated by using a study from the literature.

Heat exchanger optimization is done in Chapter 5. Operating conditions of the heat exchanger is determined first and thermal model is developed by using ε-NTU method. Then, three important objective functions, which are maximizing the heat transfer, minimizing the volume, and minimizing the ram air mass flow rate, are presented with the operating conditions and the constraints. After determining the optimization parameters and design space, Design of experiments (DOE) is used to predict third order response surface equations for f and j factors. Two hundred fifty CFD runs in total are conducted for wavy fins and offset-strip fins. Then, multi-objective optimization is implemented by using genetic algorithm and the most suitable optimum solution is selected by using a developed selection function.

In Chapter 6, porous media validation study is done by comparing physical heat exchanger CFD solution with porous media CFD solution. Then, the selected optimum

result is verified by comparing the analytical solution with full-scale porous media analysis.

Chapter 7 contains the concluding remarks and future works to be done.

CHAPTER 2

LITERATURE SURVEY

In this chapter, literature survey on similar studies is reviewed and results are presented in the following paragraphs.

2.1. Heat Exchanger Types

In aircraft industry, several heat exchanger types have been employed but weight and volume considerations allow mostly the selection of compact (large heat transfer areas per volume [5]) plate-fin or shell and tube heat exchangers. In low-pressure applications (below 2.07 MPa (300 psia)), plate-fin heat exchangers are employed mostly and shell and tube heat exchangers suit for high-pressure applications [6]. Since jet fighters have low-pressure ECS applications (generally max. 0.69 MPa (100 psia)) and require low-volume components, plate-fin heat exchangers are used as the main heat exchangers. Since plate-fin heat exchangers are convenient for aircraft air conditioning applications, only this type is considered for the design and the optimization in this thesis.

The compact plate-fin heat exchangers can provide very large heat transfer area per unit volume. Moreover, this type of heat exchanger is especially useful if both fluids are gases which is suitable for aircraft air to air heat exchanger applications. Plate-fin heat exchangers can be classified as plain fins, louvered fins, offset-strip fins, wavy fins, pin fins, and perforated fins [5]. Some 3-D and 2-D examples are shown in Figure 5 and Figure 6, respectively. Plate-fin heat exchangers offer very high compactness ratios (700-5000 m^2/m^3) which is the total heat transfer area per unit volume of the heat exchanger [6]. These high surface densities make it possible to design smaller heat exchangers. Moreover, high surface densities also allow designing smaller hydraulic diameters that promote high heat transfer coefficients.

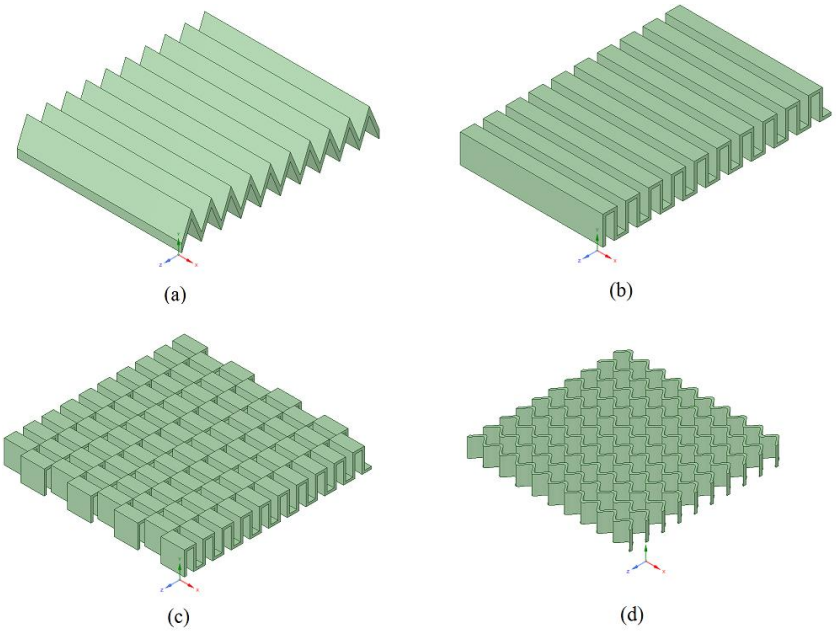

Figure 5: Corrugated fin geometries for plate-fin heat exchangers: (a) plain triangular fin; (b) plain rectangular fin; (c) offset-strip fin; (d) wavy fin

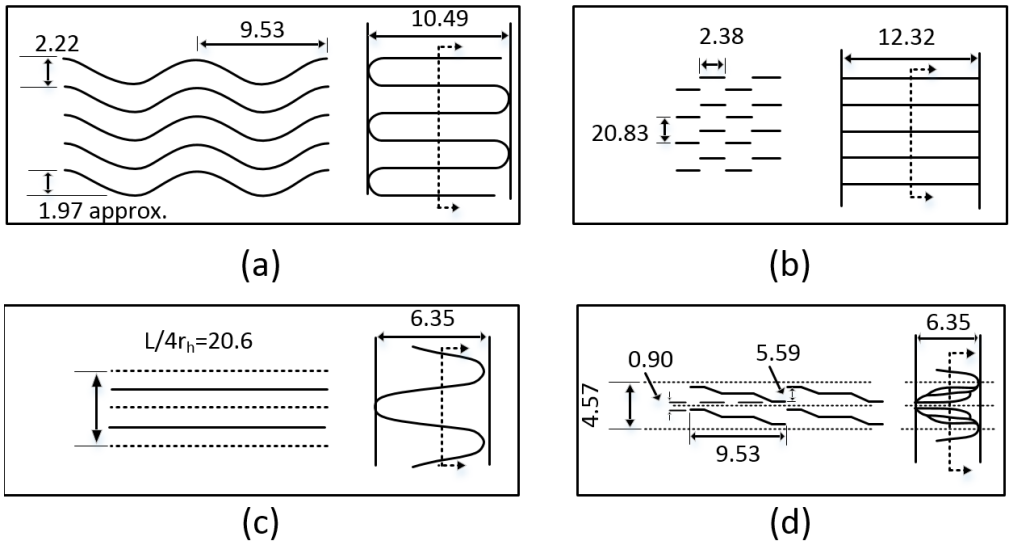

Figure 6: Different Fins with Similar Compactness Ratios: (a) Wavy Fin (11.44-3/8W); (b) Offset-strip Fin (3/32-12.22); (c) Plain Fin (11.1); (d) Louvered (3/8 - 11.1) (Note: Dimensions are in millimeters) [5]

In literature, there are some studies about selecting the most suitable heat exchanger surfaces. Cowell [7] made a comparison between plain fin and offset-strip fin. Total heat transfer and number of transfer units (NTU) were taken as fixed in the first part of the paper for a defined heat transfer problem. After that, three of the five parameters (total volume, pumping power, frontal area, hydraulic diameter, and NTU) were investigated while other two parameters were taken as fixed. As a result of these, relative change of aforementioned three parameters plots were presented. Moreover, other fins such as pin fin, finned round tube and flat tube were also compared according to relative pumping powers and hydraulic diameters. As a result, it was shown that performance parameters of heat exchanger are strictly related to each other. Lastly, results were compared with other literature studies.

Picon-Nunez et al. [8] investigated compact plate-fin heat exchangers to develop a selection methodology. Thermo-hydraulic model was presented with allowable pressure drop constraint and volume performance index was developed to present a simple approach for the surface selection. Volume performance index was basically the heat transfer per volume ratio that directs the selection of heat exchanger to high performance small volume (compact) heat exchangers. Defined heat transfer problem was applied for counter and cross flow arrangements. Results were compared with the studies in literature and showed very close agreement.

Hall et al. [9] conducted a study to select the most suitable compact heat exchangers from literature data. Fin data were taken from Kays & London Compact Heat Exchangers Book [5]. The purpose of their study was to guide a thermal engineer for designing airborne and military electronics cooling system. Several fin types such as straight, louvered, wavy, offset-strip, and pin fins were investigated. Dimensionless heat transfer coefficient (Colburn j factor) per dimensionless pressure drop for internal flow (fanning friction factor) was suggested for comparison of the fins. Besides, heat transfer per unit height and heat transfer per unit weight for fins were also compared. Lastly, specified fins were compared according to pressure drop, size, weight, and cost. These parameters were ranked from 1 to 5 and offset-strip fin was found to be the best.

2.1.1. Compact Heat Exchanger Applications on Civil and Military Aircrafts

Compact plate-fin heat exchangers are one of the widely-used heat exchanger types both in civil and military applications. Plate-fin heat exchangers can be found in the following aircraft applications [10]:

- Engine Bleed Air Precoolers
- Air Cycle ECS Heat Exchangers
- Air Cooled Oil Coolers
- Air Cooled Fuel Coolers
- Ram Air Coolers
- Electronic Liquid Cooling Loop Heat Exchangers
- Electronic Pod Coolant Heat Exchangers
- Vapor Cycle Evaporators
- Vapor Cycle Condensers

Commercial aircrafts generally have two-wheel bootstrap air cycle air conditioning system as described in Section 1.1. For example, Boeing 767 and 747-8 aircrafts have two-wheel bootstrap air cycle systems which contain compact heat exchangers [11], [12]. The only difference of this cycle between commercial and military applications is recirculation air. Commercial aircrafts can recirculate some portion (up to 50%) of the cabin air. However, military aircrafts are not allowed to use the cabin recirculation air. Additionally, single air conditioning pack is generally not enough to provide required air conditioning mass flow rates for commercial aircrafts. Two or more packs can be used for this purpose [11].

Recently, electric aircraft concept has become popular in aviation. Instead of taking bleed air from the engine, aircraft air conditioning air is supplied by independent electrically-driven compressors. This concept is called as ‘bleedless’ air conditioning systems. Exit pressure and temperature of this compressor are not as high as an engine compressor exit but the temperature is still hot enough, which has to be conditioned. Therefore, compact heat exchangers are still utilized for this bleedless systems. To

illustrate, Boeing 787 Dreamliner commercial aircraft has been produced with bleedless ECS systems and there are compact heat exchangers at the exit of two electrically driven ECS packs [13].

Compact heat exchangers are also used for military applications. Military aircrafts generally have numerous electronic equipment and must be cooled via liquid coolant or air. For example, radars and avionics bays of fighter aircrafts are generally cooled by using polyalphaolefin fluid coolant and forced air.

F-18 fighter aircraft has several ECS configurations that contains both liquid and air cooling [4]. In some of these configurations, two-wheel bootstrap air cycle system is modified to provide cooling not only for avionics bay and cabin but also for air to liquid heat exchanger. Hot fluid from radar exit is cooled by using conditioned cooling air. Additionally, there are also air to fuel heat exchangers, vapor cycle evaporators, and condensers.

F-22 fighter aircraft has a unique ECS configuration that contains two polyalphaolefin liquid loops for the forward and the aft side of the aircraft [14]. Moreover, these two loops are connected by a vapor cycle system that reject excess heat to another loop. Additionally, these loops are cooled by two-wheel bootstrap air cycle. The aft loop can reject some portion of heat to fuel by air to fuel heat exchanger. Furthermore, there are also fuel to hydraulic oil and fuel to engine lube oil heat exchangers. In the ECS configuration, there are eight compact heat exchangers.

The most advanced version of ECS belongs to the next generation power and thermal management system. This system is not only for ECS but also for auxiliary power unit and thermal management system. There is a single integrated pack which is responsible for all of these systems instead of numerous individual systems [15]. Power and thermal management system can operate in different modes such as main engine start mode, cooling mode, and emergency power mode. It contains three-wheel air cycle machine, fan duct heat exchangers, auxiliary heat exchanger, engine oil heat exchanger, condenser, reheater, recuperator, combustor, regulators, valves etc. Some

of these heat exchangers are advanced type of micro channel compact heat exchangers [15].

Consequently, compact heat exchangers have been widely used in aviation which is the reason of their selection in this thesis.

2.1.2. Compact Heat Exchanger Studies

In literature, there are numerous experimental and numerical studies about compact heat exchangers. Strace et al. [16] proposed a new compact heat exchanger design procedure that utilized both numerical and analytical approaches. The purpose was to have more detailed procedure than epsilon-number of transfer units (ε-NTU) method or log mean temperature difference method. In their study, offset-strip fin and wavy fin were applied for hot and cold side of the heat exchanger, respectively. These sides were divided into a set of control volumes and thermo-hydraulic performance was predicted by using numerical regression technique instead of iterative process. As a result, the new method was compared with ε-NTU method. It was found that the heat transfer rate was underestimated, which leads to oversize the heat exchanger to be on the safe side.

Saad et al. [17] worked on the flow distribution inside a compact heat exchanger both numerically and experimentally. Inlet distributor effects on flow maldistribution was also investigated. Air and water were the working fluids of the vertical compact heat exchanger. CFD interface tracking method was employed for two-phase flow simulation and the results were compared with experimental ones. As a result, CFD was found to be a satisfying tool in order to predict non-uniformity of the gas and liquid distribution inside the heat exchanger.

Camilleri et al. [18] conducted a study to predict the flow distribution in compact parallel flow heat exchangers. Effects of several boundary, operational, and geometric conditions were also investigated. In their study, nine parallel circular pipes were designed with U-type and Z-type flow arrangements. A network was created to solve head loss of the pipes. An algorithm was written and solved iteratively by using Matlab

commercial software. As a result, tube to header area ratio was found as an important parameter that is affected easily by Reynolds number and parallel pipe length.

2.2. Computational Fluid Dynamics

Computational Fluid Dynamics (CFD) is a numerical method that can solve the fluid mechanics and heat transfer problems using computers [19]. The history of CFD has been started in 1960s to predict the external aerodynamics of flying bodies. Using CFD is beneficial due to numerous advantages such as it is inexpensive compared to conducting experiments, dangerous experiments (combustion, detonation etc.) can be simulated, analyses can be done faster without geometrical restrictions compared to experiments etc. However, there are some disadvantages such as it requires considerable experience to use, some flows such as two-phase flows cannot be modeled accurately and judging the correctness of the results are not easy etc. Today, CFD is an important tool to predict many fluid flows such as:

- External flows
- Internal flows
- Air conditioning applications
- Combustion modelling
- Electronics equipment cooling
- Biomedical applications.

There are numerous commercial CFD tools in the literature. Generally, finite volume method (FVM) is used to solve the non-linear fluid problems. A CFD problem can be solved by the following three steps:

1) Pre-Processing
    a. Defining the problem geometry
    b. Mesh Generation
    c. Mathematical Model Selection
    d. Defining Boundary Conditions
2) Solution (generally using FVM)

3) Post-Processing (contour plots, average values etc.)

CFD has been also used to determine thermo-hydraulic characteristics of heat exchangers. There is a wide range of CFD usage on heat exchangers from fin modelling to full-sized heat exchanger modelling. Additionally, porous media approach is one of the widely used method for determining the thermo-fluid characteristics of compact plate-fin heat exchangers. In this thesis, CFD is utilized to predict thermo-hydraulic characteristics of compact heat exchanger fins and full-sized porous media approach.

2.2.1. Heat Exchanger Applications

CFD has been widely used on heat exchanger applications. Numerous heat exchanger types such as shell and tube, tube fin and plate-fin heat exchangers are modelled and solved successfully by using CFD. Since modelling heat exchangers by CFD is a mature topic, there are plenty of CFD studies in the literature. CFD modelling of heat exchangers generally requires solving energy equation as well as continuity and momentum equations unless only hydrodynamic characteristics are investigated. In order to model heat exchangers correctly, several CFD parameters such as turbulence model and pressure-velocity coupling scheme should be determined. In the literature, there are numerous turbulence models that are used in the heat exchanger design from spalart-allmaras to k-ω turbulence models. These CFD parameters can be selected more accurately via experience.

CFD modelling is generally used for evaluating the performance of heat exchanger thermally and hydrodynamically. Geometrical or flow parameters, such as fin density, tube diameters, Reynolds number and working fluid, can be varied in defined intervals in order to analyze the effects of parameters on heat transfer or pressure drop. Several studies from the literature about CFD usage on heat exchangers will be presented in the following paragraphs.

Yaïci et al. [20] investigated the flow maldistribution effects on heat exchanger performance. They studied plate-fin and tube heat exchangers by using CFD. Inlet air

flow distributions and geometrical parameters were analyzed computationally for different longitudinal, transversal, and fin pitches. Colburn j factor, fanning friction factor and j/f factor were found from the analyses. It was reported that flow maldistribution and geometrical parameters have severe impact on thermal and hydraulic performance.

Ozden et al. [21] worked on the effects of shell side design parameters on pressure drop and heat transfer by using CFD. In their study, a set of CFD simulations was conducted to predict the most suitable turbulence model. The results were compared with the analytical results which was obtained from Bell-Delaware method. Two baffle cut values and baffle spacing to shell diameter ratio were investigated with various flow rates. It was found that k-ε realizable turbulence model with fine mesh and first order spatial discretization are the best method compared to Bell-Delaware analytical results. Additionally, it was found that Kern method underpredicts the heat transfer. Lastly, it was concluded that CFD can improve shell and tube heat exchanger design with the help of experiments.

Rehman [22] investigated unbaffled shell and tube heat exchanger by using CFD. The heat exchanger contained 19 plain tubes and 5.85 m long shell. Mesh independence study and a set of CFD analysis were done and the results were compared with the experimental results. Several turbulence models with different wall treatments were also investigated and it was found that k-ω shear stress transport turbulence model provides better results than other models. Another finding from CFD analyses was that 2/3 of the shell side flow bypassed the tubes and created heat transfer inefficiency. As a result of this study, design modifications for the heat exchanger was suggested to improve the heat transfer.

Pan et al. [23] studied helical rectangular channel heat exchangers which have three different height to width ratios. Ansys Fluent commercial software was used for CFD simulations. Constant temperature wall boundary condition was set for walls and inlet velocity was defined as a function of fanning friction factor, hydraulic diameter and kinematic viscosity by using user defined functions. The results showed that largest

length to width ratio improves the heat transfer and pressure drop characteristics. Additionally, CFD results were found to be very close to the experimental results.

Rois-Iribe et al. [24] conducted a CFD study to investigate non-Newtonian thermo-hydraulic effects on plate heat exchanger. Single pass U-type plate heat exchanger was considered without baffles and thermo-hydraulic characteristics of the heat exchanger were investigated by changing number of plates and distance between plates. Fanning friction factor correlation was developed as a function of Reynolds number, friction characteristic length, and flow trajectory length. As a result, it was found that simple correlations can be derived for these types of highly complex flow patterns. Moreover, CFD were considered as a powerful tool in plate heat exchanger design and analysis.

Amanowicz et al. [25] worked on a validation study of experimentally investigated earth-to-air heat exchanger which has five flow pipes in Z type flow arrangement. Ansys Fluent was used to validate the heat exchanger flow characteristic as a CFD tool. In the analyses, k-ε realizable turbulence model with enhanced wall function near wall treatment was used. The results showed that experimental and numerical pressure losses are in good agreement and the relative errors of these are generally lower than 10%.

2.2.2. Compact Heat Exchanger CFD Studies

Recently, CFD has been widely used in compact heat exchanger analysis. Hosseini et al. [26] studied the effect of particle size on deposition in compact heat exchangers. In their work, ANSYS Fluent software was used in order to solve Reynolds-Averaged Navier Stokes equations. Suitable turbulence models were assessed and standard k-epsilon turbulence model with standard wall function was found as appropriate. Semi-implicit pressure linked equations was selected as pressure velocity coupling scheme. As a result, numerical study revealed that particle deposition increases with increasing particle size.

Ismail et al. [27] worked on compact heat exchanger fins by using CFD. Analyses were done to predict f and j factors for wavy and offset-strip fin by using Ansys Fluent

commercial software. Periodic boundary conditions were applied to get rid of entrance effects of inlets. Offset-strip fin and wavy fin analyses were validated with the data from the literature. It is emphasized that there are numerous offset-strip fin f and j factor correlations in the literature and these correlations show discrepancy compared to each other. Moreover, new f and j factor correlations were developed as a function of Reynolds number and geometrical fin parameters for wavy fin. Finally, these correlations were compared with other correlations from the literature.

Rao et al. [28] investigated plain fin compact heat exchanger f and j factors by using CFD. Only plain fins were considered in their study. Rectangular flow geometry was modelled by taking one quarter of the cross section due to symmetry. The analyses were done by using standard k-ε turbulence model with enhanced wall function near wall treatment. The model was validated with the experimental data from the literature and then new correlations of f and j factors for rectangular plain fins were presented.

Girgin [29] investigated the effects of compact heat exchanger vortex generator configurations on heat transfer via CFD. In his study; common flow up, common flow down, and mixed type vortex generator orientations with several angle of attacks were analyzed. Moreover, number of vortex generator pairs was changed from two to three. Ansys Fluent was utilized as a CFD tool. As a result, three pairs of common flow down configuration with 30^o and 45^o angle of attacks gave the best heat transfer performance.

2.2.3. Porous Media Approach

Porous media approach has been widely used especially in fluidized beds, reactors, and heat sinks. This approach has also been used for compact heat exchangers. Since CFD modelling of compact heat exchangers with fins requires highly detailed and extremely fine mesh, solving this may not be efficient in terms of time and computational source. This difficulty can be overcome with the help of porous media approach. Since there are no highly detailed geometrical sections in porous media geometry, it requires very low number of CFD mesh elements compared to detailed mesh.

Several studies have been done on porous media heat exchanger modelling. For example, Güler [30] modelled a tractor radiator, which was a cross flow fin and tube type heat exchanger. The engine coolant was modelled as water and located at the tube side of the radiator. Air was considered as radiator coolant fluid which is located at the fin side of the radiator. Since there were no fins on water tube side, only air side was modelled with porous media. After extracting porous inertial and viscous coefficients, the results were obtained and compared with experimental results. The total numerical and experimental transferred heat was found as 55.8 kW and 54.4 kW, respectively.

Musto et al. [31] studied porous media on a turboprop aircraft's oil cooler. The aircraft was assumed to fly at cruise conditions (9000 ft). The main purpose was to investigate the pressure drop and heat transfer characteristics of the cooler using the porous media model. The numerical results were analyzed and compared with the experimental data which were found as satisfactory. As a result, heat exchanger CFD modelling with porous media approach was found as a suitable approach.

Wang et al. [32] investigated hydrodynamic characteristics of a full-sized plate-fin heat exchanger. CFD was utilized with the help of porous media approach to predict the effects of fluid dynamic viscosity and perforated fins on the pressure drop and flow distribution. Ansys Fluent commercial software and standard k-ε turbulence model with enhanced wall function were used in CFD analyses. The results were found to be in good agreement with the experimental results. Consequently, two suggestions were made to improve the flow distribution of the heat exchanger.

Mao et al. [33] conducted a study to predict the thermal performance of a heavy-duty radiator. The flow in the radiator was solved by using CFD with porous media approach. Since there were two regions of radiator as water and air side, dual porous zone method was applied. Ansys Fluent was used to solve flow equations in the heat exchanger. Moreover, structural analysis was also coupled with CFD and done by using ABAQUS finite element analysis commercial software in order to investigate possible structural failure locations. As a conclusion, the results were compared with the experimental results and showed good agreement. Moreover, it was emphasized

that porous media approach was helpful to overcome modelling difficulties of compact heat exchanger fins.

Hayes et al. [34] studied heat transfer and hydraulic characteristics of a matrix heat exchanger. In their study, both numerical and experimental studies were conducted. Ansys Fluent was used as a CFD tool with porous media approach. Energy equation was solved by using non-equilibrium thermal model which has coincident zones with the same number of mesh elements for modelling solid and fluid separately. These are generally called as porous solid and porous fluid. In this model, porous fluid and porous solid temperatures are assumed to be not equal. As a result, thermal non-equilibrium model was verified with the experimental data. Additionally, a correlation was suggested to predict the Nusselt Number as a function of the Reynolds number.

Zhang et al. [35] investigated an Intermediate Heat Exchanger of a pool-type sodium-cooled neutron reactor via CFD. Flow field and temperature distributions were examined in their study using Ansys Fluent commercial software. In order to reduce computational effort, porous media approach was utilized instead of modelling a number of tubes. Porous coefficients were predicted from empirical relationships. As a result, larger inlet area and non-uniform inlet velocity distribution design model was found to be the most suitable design by considering the maximum permitted temperature difference and radial velocity.

2.3. Heat Exchanger Optimization

In the last few decades numerous methods for heat exchanger optimization have been developed [36, 37, 38, 39, 40, 41, 42]. Mathematical programming methods and stochastic methods are widely used optimization methods for heat exchangers. The former methods are very effective ones which converge faster and gives accurate results. However, they require good initial points to get a global optimum solution. Because of this reason, there may be some problems if non-convex problems are tried to be solved. On the contrary, the latter methods work well for global searching due to ability of rapidly exploring and finding good solutions on design space. These methods have capability to handle complex non-linear problems. Moreover, they are not

affected from discontinuities or non-convexities [37]. There are some examples of both mathematical programming methods and stochastic methods in the literature.

Zalewski et al. [43] conducted a study about optimization of evaporative fluid coolers. Mathematical formulation of the heat and the mass transfer was developed initially. Two non-linear objective functions with some equality and inequality constraints were introduced. Objective functions were the minimizing the total cost with the maximizing the heat capacity and the minimizing the operating cost. The problem was solved by using Schittlowski's method which is based on quadratic programming. Consequently, the results were obtained and validated by experiments.

Gonzalez et al. [44] worked on air-cooled heat exchanger optimization by using mathematical programming. The heat exchanger was tube fin heat exchanger which contains hot fluid flow inside of the tubes and cold fluid (air) flow outside of the tubes. The heat transfer problem was taken from another literature study. Objective function was the minimizing the cost by keeping heat duty constraint. There were ten optimization variables such as tube outside diameter, fin per meter, number of tube passes with five different constraints. Mathematical heat transfer formulation was solved by using Successive Quadratic Programming and the results showed that optimum heat exchanger parameters gave lower cost than the previously installed heat exchanger.

Stewart et al. [45] studied the optimization of the finned tube condenser of a 9 kW vapor cycle cooling system. Objective function of the study was the minimizing the coil cost of the system. Simplex Search Method was used as the optimization method and it was emphasized that the algorithm might give a good solution instead of global optimum solution. The results were obtained and 23% improvement of coil cost was achieved with the same coefficient of performance.

Zarea et al. [46] used stochastic bee algorithm to optimize a plate-fin heat exchanger. In their study, two different objective functions were considered as the maximizing the heat exchanger effectiveness and the minimizing the number of generation units (rate of entropy generation per heat capacity rate). ε-NTU method was used for heat transfer

model. Seven different optimization parameters were introduced with some constraints which were embedded into the optimization code as penalty functions. The results were obtained and several comparison studies were carried out between bee algorithm, particle swarm optimization, and genetic algorithm.

Zhao et al. [47] studied a network-based optimization for a two-phase heat exchanger such as evaporator or condenser. In their study, the heat exchanger was divided into zones and a thermal circuit was introduced. Additionally, fluid thermo-physical property variation was investigated in the circuit. Energy balance for all nodes in the circuit was written and combined with constraints. As a result of this, a complex Lagrange function was obtained and solved. The results were compared with ε-NTU method and it was concluded that thermal circuit method was accurate.

2.3.1. Compact Heat Exchanger Optimization

Vargas et al. [48] optimized a compact aircraft ECS heat exchanger by using the entropy generation minimization method. In their study, main components of a two-wheel bootstrap air cycle system such as the air cycle machine were also taken into consideration to extend inlet and outlet streams of the heat exchanger. Two types of the heat exchanger were considered as finned and smooth parallel plates. Thermodynamic model of the system was written with some constraints and it was solved by functional iteration. Maximum functional tolerance was selected as 10^{-6}. As a result, several design graphs were presented and it was concluded that the applied optimization method was applicable to any system which included limited amount of fuel.

Bello-Ochende et al. [49] studied the optimization of the primary and secondary heat exchangers of a two-wheel bootstrap air cycle for an aircraft ECS system. The heat exchanges were selected as compact plate-fin heat exchangers with offset-strip fins. Entropy generation minimization technique was applied to optimization algorithms. ε-NTU method was used with f and j factor correlations from the literature. Moreover, parameters for cold and hot air sides of the heat exchangers were taken separately. Flow parameters such as mass flow rates were taken from C-17A aircraft. The system

had 14 non-linear equations with 14 unknowns and they were solved by using Mathcad 15.0 commercial software which is based on Quasi-Newton methods. Consequently, optimum primary and secondary heat exchanger parameters were presented.

Rao et al. [50] optimized a compact plate-fin heat exchanger by using Jaya optimization algorithm. Offset-strip fins were employed to both sides of the heat exchanger. Seven design variables and nine constraints governed the optimization algorithm. Heat exchanger model was developed by using the ε-NTU method. f and j factor correlations were taken from the literature. Four different objective functions which were the total annual cost minimization, the total heat transfer area minimization, the total pressure drop minimization, and the effectiveness maximization were evaluated. The results were obtained and compared with the studies from the literature. As a result, it was concluded that the algorithm could be successfully applied for the optimization of plate-fin heat exchangers.

Raja et al. [51] conducted a study of cross flow plate-fin heat exchanger optimization. Four objective functions as the maximization of the effectiveness and the minimization of the total annual cost, the number of entropy, and the total weight were implemented simultaneously. Moreover, multi-objective transfer search algorithm was implemented as an optimization algorithm. The results were obtained and a comparison between four-objective and two-objective Pareto-optimal fronts (set of optimal solutions) was made. A final optimal solution was found by using decision making methods such as LINMAP and Fuzzy.

Bari et al. [52] used CFD to optimize the compact heat exchanger of a diesel engine heat recovery system. Two types of heat exchangers were considered as pancake-shaped and round-shaped heat exchangers. The analyses were done by using Ansys CFX commercial CFD tool. Turbulence model was chosen as k-ω shear stress transport and necessary mesh independence studies were done. Some parameters such as tube diameters and heat exchanger length were taken as optimization parameters. As a result, power improvements of pancake-shaped and round-shaped heat exchangers were 25.1% and 23.6%, respectively.

2.3.2. Genetic Algorithm Optimization Studies

Genetic algorithm is a metaheuristic optimization method for solving constrained and unconstrained optimization problems. The algorithm is inspired by natural selection and evolutionary processes which can provide some good optimal solutions. Nevertheless, the best solution may not always be provided. The genetic algorithm continuously modifies individual solutions in order to find a better solution. At each iteration, individuals are selected randomly to be parents and to produce the next generation. The population converges to an optimal solution or a set of optimum solutions after some created generations. The main advantage of the genetic algorithm is that it can be applied for a wide variety of problems such as highly non-linear, non-differentiable, and discontinuous problems.

The algorithm basically creates a generation by using three rules named as selection, crossover, and mutation. Selection process is selecting random pairs under a given probability from previously generated population in order to choose parents. The possibility of to be selected depends on the fitness which is the output value of objective function. Higher fitness means higher selection probability. After selection, crossover process recombines the parents to form children for the next generation. Lastly, mutation process applies random changes to parents in order to form children. This process is very useful to converge from local maxima to global maxima. Some commercial optimization codes are programmed only to minimize the objective function. The fitness is increasing with decreasing objective function value in this case. For example, genetic algorithm available in the Matlab software can do only minimization. The following literature studies are given as examples of Genetic Algorithm (GA) optimization method application on different types of heat exchangers.

Najafi et al. [53] conducted a study about optimization of a plate heat exchanger by using GA. The maximization of the overall heat transfer coefficient and the minimization of the pressure drop were selected as multi-objective objective functions. Water was used as the working fluid. Six parameters such as plate thickness, diameter

of the ports, and enlargement factor were taken as optimization parameters. Other parameters such as chevron angle, number of passes, and thermal conductivity of the plates were taken as constant. Multi-objective GA was run by using Matlab commercial software. Consequently, pareto front (set of optimal solutions) was presented. It was emphasized that the most suitable solution of the result could be selected by design engineer.

Sadeghzadeh et al. [54] studied shell and tube heat exchanger optimization by using multi-objective GA. Objective functions were determined as the maximization of the heat transfer and the minimization of the cost. Eight parameters such as tube arrangement, tube length, and fin thickness were selected as optimization parameters. Moreover, baffle cut was fixed to 20 percent. Delaware modified method was applied to determine thermo-hydraulic characteristics. The algorithm was run and a set of optimal solutions was obtained. Four different optimal solutions were suggested from the pareto front. One of them was for the maximum heat transfer and another one was for the minimum cost. Other two suggestions were from somewhere between the first two suggestions.

Hajabdollahi et al. [55] worked on shell and tube heat exchanger optimization using both particle swarm optimization and GA. The objective function was determined as minimizing the total cost which contains investment and operational cost. Heat transfer was modelled by using log mean temperature difference method. Five different design parameters such as tube number, number of pass, and inlet diameters were selected as optimization parameters. The results showed that GA gives better results than particle swarm optimization method. Additionally, sensitivity analyses were done on the optimum solution by changing only one design parameter at a time and keeping all other parameters as constant.

Yadav et al. [56] optimized a louvered fin flat tube compact heat exchanger. Single objective GA was employed to find one of the best solutions on the heat transfer. ε-NTU method was employed for thermo-hydraulic heat exchanger characteristics. Twelve optimization parameters such as fin pitch, louver angle, and number of fins

were selected. As a result, 22.56% heat transfer enhancement was accomplished by increasing the tube side and fin side compactness.

Xie et al. [57] optimized a plate-fin compact heat exchanger considering both the minimizing the volume and the cost objective functions. In their study, fin parameters were taken as constants and retrieved from the literature. Corresponding experimental f and j factors of the fins were converted to curve-fitting formulae which were functions of the Reynolds number. Three external dimensions of the heat exchanger were selected as optimization parameters. ε-NTU method was adopted and genetic algorithm was run. As a result, 30% lower volume and 15% lower annual cost were achieved with pressure drop constraint and 49% lower volume and 16% lower annual cost were achieved without pressure drop constraints.

Mishra et al. [58] conducted a study on the optimization of crossflow plate-fin heat exchangers with offset-strip fins. GA was selected as suitable optimization algorithm. In their study, total number of entropy generation units was minimized for a specified heat duty with space restrictions total number of entropy generation units (rate of entropy generation per heat capacity rate). Both fin parameters and external heat exchanger diameters were selected as optimization parameters. Consequently, the optimum solution was obtained and graphical contours were presented in feasible design space in order to select convenient designs.

In addition to these studies, other studies on the heat exchanger GA optimization can be found in the literature [59, 60, 61, 62, 63, 64]. Modified versions of GA such as constructal theory and combination of neural network with GA are also used in some of these studies.

2.4. Design of Experiments

Design of experiments (DOE) aims to collect an illustrative set of data to compute a response equation and to predict reaction of other design points in design space. Convenient DOE methods can decrease required design points and unnecessary experiments can be discarded. As a result of this, considerable amount of time and

workload can be saved. Accuracy of the response equation significantly depends on the DOE scheme. In literature, there are numerous DOE schemes. To illustrate, Randomized Complete Block Design, Latin Square, Full Factorial, Fractional Factorial, Central Composite, Box-Behnken, Plackett-Burman, Taguchi, Random Space Filling, Halton, Faure, and Sobol Sequences, Latin Hypercube and Optimal Design Techniques are the main techniques which are used in practice. Experimental designer has several choices but there is no best choice. To select a suitable DOE method, the number of experiments (N) which can be afforded, the number of parameters (k), the number of levels (L) for each parameter, and the aim of the DOE can be considered [65]. In Table 1, various DOE methods are summarized.

Table 1: DOE methods synoptic table [65]

Method	Number of experiments	Suitability
Randomized Complete Block Design	$N(L_i) = \prod_{i=1}^{k} L_i$	Focusing on a primary factor using blocking techniques
Latin squares	$N(L) = L^2$	Focusing on a primary factor cheaply
Full factorial	$N(L,k) = L^k$	Computing the main and the interaction effects, building response surfaces
Fractional factorial	$N(L,k,p) = L^{k-p}$	Estimating the main and the interaction effects
Central composite	$N(k) = 2^k + 2k + 1$	Building response surfaces
Box-Behnken	*N(k)* from tables	Building quadratic response surfaces

Table 1 Continued: DOE methods synoptic table [65]

Plackett-Burman	$N(k) = k + 4 - \mathrm{mod}\left(\frac{k}{4}\right)$	Estimating the main effects
Taguchi	$N(k_{in}, k_{out}, L) = N_{in} N_{out}, N_{in}(k_{in}, L), N_{out}(k_{out}, L)$	Addressing the influence of noise variables
Random	chosen by the experimenter	Building response surfaces
Halton, Faure, Sobol	chosen by the experimenter	Building response surfaces
Latin hypercube	chosen by the experimenter	Building response surfaces
Optimal design	chosen by the experimenter	Building response surfaces

In literature, there are various DOE studies applied on heat exchangers. Kumar and Lee [66] combined CFD with DOE. In their study, cross flow finned-tube heat exchanger was analyzed and the most effective parameters on the temperature difference and the pressure drop were investigated. Four independent design parameters were defined with three levels for each. In order to minimize the number of experiments required, L_9 Taguchi Orthogonal Array was used. Analysis was done by Ansys-CFX. Solid geometry was simplified by neglecting the fins and decreasing the total number of tubes from 484 to 36. Moreover, Analysis of Variance was used to evaluate the collected data. Consequently, the DOE using L_9 orthogonal array showed that the most effective parameter was the inner diameter and the thickness of the tube among other parameters had more influence on the heat transfer rate.

Sahin et al. [67] used DOE to investigate the effects of the longitudinal and lateral separations on specifically arranged fin pairs experimentally. Some fin parameters

such as the fin height, the fin width etc. were changed to observe the effects on the heat and pressure drop characteristics. L_{18} Taguchi Orthogonal Array was selected for eight parameters in total. They found out the most important fin parameters on the heat transfer and the pressure drop. Then, the goals were considered together and the optimum result was obtained.

Additionally, some compact heat exchanger DOE studies are available in the literature. Kim et al. [68] conducted numerical DOE studies to predict fanning friction factor and Colburn j factor for offset-strip fin heat exchanger. DOE table was generated by using Central Composite Design. Not only a comparison between the literature and developed correlations was made, but also new relations were derived for different working fluids such as diesel fuel and water. Finally, found relations were optimized and 24% improvement was observed on the offset-strip fin Colburn j factor/f factor value.

Liu et al. [69] tried to develop a plate-fin heat exchanger for hydraulic application. They utilized DOE to predict the fanning friction and the Colburn j factors of the offset-strip fin heat exchanger. Sample points were generated using Optimal Latin Hypercube DOE method. After generating f and j factors, Non-Dominated Sorting Genetic Algorithm was employed for the optimization. Consequently, Colburn j factor was increased by 12.83% and fanning friction factor was decreased by 26.91%.

2.5. Response Surface Method

Response surface method is a surface fitting method for a given set of inputs and outputs. Non-linear solution sets can be predicted by using these simple equations. Second order response surface equation can be written as below [70].

$$y = \beta_0 + \sum_{i=1}^{k} \beta_i x_i + \sum_{i=1}^{k} \beta_{ii} {x_i}^2 + \sum_{i=1}^{k} \sum_{j=1}^{k} \beta_{ij} x_i x_j + \varepsilon \qquad (1)$$

where, x and y denote input and output parameters, respectively. β and ε represent equation coefficients and numerical error, correspondingly. If accuracy of the equation is not sufficient, order of the equation can be increased. However, increasing order of equation requires more data. In this study, second order response surface method will be used at first to create correlations between f and j factors and design parameters. Input parameters will be generated by using DOE and corresponding outputs will be obtained by using CFD.

In the literature, there are some studies about response surface methodology. Wang et al. [71] optimized shell and tube heat exchanger by using multi objective GA. Second order response surface method was utilized to examine the effects of fold baffle configuration parameters on the heat transfer and the pressure drop. Three dimensional parameters of the shell and tube heat exchanger were chosen as optimization parameters in order to maximize the heat transfer and minimize the pressure drop. Analysis was run and a set of optimal solutions was obtained. Consequently, the optimization results showed a good agreement with CFD results. Moreover, empirical correlations were suggested which gives Nusselt Number and f factor as functions of heat exchanger dimensional parameters and the Reynolds number.

Liu et al. [72] studied a thermoelectric generator in order to optimize the heat transfer and the pressure drop characteristics. Four optimization parameters were selected as a function of five fin design parameters. L_{16} orthogonal array CFD simulations were analyzed. In their study, a third order response surface approach was applied to extract variation regularity between input and output parameters. As a result of this, the horizontal temperature difference was reduced and 20% pressure drop improvement was obtained.

Shirvan et al. [73] conducted a study on 2-D porous media application on a double pipe heat exchanger. In their study, response surface method was used to predict the effects of the Reynolds number, the Darcy Number and the porous substrate thickness on the Nusselt Number. Three levels of parameters were selected and first order response surface equation was used. Moreover, a face centered central composite

design (CCD) DOE method was applied to generate experiments. As a result of this, fitting quality was found to be satisfying. Additionally, sensitivity analysis was done to assess the effects of response surface method input parameters on heat transfer and heat exchanger effectiveness.

CHAPTER 3

METHOD OF APPROACH

In this chapter, the selection of the fin types for the compact heat exchanger and the details of the CFD analyses, the optimization method, and the DOE studies with response surface methodology are explained.

3.1. Compact Heat Exchanger Fin Selection

The most suitable fin type for the plate-fin heat exchanger can be selected by comparing Colburn j factor and f factor. Since minimizing the heat exchanger volume is important for aircrafts, a comparison is made between these different fin surfaces with similar compactness ratios which is given in Table 2. Properties of compared fins are taken from the reference [5]. Colburn j factors and friction factors are compared in Figure 7 and Figure 8, respectively. Since the air pressure from engines (up to 1.03 MPa (150 psig)) are higher than working pressure of main heat exchangers (up to 0.55 MPa (80 psig)), there are some pressure regulators on aircraft ECS line. This makes it possible to allow high pressure drops on heat exchangers. Therefore, using high friction factor fins on the heat exchangers can be tolerable. Due to these reasons, only Colburn j factor will be evaluated for fin selection procedure. In Figure 7, wavy fin and offset-strip fin offer higher Colburn j factors compared to other fins for the same Reynolds number. Therefore, only these two fins will be assessed in this study.

Table 2: Similar Compactness Fin Parameters [5].

Parameters	Wavy Fin (11.44-3/8W)	Offset-strip Fin (3/32-12.22)	Plain Fin (11.1)	Pin Fin (PF-3)	Louvered (3/8 - 11.1)	Perforated (13.95(P))
Compactness	1152	1115	1204	1112	1204	1250
Fin Area/ Total Area	0.847	0.862	0.756	0.835-4	0.756	0.705
Fin Thickness [mm]	0.152	0.102	0.152	-	0.152	0.305
Hydraulic Diameter [mm]	3.23	3.41	3.08	1.636	3.084	2.504
Plate Spacing [mm]	10.49	12.3	6.35	19.1	6.35	5.08
Fins per meter	450.4	480.3	437.0	-	437.0	549.2

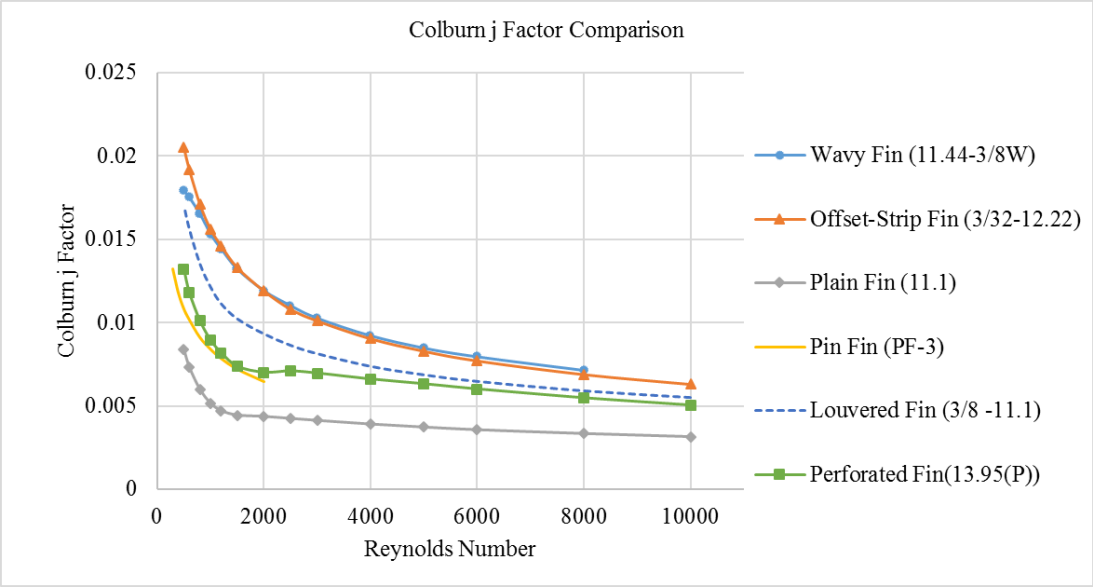

Figure 7: Colburn j Factor Comparison of Different Fins [5]

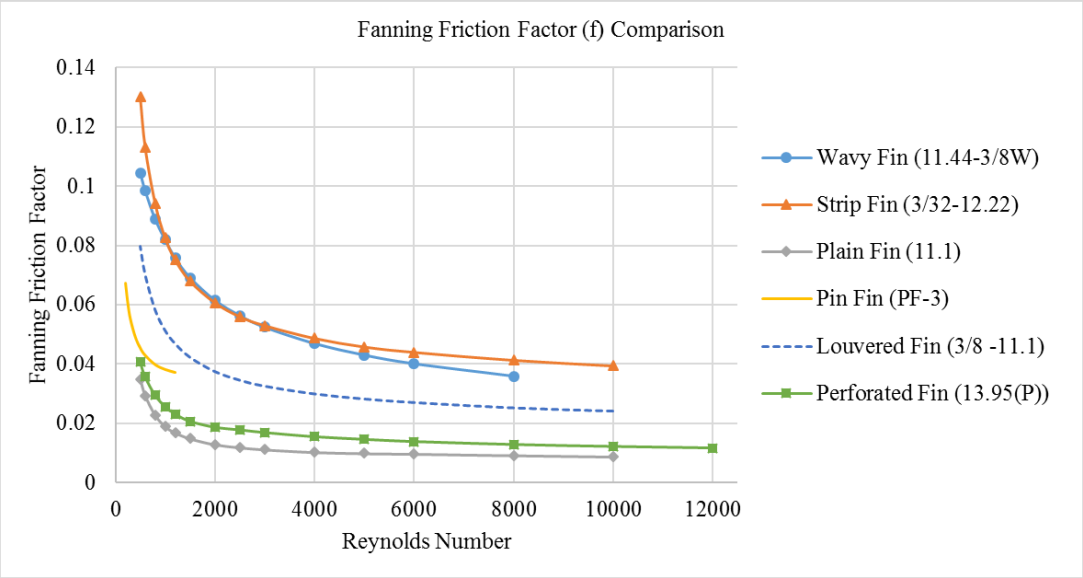

Figure 8: Friction Factor Comparison of Different Fins [5]

3.2. Computational Fluid Dynamics

In CFD, Navier-Stokes equations are solved by assuming the fluid to be continuum. These equations are derived from the conservation of mass and the Newton's law of motion for the fluid flow. The conservation of mass equation (continuity equation) is given below:

$$\frac{\partial \rho}{\partial t} + \nabla . \left(\rho \vec{V}\right) = 0 \tag{2}$$

Conservation of momentum equation for x-direction can be written as below. Other components (y and z) can be written similarly.

$$\frac{\partial (\rho u)}{\partial t} + \nabla . \left(\rho u \vec{V}\right) = -\frac{\partial p}{\partial x} + \nabla . (\mu \nabla \mathrm{u}) + S_x \tag{3}$$

Lastly, the energy equation can be written as;

$$\frac{\partial(\rho e)}{\partial t} + \nabla.\left(\rho e\vec{V}\right) = -p\left(\nabla.\vec{V}\right) + \nabla.(k\nabla \mathrm{T}) + S_e + \phi \tag{4}$$

These five scalar equations contain 7 unknowns (ρ, u, v, w, p, e, T). Two more equations are required to solve the equations. One of them comes from equation of state and the other one comes from internal energy and temperature relation. The equations are shown below.

$$p = \rho RT \tag{5}$$

$$\Delta e = C_v.\Delta T \tag{6}$$

The parameters in these equations are defined in Table 3.

Table 3: CFD Terms

ρ	Density
t	Time
$\vec{V}$	Velocity Vector
u	x-component of Velocity Vector
v	y-component of Velocity Vector
w	z-component of Velocity Vector
p	Pressure
μ	Dynamic Viscosity
S_x	Body Forces

Table 3 Continued: CFD Terms

e	Internal energy per mass
k	Thermal Conductivity
T	Temperature
S_e	Energy source terms
ϕ	Viscous Dissipation Term
C_v	Constant Volume Specific Heat

Solving these 7 equations is almost impossible analytically. Therefore, they are generally solved numerically. Partial derivatives are discretized by using convenient methods and resulting equations can be solved with appropriate techniques. In this study, the abovementioned governing equations are solved using Ansys Fluent 16.0 commercial CFD software.

3.3. Porous Media Approach

Porous media CFD modelling includes continuity and momentum equations that are similar to CFD equations given in Section 3.2. Since volume blockage is not modelled physically in porous media approach, superficial velocity can be defined which does not account for porosity when calculating the convection and diffusion terms of the transport equation. Besides, more accurate physical velocity model can also be chosen instead of superficial velocity. In this thesis, both velocity models are applied and it is seen that there is not a substantial difference between the results. Therefore, superficial velocity is preferred for the sake of simplicity. Besides, porous media momentum equations include a momentum source term which is the only difference between Navier-Stokes momentum equations and porous media momentum equations. This source term contains two terms, namely, a viscous loss term (first term on the right-

hand side of Equation (7)) and an inertial loss term (second term on the right-hand side of Equation (7)) [74]:

$$S_i = -\left(\sum_{j=1}^{3} D_{ij}\mu v_j + \sum_{j=1}^{3} C_{ij}\frac{1}{2}\rho|v|v_j\right) \tag{7}$$

where, S_i indicates the source term for the i_{th} momentum equation. Additionally, D_{ij} and C_{ij} are prescribed matrices. $|v|$ denotes the magnitude of the velocity [74]. This equation reduces to Equation (8) for simple homogenous porous media:

$$S_i = -\left(\frac{\mu}{\alpha}v_i + C_2\frac{1}{2}\rho|v|v_i\right) \tag{8}$$

where, α is the permeability and C_2 is the inertial resistance factor. For all laminar flows, inertial loss term can be considered as zero. Similarly, viscous loss term can be considered as zero for high flow velocity cases.

Energy equation can be solved in two different ways in porous media approach. The first one is the equilibrium model which is used when the porous medium and the fluid flow are assumed to be in thermal equilibrium. The second one is the non-equilibrium model which is used when the porous medium and the fluid flow are assumed not to be in thermal equilibrium. Since heat exchanger problems are solved by non-equilibrium model, only this equation is given below:

$$\frac{\partial}{\partial t}\left(\gamma\rho_f E_f\right) + \nabla.\left(\vec{V}(\rho_f E_f + p)\right) = \nabla.\left(\gamma k_f \nabla \mathrm{T}_f - \left(\sum_i h_i J_i\right) + \left(\bar{\bar{\tau}}.\vec{V}\right)\right) + S_f^h + h_{fs}A_{fs}(T_s - T_f) \quad (9)$$

And the energy equation solved for the solid zone is

$$\frac{\partial}{\partial t}\left((1-\gamma)\rho_s E_s\right) = \nabla.\left((1-\gamma)k_s \nabla T_s\right) + S_s^h + h_{fs}A_{fs}(T_f - T_s) \quad (10)$$

The parameters used in these equations are defined in Table 4.

Table 4: Porous Media Approach CFD Terms [74]

E_f	Total Fluid Energy
E_s	Total Solid Medium Energy
ρ_f	Fluid Density
ρ_s	Solid Medium Density
γ	Porosity of the Medium
k_f	Fluid Phase Thermal Conductivity
k_s	Solid Medium Thermal Conductivity
h_{fs}	Heat Transfer Coefficient for the Fluid / Solid Interface
A_{fs}	Interfacial Area Density
T_f	Temperature of the Fluid
T_s	Temperature of the Solid Medium
S_f^h	Fluid Enthalpy Source Term
S_s^h	Solid Enthalpy Source Term

3.4. Optimization

In this thesis, Matlab commercial software will be used for all optimization studies. There are different options for main rules of genetic algorithm (choosing, crossing and mutation) in the literature. For instance, stochastic uniform, remainder, uniform, roulette and tournament choosing options are available in the Matlab for single objective genetic algorithm [75]. In multi-objective genetic algorithm, only tournament choosing is available. Moreover, some crossover options are available in the same optimization tool namely scattered, single point, two point, intermediate, heuristic and arithmetic. Lastly, mutation options can be classified as Gaussian, uniform and adaptive feasible. The best options will be determined by sensitivity analysis in this thesis. The detailed information about other multi-objective genetic algorithm options such as pareto fraction and distance measure of individuals can be found in the reference [75]. The flowchart of the genetic algorithm, which is used in this thesis, is given in Figure 9 to provide better illustration.

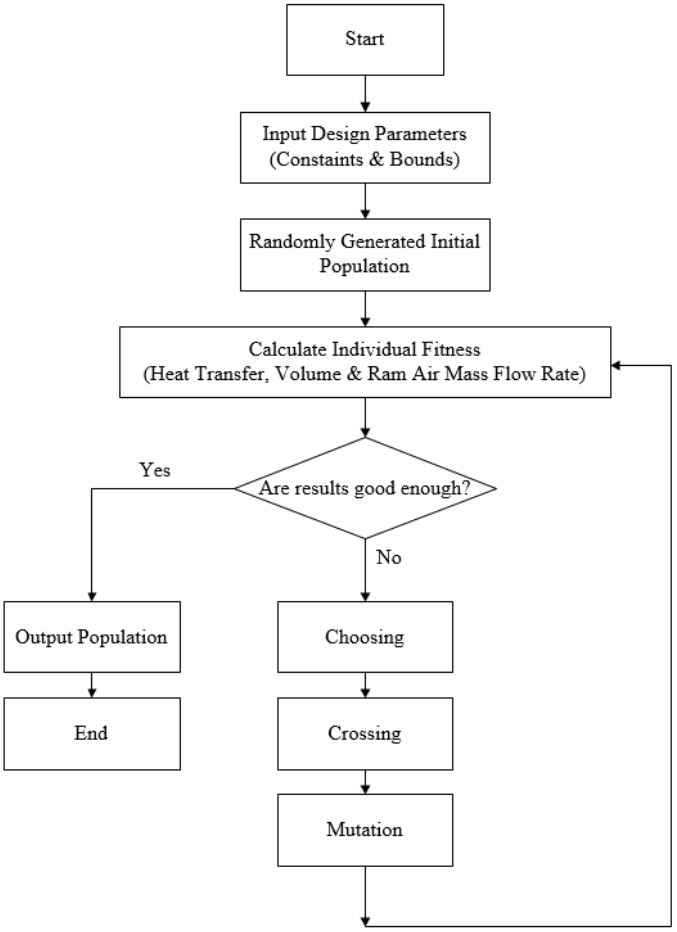

Figure 9: Schematic of Genetic Algorithm

GA is selected as a suitable optimization algorithm for this thesis beyond this point. An air to air aircraft ECS primary heat exchanger will be optimized by using multi objective GA algorithm.

3.5. DOE & Response Surface Method

As mentioned before in Section 3.1, offset-strip fin and wavy fin were found as convenient fins for aircraft cooling applications. Four geometric parameters and one flow parameter are selected for each fin type namely the fin pitch, the plate spacing, the fin inclination angle, the offset length, and the Reynolds number for the offset-strip

fin and the fin pitch, the plate spacing, the wavelength, the amplitude, and the Reynolds number for the wavy fin. Considering number of experiments in the Table 1, Central Composite Design (CCD) gives 43 experiments for each fin type. This means 86 experiments in total for the two fin types, which is computationally affordable. Additionally, CCD covers all extremes, which is desirable for this study. Lastly, Ansys DesignXplorer notes indicates CCD as a good default choice [76]. Consequently, CCD will be used as a DOE method beyond this point. After DOE experiments are done, Response Surface Method will be utilized to create f and j factors correlations for the wavy fin and the offset-strip fin. In other words, discrete f and j factors results for a set of CFD runs will be correlated with geometrical and flow parameters in order to have continuous correlations. ModeFrontier 2014 commercial data analysis software will be used for this purpose [77].

All in all, DOE with Response Surface Method will be used to create the initial experimental input data points for predicting f and j factor formulae of offset-strip and wavy fins in this thesis.

CHAPTER 4

VALIDATION STUDIES

In this chapter, several validation studies are done to support further studies in the coming chapters. Periodic flow approach is explained and CFD validation studies are done for offset-strip fin and wavy fin. Additionally, GA optimization case study is done.

4.1. Periodic Flow Approach

CFD analyses are done by implementing periodic boundary condition as described in the paper of Patankar et al. which formulates a generalization of the concepts of fully developed flow and heat transfer [78]. This method is used in order to get rid of entrance effect of developing flows. In Figure 10, staggered array of plates which was used in the aforementioned study is shown.

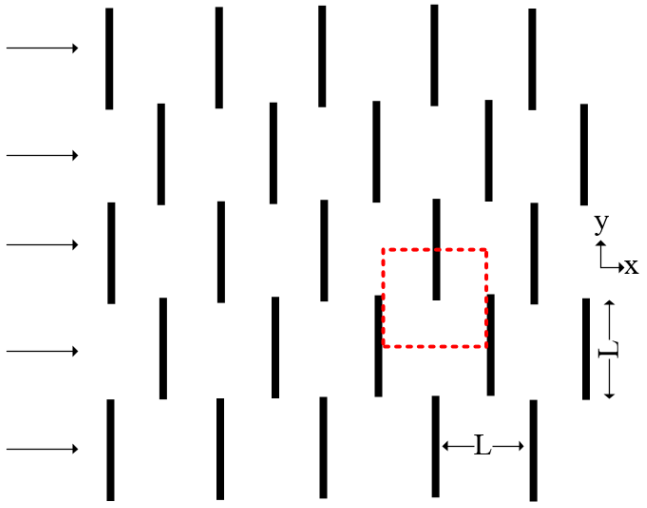

Figure 10: Transverse Plate Array Schematic Diagram [78]

In the periodic flow approach, velocity components show periodic behavior as follows;

$$u(x,y) = u(x+L,y) = u(x+2L,y) = \cdots \quad (11)$$

$$v(x,y) = v(x+L,y) = v(x+2L,y) = \cdots \quad (12)$$

where u and v are the x and y component of the velocity field, respectively. However, pressure and temperature fields (for heating case) show constant change far from inlet as follows:

$$p(x,y) - p(x+L,y) = p(x+L,y) - p(x+2L,y) = \cdots \quad (13)$$

$$T(x+L,y) - T(x,y) = T(x+2L,y) - T(x+L,y) = \cdots \quad (14)$$

where p and T are the pressure and temperature, accordingly. The details of the periodic flow approach can be found in the reference [78].

4.1.1. 1/8-19-86 Offset-Strip Fin Validation

Fanning friction factor and Colburn j factor for a specific fin can be predicted by using CFD. In this study, 1/8-19.86 offset-strip fin f and j factors are used as a case study [5]. The number of 19.86 denotes fin per inch and 1/8 denotes offset length of the fin in inches. Experimental results are retrieved from Kays and London Compact Heat Exchangers book [5]. Ansys Fluent User's Guide indicates that the thermodynamic properties cannot be functions of temperature when periodic boundary condition is applied [74]. If the properties are taken as a function of temperature, there may be convergence problems according to the author's experience. Therefore, air properties are taken as constant at 315 K, which is the average of the inlet and outlet temperatures at 1atm. Dynamic viscosity and density are found as 1.92E-5 Pa.s and 1.10 kg/m^3 , respectively. Since the experiments in Kays & London's Book are done by using condensing steam, constant temperature wall boundary conditions are applied with 373.15 K. Moreover, air upstream bulk temperature is taken as 300 K. Inlet and outlet static temperatures are obtained by using area-weighted average. According to the author's experience, it is better to get scalar quantities with area-weighted-average such as temperature or pressure. Since the flow is periodic, there is no standard inlet or outlet boundary condition. Only periodic mass flow condition is implemented. The geometry of the fin and applied boundary conditions are shown in Figure 11. In the

geometry, azure and red colors indicate periodic boundary conditions (separate pairs) and green color indicates wall boundary condition.

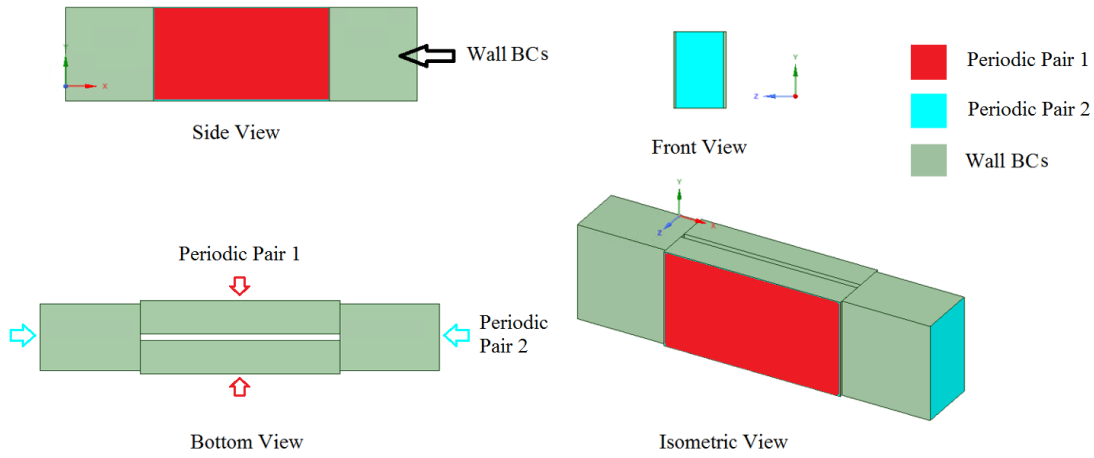

Figure 11: 1/8-19.86 Fin Channel Geometry

Mesh independence study is conducted first. Since the flow geometry is quite small, enhanced wall function with realizable k-ε turbulence model is used first to solve thin boundary layers near walls. The Reynolds number is kept approximately at 3750 which is close to the maximum for the corresponding fin configuration (Max Re=4000) in the reference book [5]. Convergence criteria are selected as 10^{-3} for k and ε, 10^{-6} for energy, and 10^{-5} for other residuals. Moreover, mesh is created by using edge sizing and biased through the walls which is shown in Figure 12. Mesh is refined at the fin edges and walls where velocity and pressure gradients are high in order to provide good resolution and to keep y^+ (dimensionless wall distance) below 1.

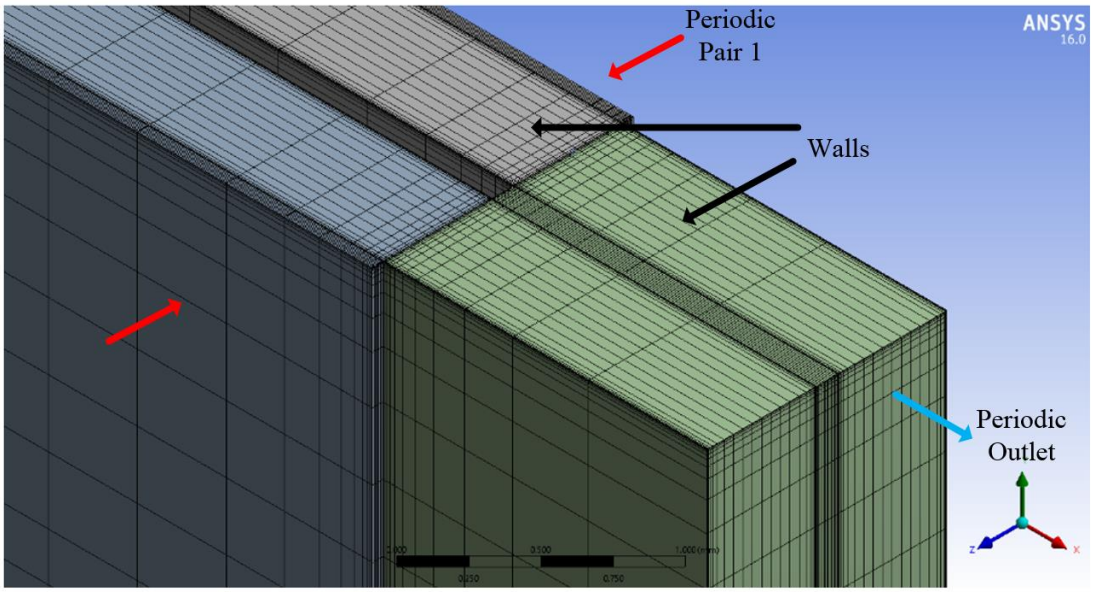

Figure 12: Created mesh for mesh independence study

Calculations are done by using semi-implicit pressure linked equations pressure-velocity coupling scheme with second order upwind scheme for momentum, turbulent kinetic energy and turbulent dissipation rate. Least squares cell based and second order discretization methods are used for gradient and pressure discretization, respectively. Pressure drop per meter values are obtained from periodic boundary condition section. Fanning friction factor is calculated using Equation (15). The results of mesh independency study are shown in Figure 13. Since increasing mesh size does not affect the solution significantly, using 173000 elements mesh is beneficial for computational time cost. Further increase of the number of elements gives not more than 2% change. Beyond this point, this mesh will be used for future calculations.

$$f = \frac{D_h \rho_{ave} \Delta P}{2LG^2} \tag{15}$$

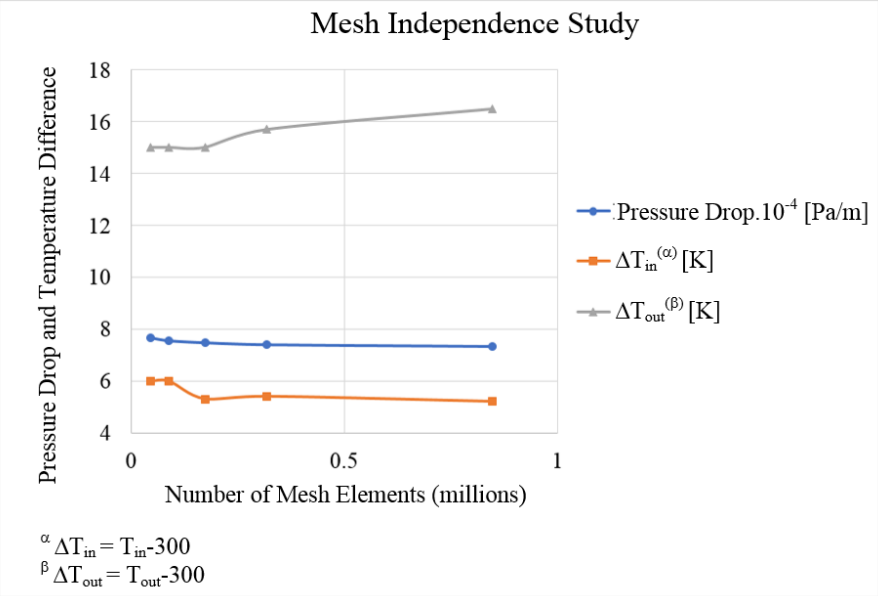

Figure 13: Mesh Independence Study

Standard and realizable k-ε turbulence models are also investigated with standard, enhanced, and Menter-Lechner wall functions as a next step. Since every wall function has its own dimensionless wall distance (y^+) characteristics, different meshes are implemented for different wall functions. Standard wall function accuracy deteriorates when $y^+<15$ and enhanced wall function requires maximum $y^+\leq1$ for a good solution [79]. Additionally, Menter-Lechner wall function is y^+ independent. Enhanced wall function mesh is created by using edge sizing bias factor as 100 to keep y^+ value below 1 but the mesh for Menter-Lechner and standard wall functions contains no bias. Created meshes are shown below in Figure 14 and Figure 15.

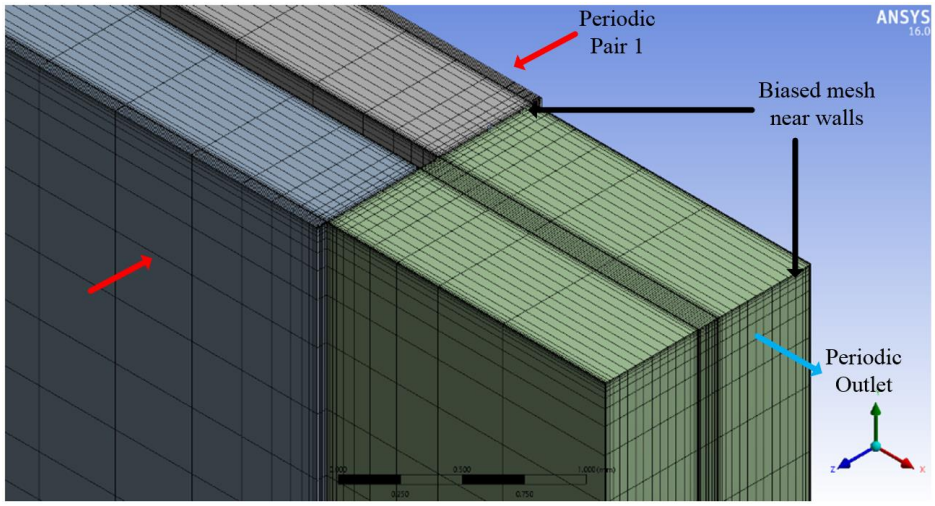

Figure 14: Used Mesh for Enhanced Wall Function

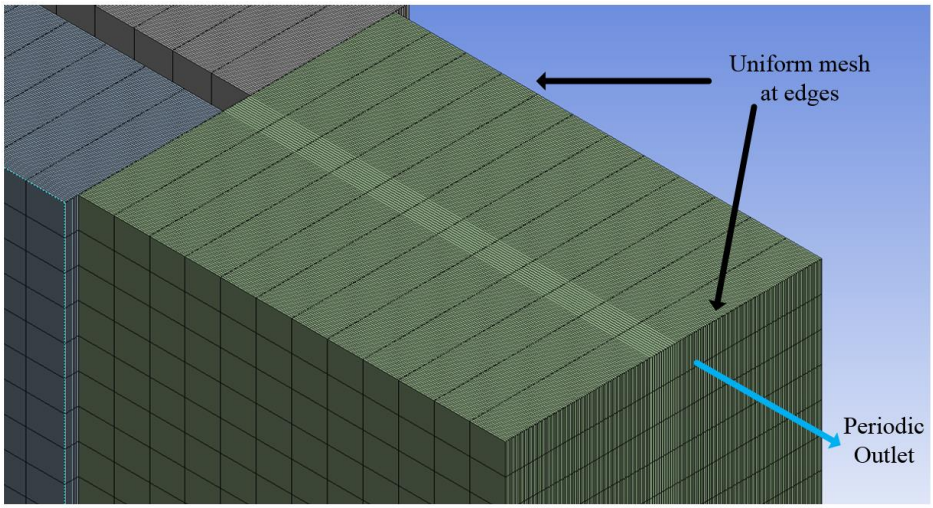

Figure 15: Used Mesh for Other Wall Functions

The results are shown in Table 5. Since there is ±5% uncertainty in experimental results of Kays and London's book, standard k-ε with enhanced wall function can be acceptable to predict f and j factors. The reason of this may be that realizable and RNG k-ε models are beneficial where there are strong streamline curvature, vortices, and rotation but there is no strong streamline curvature in the geometry [79].

Table 5: Turbulence Model Evaluation

Re	**Pressure Drop [kPa/m]**	**f Real×10^2** [5]	**f CFD×10^2**	**Relative Error [%]**	**y$^+$ near walls**	**Model**	**Number of elements**
3750	74.8	2.895	2.899	-0.15	0.93	k-ε realizable with enhanced wall function	173000
3750	**74.8**	**2.895**	**2.899**	**-0.13**	**0.88**	**k-ε standard enhanced wall function**	**173000**
3750	91.7	2.895	3.552	-22.68	3.96	k-ε standard standard wall function	173000
3750	69.2	2.895	2.681	7.40	3.92	k-ε standard menter-lechner wall function	173000
3750	55.4	2.895	2.148	25.80	3.70	k-ε realizable menter-lechner wall function	173000

After determining the best turbulence model and independent mesh settings, validation study can be done. Reynolds number is varied between approximately 1000 and 3750 which is in the transition and turbulent region [80]. Colburn j factor is calculated by using Equation (16):

$$\mathrm{j} = \frac{D_h}{4L} ln\left(\frac{T_{in} - T_{wall}}{T_{out} - T_{wall}}\right) * Pr^{2/3} \quad (16)$$

Air temperature and velocity contours of three different planes (periodic inlet, periodic outlet and y axis middle cross section) for Re=3750 are shown in Figure 16 and Figure 17, respectively. Temperature scale is in K and velocity scale is in m/s.

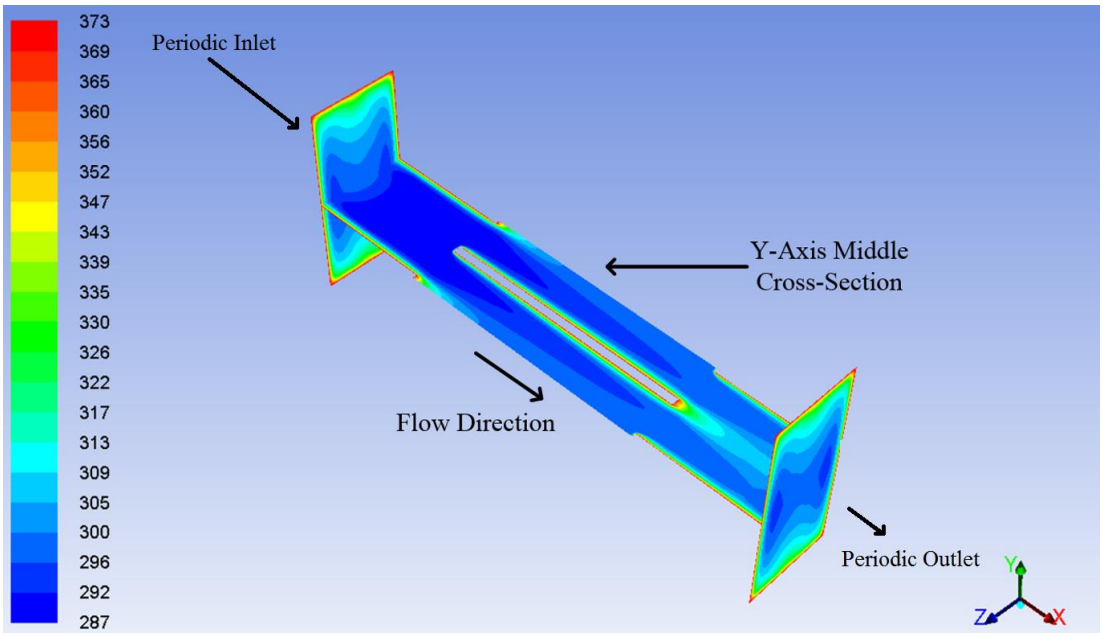

Figure 16: Offset-strip Fin Sample Temperature Contours [K]

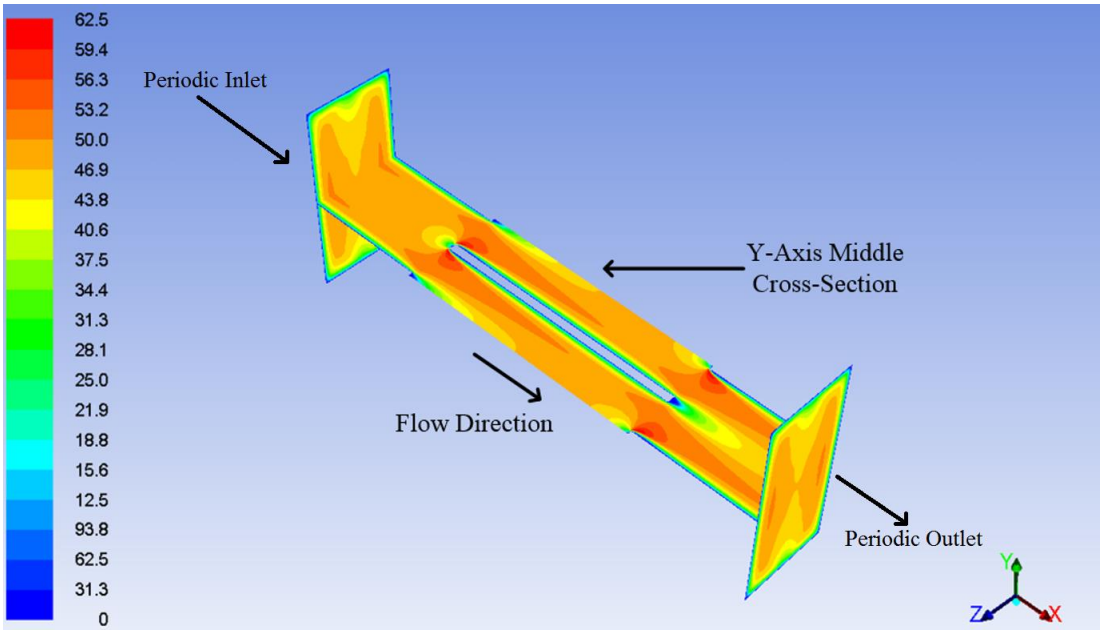

Figure 17: Offset-Strip Fin Sample Velocity Contours [m/s]

The general results are shown in Figure 18. Average relative errors for friction factor and Colburn j factor are found as 2.28% and 5.17%, respectively. Consequently, 1/8-19.86 offset-strip fin friction factor and Colburn j factor are predicted successfully.

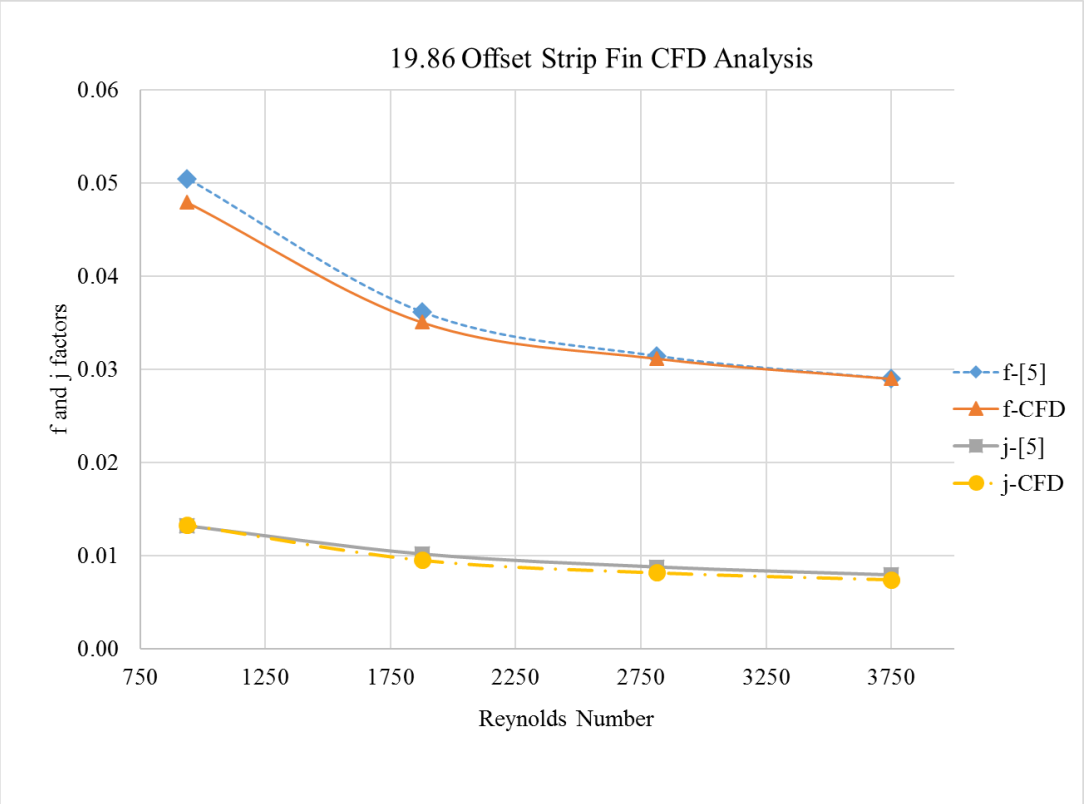

Figure 18: 1/8 19.86 Offset-Strip Fin Validation Results

4.1.2. 3/8-11.44 Wavy Fin Validation

The procedure is the same as in the case of offset-strip fin. The geometry of the fin and applied boundary conditions are shown in Figure 19. In the geometry, azure and green colors indicate periodic boundary conditions and wall boundary conditions, respectively. As in the previous case all walls are set to 373.15 K constant temperature.

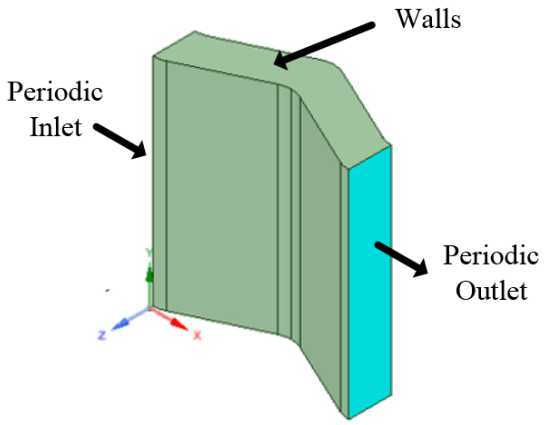

Figure 19: 3/8-11.44 Fin Channel Geometry

Mesh independence study is done by using the same settings of offset-strip fin case. Relatively finer mesh is used, which is shown in Figure 20,compared to offset-strip fin case to keep y^+ value below 1.

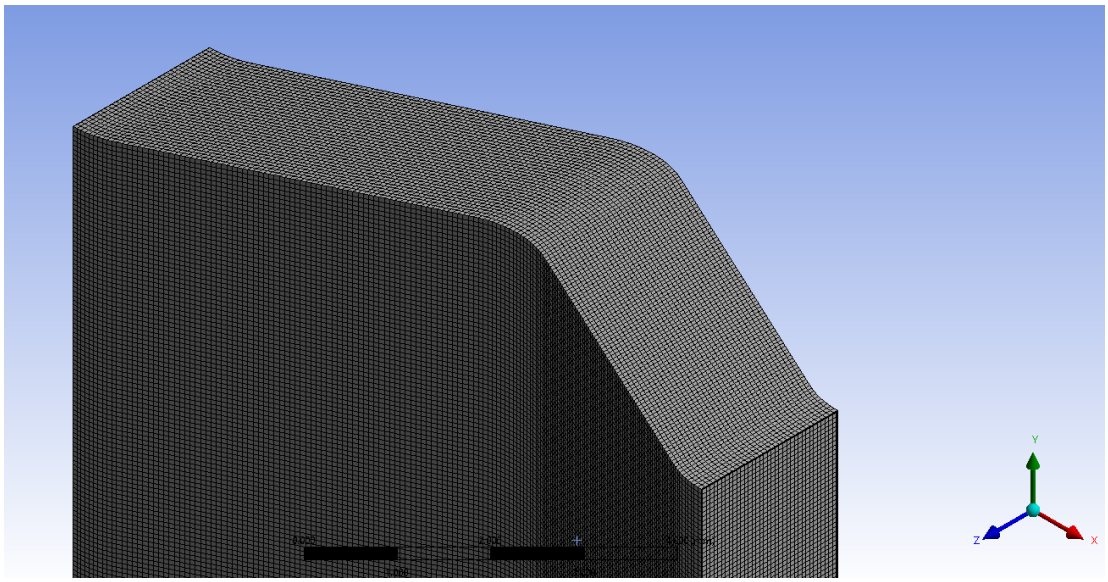

Figure 20: Used Mesh for Wavy Fin

Since the geometry contains curvature structure, realizable k-ε turbulence model is preferred than standard k-ε turbulence model [79]. Mesh independence study is conducted at Re=7500 and shown in Figure 21. The results show that 130000 element mesh is sufficient for further calculations.

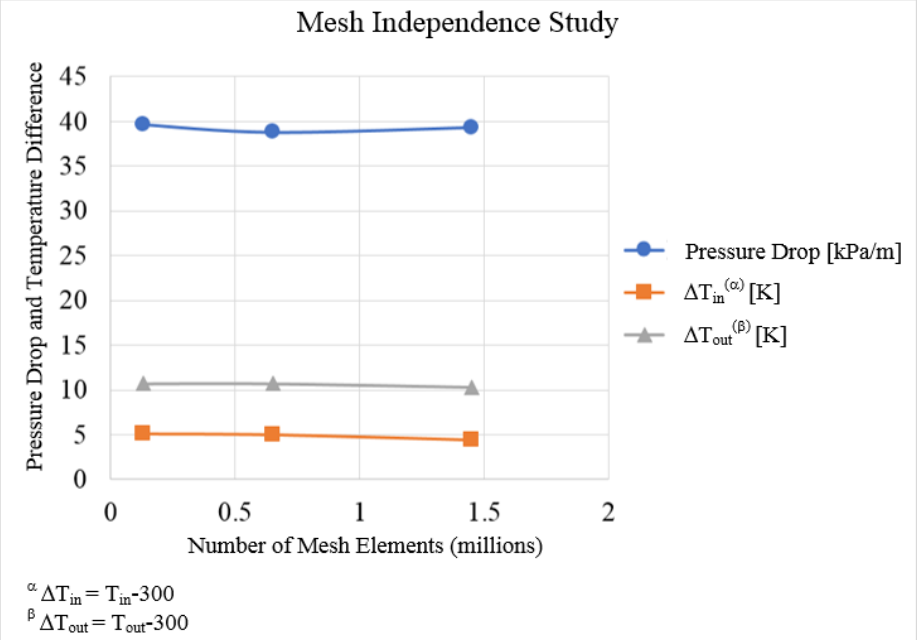

Figure 21: Wavy Fin Mesh Independence Study for 3/8-11.44(W)

Air temperature and velocity contours of three different planes (periodic inlet, periodic outlet and y axis middle cross section) for Re=7500 are shown in Figure 22 and Figure 23, respectively. Temperature scale is in K and velocity scale is in m/s.

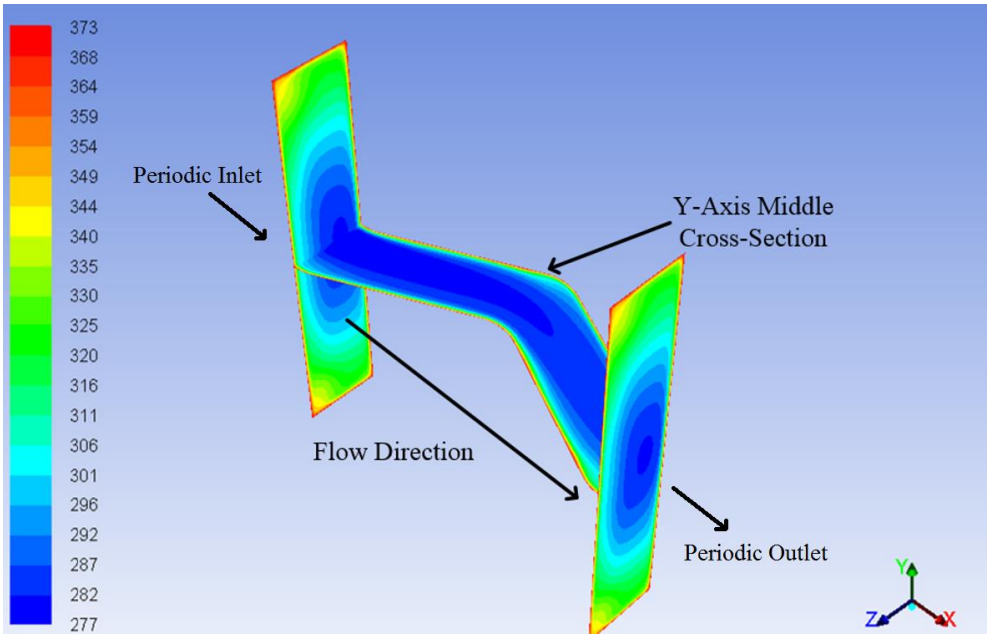

Figure 22: Wavy Fin Sample Temperature Contours [K]

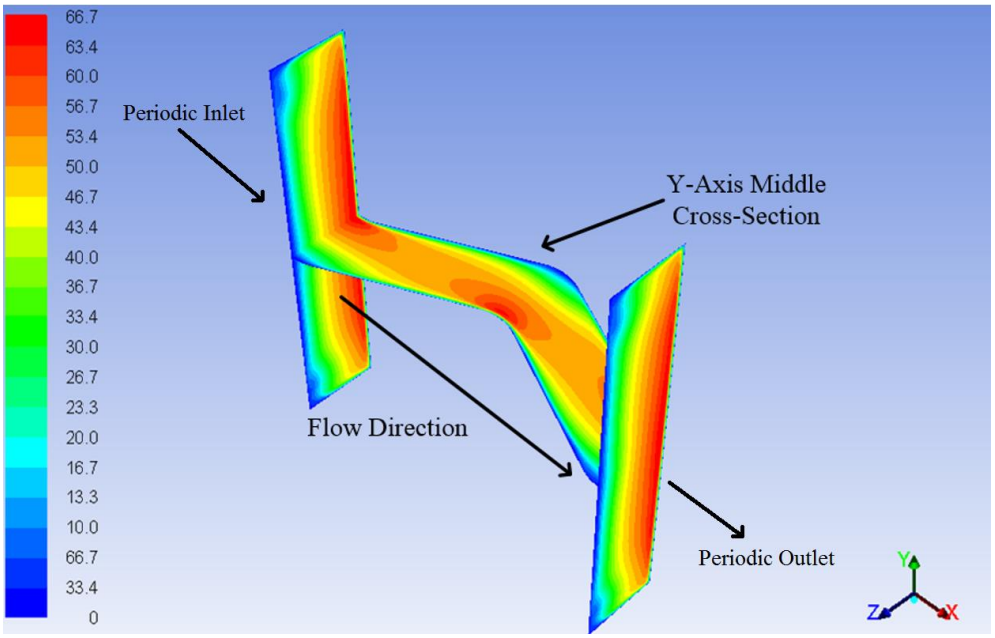

Figure 23: Wavy Fin Sample Velocity Contours [m/s]

The general results are shown in Figure 24. The average relative errors for friction factor and Colburn j factor are found as 3.93% and 16.5%, respectively. Consequently, 3/8-11.44 wavy fin friction factor is predicted successfully. The deviation of the Colburn j factor may be resulted from wavy tip radius or wave shape such as sinusoidal wave or other type which are not given in the reference [5].

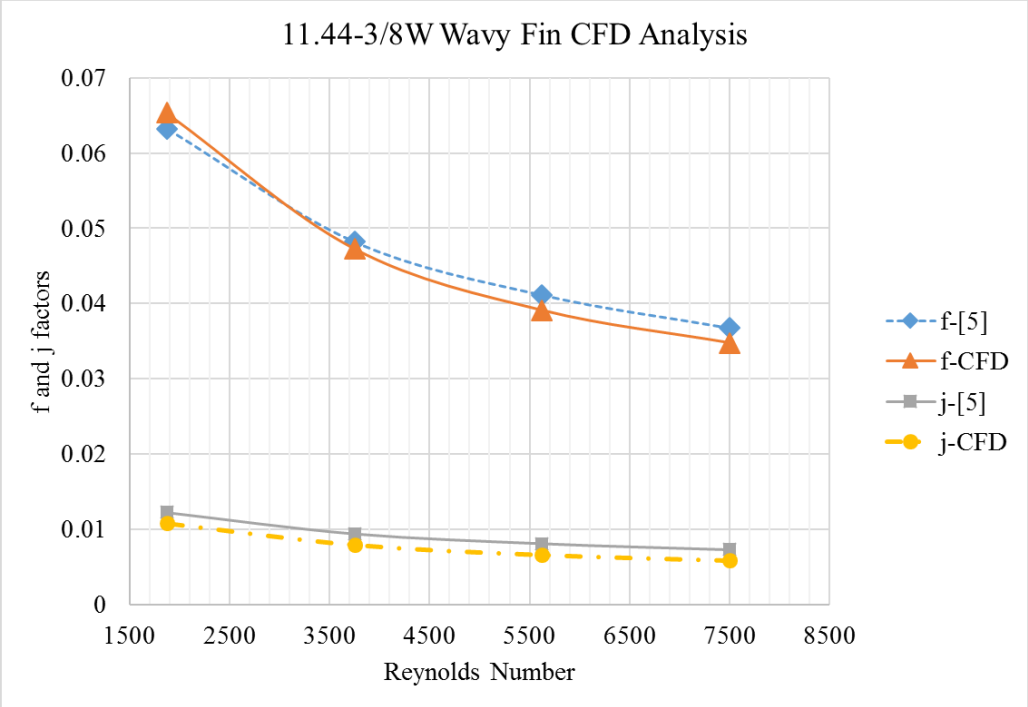

Figure 24:3/8 11.44 Wavy Fin Validation Results

4.2. GA Optimization Case Study

The work of Imran et al. [41] is used to validate the genetic algorithm used in this thesis. In their study, water to water plate heat exchanger (Figure 25) is optimized. Heat transfer and pressure drop are selected as objective functions. Multi-objective genetic algorithm is applied as an optimization tool. The results are shown in Figure 26. The source of the small deviation may be the unknown fluid properties. Properties are assumed as constant at the average of inlet and outlet temperatures. Additionally,

number of total generations was not given in their study. Since GA heat exchanger optimization studies generally converge number of generations lower than 3000 by the author's experience, it is taken as 3000 in order to be on the safe side. Aforementioned small deviation may have resulted from unknown number of generations.

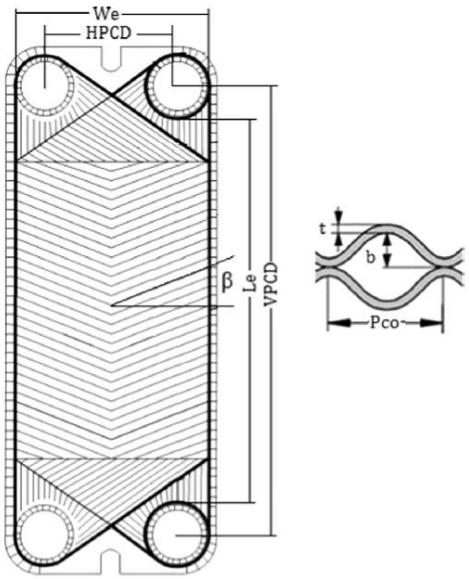

Figure 25: Used Plate Heat Exchanger [41]

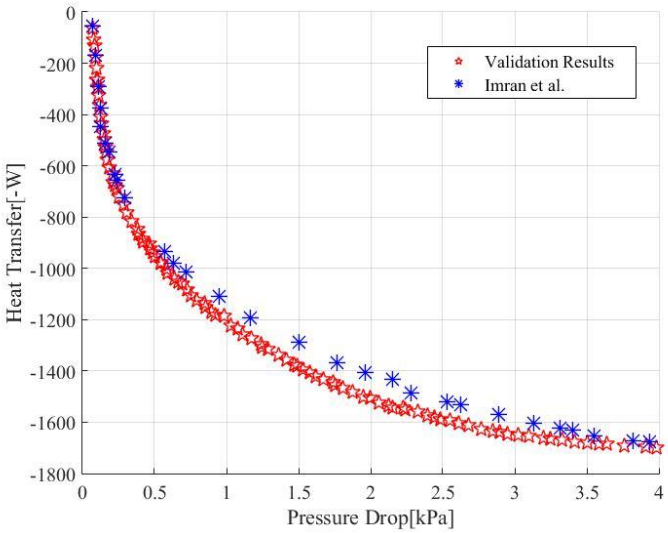

Figure 26: Pareto Front Comparison

CHAPTER 5

HEAT EXCHANGER OPTIMIZATION

5.1. Supersonic Aircraft Flight Conditions

Air conditioning heat exchangers should give good performance in all extreme conditions. Matullch studied most critical flight envelope points for F-15 jet fighter [3]. In Figure 27, typical flight envelope of a supersonic aircraft is given. In this figure, most critical 5 flight conditions are shown according to the available heat sink. In case 1, aircraft is flying at sea level with Ma=0.3 speed. At this condition, ram air mass flow rate may not be sufficient due to low speed. In case 2, aircraft speed is slightly higher than Ma=1 and the altitude is again at sea level. At this condition, air density and air recovery temperature are quite high due to compressible flow and aerodynamic heating. In case 3, aircraft speed is about Ma=2.15 and the altitude is at about 11 km (36000 ft). At this condition, air recovery temperature is again high but air density is dramatically decreased due to altitude which decreases ram air mass flow rate. In case 4, the mass flow rate of the ram air is decreased due to low aircraft speed and low air density. Lastly, the fastest point of flight envelope is considered which is case 5. The details of the flight envelope points are given in Table 6 [3].

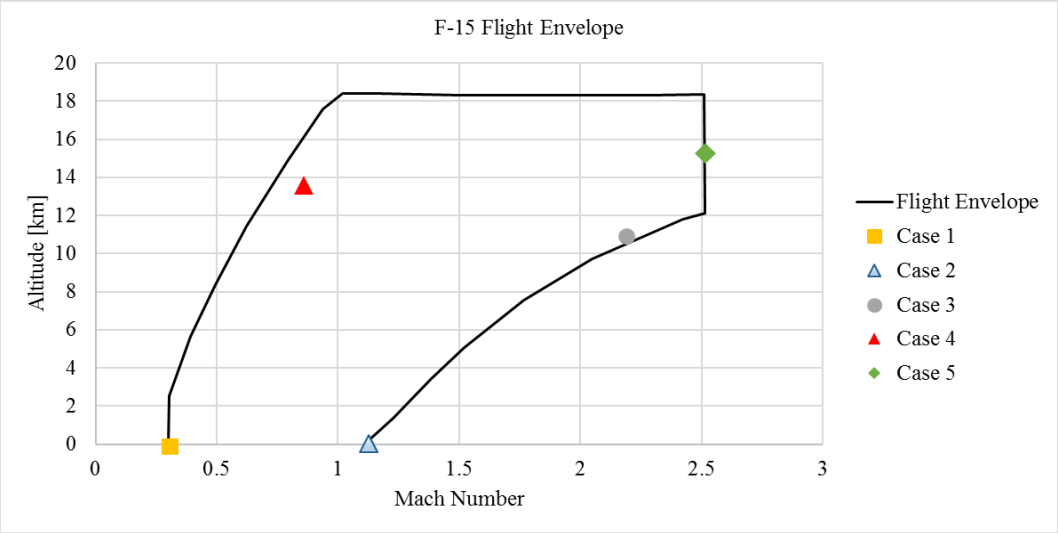

Figure 27: Typical Flight Envelope of a Jet Fighter [3]

Table 6: Details of Critical Thermal Points of Flight Envelope [3]

Case	**Altitude [km]**	**Mach No**	**Day**	**Total Bleed Air Flow [kg/s]**	**Total Ram Air Flow [kg/s]**
1	Sea Level	0.3	Hot	1.15	2.74
2	Sea Level	1.14	Hot	1.20	14.49
3	11	2.15	Hot	1.02	9.96
4	13.7	0.85	Standard	0.64	1.24
5	15.2	2.5	Standard	0.86	6.74

Critical points are investigated thermodynamically according to temperature-entropy graphs of the Matullch's study [3]. The calculated results are given in Table 7. Since F-15 aircraft contains two engines and two primary heat exchangers, total bleed air mass flow rate is divided by 2. Moreover, some portion of air is discharged from ejectors (in Case 1) before reaching the primary heat exchangers for cooling purposes which explains the difference of the bleed air mass flow rates between Table 6 and

Table 7. Additionally, it is assumed that ram air flow rate per heat exchanger is equal for two primary and one secondary heat exchangers. Hot day conditions are taken from MIL-HDBK-310C for 5% geometric altitude and standard day conditions are taken from International Standard Atmosphere [81]. Recovery air temperature is calculated according to formula below [82]:

$$T_r = T_o \left[1 + r\left(\frac{\gamma - 1}{2}\right) M^2\right] \tag{17}$$

where, T_r [R], T_o [R], r, γ, and Ma are the recovery temperature, the outside ambient temperature, the recovery factor, the specific heat ratio, and the Mach number, respectively.

Consequently, Case 2 requires the highest amount of heat transfer for primary heat exchanger (PHX), which is about 243 kW per heat exchanger. Therefore, in this study, optimization study will be performed by considering Case 2 conditions.

Table 7: Operating Parameters Calculation

Case	**Cp,air [J/kgK]**	**Bleed Air Flow [kg/s]**	**Ram Air Flow [kg/s]**	**Bleed Air Inlet Temp [K]**	**Bleed Air Outlet Temp [K]**	**Ram Air Inlet Temp [K]**	**PHX HT [kW]**	**Max HT [kW]**
1	1029.12	0.44	0.91	606.27	400.65	327.02	92.82	126.05
2	1056.92	0.60	4.83	831.63	447.20	392.49	243.17	277.78
3	1072.46	0.51	3.32	905.48	506.38	450.94	219.04	249.46
4	1032.22	0.32	0.41	602.88	438.36	244.76	53.52	116.50
5	1075.08	0.42	2.25	910.84	522.81	456.02	177.13	207.63

5.2. Thermal Model

In this study, ε-NTU method is applied to air to air crossflow heat exchanger for analyzing the heat exchanger performance. The simple outside dimensions of the heat exchanger and fin parameters are shown in Figure 28 and Figure 29, respectively. There are 12 parameters for each fin type. Some of them are common but others are different for each fin. All common and different optimization parameters are shown in Table 8. Since no-flow length in Figure 28 is dependent on other parameters such as hot side number of plates, cold side plate spacing, hot side plate spacing and plate thickness, it is not taken in the parameters table. In the analysis, the variations of physical properties of fluids with temperature are neglected and air at both sides is considered as ideal. Other assumptions are given as follows:

1- Number of cold side fin layer is taken as one more than hot side fin layers.
2- Thermal contact resistance of the walls is neglected.
3- Fouling is neglected since the heat exchanger is air to air.
4- Transient effects are neglected.
5- Heat transfer coefficient is assumed as constant and uniform.
6- Heat exchanger material is taken as Inconel due to high temperature melting point with 18 W/mK thermal conductivity.
7- No manufacturing technique is considered.
8- Fin metal thickness is taken as constant (0.05 mm)

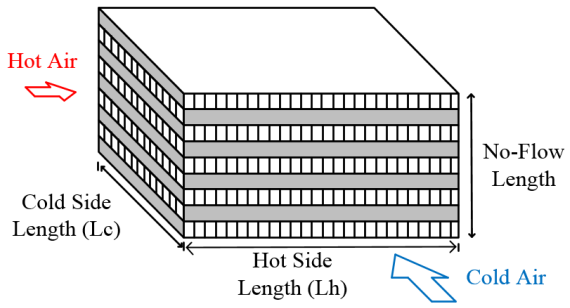

Figure 28: Heat Exchanger Full Dimension Parameters

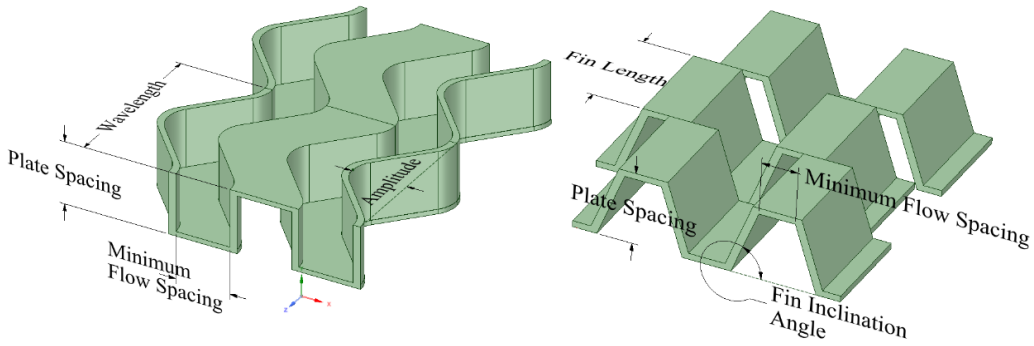

Figure 29:Wavy Fin and Offset-Strip Fin Optimization Parameters

Table 8: Heat Exchanger Input Parameters for Wavy Fin and Offset-Strip Fin

Parameter Number	Wavy Fin	Offset-Strip Fin
1	Hot Flow Length (L_h)	
2	Cold Flow Length (L_c)	
3	Hot Side Number of Plates (N_h)	
4	Cold Side Minimum Flow Spacing (MFS_c)	
5	Hot Side Minimum Flow Spacing (MFS_h)	
6	Cold Side Plate Spacing (PS_c)	
7	Hot Side Plate Spacing (PS_h)	
8	Cold Side Wavelength (Wl_c)	Cold Side Fin Length (Fl_c)
9	Hot Side Wavelength (Wl_h)	Hot Side Fin Length (Fl_h)
10	Cold Side Amplitude (Amp_c)	Cold Side Fin Inclination Angle (FIA_c)
11	Hot Side Amplitude (Amp_h)	Hot Side Fin Inclination Angle (FIA_h)
12	Ram Air Total Mass Flow Rate (MFR_c)	

The operating conditions are taken as constant for each side due to periodic flow restriction which is explained in Section 4.1.1. Hot side air temperature is assumed as 640 K average temperature with 0.6 kg/s constant mass flow rate in order to calculate material properties. Similarly, cold side air temperature and mass flow rate are assumed as 445 K average temperature with 2.45 kg/s mass flow rate. However, cold side mass flow rate will be taken as an optimization variable. Therefore, 2.45 kg/s is only an initial estimate. Since air thermal properties do not change with pressure significantly, they are calculated at 1atm state as a function of temperature except the density. Density is calculated by using ideal gas law and other properties are calculated by using spline interpolation method [83]. Details of operating conditions are given in Table 9. Fin thickness is taken as constant which is the minimum value of fin corresponding wavy and offset-strip fins in the reference [5]. Moreover, core dimensions of the fins are shown in Figure 30 and Figure 31.

Table 9: Supersonic Aircraft Heat Exchanger Operating Parameters

Properties	Hot Side @ 527.3 kPa (76.5 psi), 640 K	Cold Side @ 209.6 kPa (30.41 psi), 445 K
Density [kg/m^3]	2.86	1.64
Specific Heat [J/kgK]	1060	1021
Viscosity [kg/m.s]	32e-6	25e-6
Prandtl Number	0.688	0.686
Mass Flow Rate [kg/s]	0.6	Optimization Variable (0.5-4)
Fin Thickness (t) [mm]	0.05	0.05

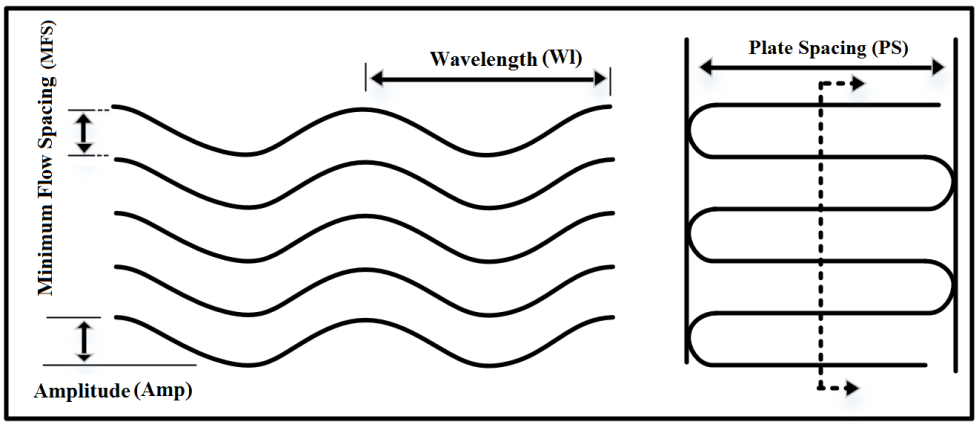

Figure 30: Wavy Fin Core Dimension Parameters

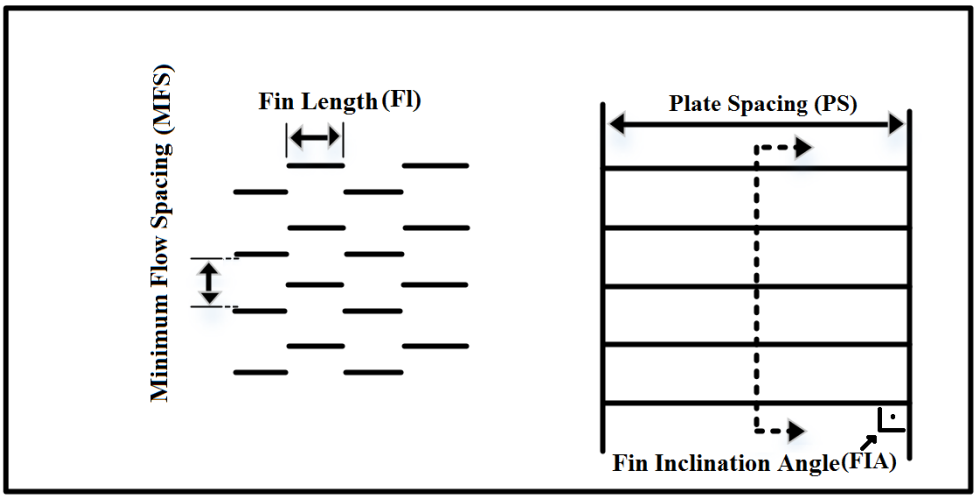

Figure 31: Offset-Strip Fin Core Dimension Parameters

Details of the thermal model is given below. To begin with, heat capacities of flows are defined as follows:

$$C_c = Cp_c \times MFR_c \quad (18)$$

$$C_h = Cp_h \times MFR_h \quad (19)$$

$$C_{min} = \min(C_c, C_h) \quad (20)$$

$$C_{max} = \max(C_c, C_h) \quad (21)$$

$$C^* = \mathrm{C_{min}}/\mathrm{C_{max}} \quad (22)$$

Free flow areas can be calculated according to frontal view of the fins as shown in the figures below:

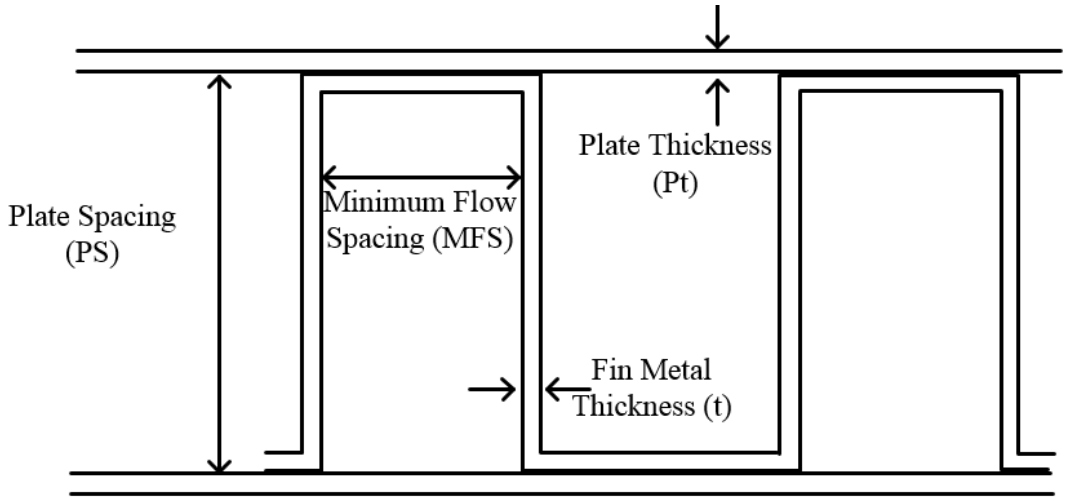

Figure 32: Wavy Fin Frontal View

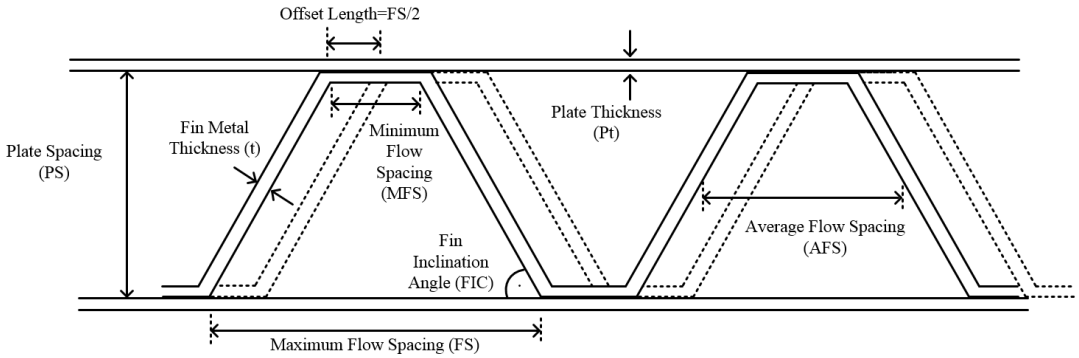

Figure 33: Offset-Strip Fin Frontal View

$$Aff_h = (PS_h - t) \times L_c \times (MFS_h/(MFS_h + t)) \times N_h \text{ for wavy fin} \quad (23)$$

$$Aff_c = (PS_c - t) \times L_h \times FS_c/(FS_c + t) \times N_c \text{ for wavy fin} \quad (24)$$

$$Aff_h = AFS_h \times (PS_h - t) \times n_h \times L_c \times N_h \text{ for offset-strip fin} \quad (25)$$

$$Aff_c = AFS_c \times (PS_c - t) \times n_c \times L_h \times N_c \text{ for offset-strip fin} \quad (26)$$

where, n is fin per meter and is defined as follows:

$$n_h = 1/(FS_h + t) \text{ for wavy fin} \quad (27)$$

$$n_c = 1/(FS_c + t) \text{ for wavy fin} \quad (28)$$

$$n_h = 2/(FS_h + MFS_h + 2 \times t) \text{ for offset-strip fin} \quad (29)$$

$$n_c = 2/(FS_c + MFS_c + 2 \times t) \text{ for offset-strip fin} \quad (30)$$

Total heat transfer areas can be divided as primary and fin heat transfer areas as below [84]:

$$Ap_h = \left(L_h \times L_c - t \times L_h \times \frac{unitlength_h}{Wl_h} \times n_h \times L_c\right) \times N_h \text{ for wavy fin} \quad (31)$$

$$Ap_c = \left(L_c \times L_h - t \times L_c \times \frac{unitlength_c}{Wl_c} \times n_c \times L_h\right) \times N_c \text{ for wavy fin} \quad (32)$$

$$\mathrm{Af_h} = (2 \times (\mathrm{PS_h} - \mathrm{t}) + \mathrm{MFS_h}) \times \mathrm{L_h} \times \mathrm{L_c} \times \mathrm{n_h} \times \frac{unitlength_h}{Wl_h} \times N_h \text{ for wavy fin} \quad (33)$$

$$\mathrm{Af_c} = (2 \times (\mathrm{PS_c} - \mathrm{t}) + \mathrm{MFS_c}) \times \mathrm{L_c} \times \mathrm{L_h} \times \mathrm{n_c} \times \frac{unitlength_c}{Wl_c} \times N_c \text{ for wavy fin} \quad (34)$$

$$\mathrm{Ap_h} = \mathrm{FS_h} \times \mathrm{n_h} \times \mathrm{L_c} \times \mathrm{L_h} \times \mathrm{N_h} \text{ for offset-strip fin} \quad (35)$$

$$\mathrm{Ap_c} = \mathrm{FS_c} \times \mathrm{n_c} \times \mathrm{L_h} \times \mathrm{L_c} \times \mathrm{N_c} \text{ for offset-strip fin} \quad (36)$$

$$\mathrm{Af_h} = \left(2 \times \frac{\mathrm{PS_h} - \mathrm{t}}{\sin(\mathrm{FIA_h})} + \mathrm{MFS_h}\right) \times \mathrm{L_h} \times \mathrm{L_c} \times \mathrm{n_h} \times \mathrm{N_h} \text{ for offset-strip fin} \quad (37)$$

$$\mathrm{Af_c} = (2 \times (\mathrm{PS_c} - \mathrm{t})/\sin(\mathrm{FIA_c}) + \mathrm{MFS_c}) \times \mathrm{L_c} \times \mathrm{L_h} \times \mathrm{n_c} \times \mathrm{N_c} \text{ for offset-strip fin} \quad (38)$$

$$\mathrm{A_h} = \mathrm{Ap_h} + \mathrm{Af_h} \text{ for both fins} \quad (39)$$

$$A_c = Ap_c + Af_c \text{ for both fins} \quad (40)$$

The wavy fin length calculation is comparatively more complex. Since the wavy fin is constructed by combining 3 arcs and 2 straight lines as shown in Figure 34, its length is calculated trigonometrically. In calculations, wavy tip radius is taken as 1 mm for all fin designs. Heat transfer area is calculated like straight fins and then the area is multiplied by unit length/wavelength ratio in order to find the exact fin length.

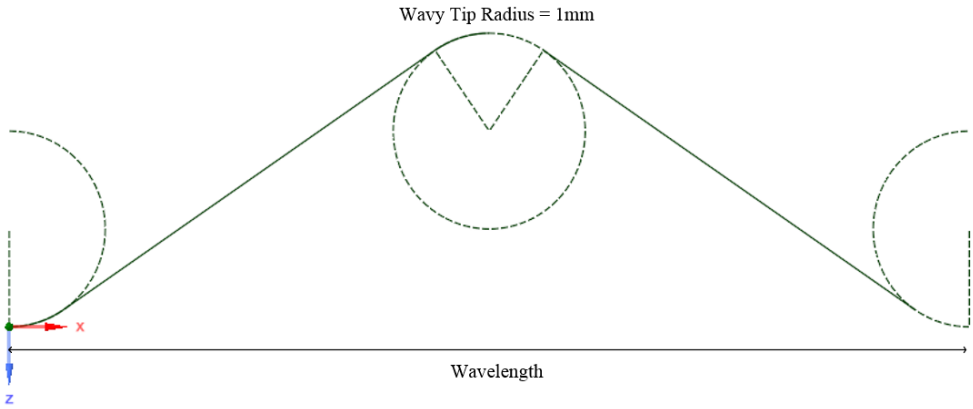

Figure 34: Wavy-Fin Fin Length Calculation

Hydraulics diameters are calculated as below:

$$(D_h) = \frac{4 \times wetted\ area}{perimeter} \quad (41)$$

$$(D_h)_h = 4 \times FS_h \times (PS_h - t)/(2 \times (FS_h + PS_h - t)) \text{ for wavy fin} \quad (42)$$

$$(D_h)_c = 4 \times FS_c \times (PS_c - t)/(2 \times (FS_c + PS_c - t)) \text{ for wavy fin} \quad (43)$$

$$(D_h)_h = \frac{4 \times AFS_h \times (PS_h - t)}{AFS_h \times 2 + 2 \times (PS_h - t)/sin(FIA_h) + 2 \times (PS_h - t) \times t/Fl_h/sin(FIA_h)) + t \times FS_h} \quad (44)$$

for offset-strip fin

$$(D_h)_c = \frac{4 \times AFS_c \times (PS_c - t)}{AFS_c \times 2 + 2 \times (PS_c - t)/sin(FIA_c) + 2 \times (PS_c - t) \times t/Fl_c/sin(FIA_c)) + t \times FS_c} \quad (45)$$

for offset-strip fin

Reynolds number can be defined as follows for both fins;

$$Re = \frac{MFR \times D_h}{Aff \times \mu} \quad (46)$$

where, μ is dynamic viscosity. Moreover, mass flux, heat transfer coefficients, fin efficiencies and overall heat transfer coefficient can be defined as follows:

$$G_h = \frac{MFR_h}{Aff_h} \quad (47)$$

$$G_c = \frac{MFR_c}{Aff_c} \quad (48)$$

$$h_h = j_h \times G_h \times Cp_h \times {Pr_h}^{-2/3} \quad (49)$$

$$h_c = j_c \times G_c \times Cp_c \times {Pr_c}^{-2/3} \quad (50)$$

$$m_h = (2 \times h_h/kf/t \times (1 + t/L_h))^{0.5} \text{ for wavy fins} \quad (51)$$

$$m_c = (2 \times h_c/kf/t \times (1 + t/L_c))^{0.5} \text{ for wavy fins} \quad (52)$$

$$m_h = (2 \times h_h/kf/t \times (1 + t/Fl_h))^{0.5} \text{ for offset-strip fins} \quad (53)$$

$$m_c = (2 \times h_c/kf/t \times (1 + t/Fl_c))^{0.5} \text{ for offset-strip fins} \quad (54)$$

$$l_h = (PS_h/2 - t) \text{ for both fins} \quad (55)$$

$$l_c = (PS_c/2 - t) \text{ for both fins} \quad (56)$$

$$nf_h = tanh(m_h \times l_h)/(m_h \times l_h) \text{ for both fins} \quad (57)$$

$$nf_c = tanh(m_c \times l_c)/(m_c \times l_c) \text{ for both fins} \quad (58)$$

$$n_{o,h} = 1 - (1 - nf_h) \times Af_h/A_h \text{ for both fins} \quad (59)$$

$$n_{o,c} = 1 - (1 - nf_c) \times Af_c/A_c \text{ for both fins} \quad (60)$$

$$UA = \left[\left(n_{o,h} \times h_h \times A_h\right)^{-1} + \left(n_{o,c} \times h_c \times A_c\right)^{-1}\right]^{-1} \text{ for both fins} \quad (61)$$

Note that friction factor (f_h and f_c) and Colburn j factor (j_h and j_c) correlations will be found later by using DOE with response surface method. Number of heat transfer units and effectiveness formula is given for both fluids unmixed as [83]:

$$NTU = UA/Cmin \quad (62)$$

$$effectiveness = 1 - e^{\frac{NTU^{0.22}\{e^{-C^*.NTU^{0.78}}-1\}}{C^*}} \quad (63)$$

Total heat transfer can be found as follows:

$$Q = effectiveness \times Cmin \times (T_{i,h} - T_{i,c}) \quad (64)$$

where, $T_{i,h}$ and $T_{i,c}$ are hot side inlet temperature and cold side inlet temperature, respectively. Pressure drop for each side can be defined as:

$$\Delta P_h = \frac{2 f_h L_h G_h^2}{\rho_h D_{h,h}} \quad (65)$$

$$\Delta P_c = \frac{2 f_c L_c G_c^2}{\rho_c D_{h,c}} \quad (66)$$

Lastly, heat exchanger no flow length and volume can be calculated as below:

$$L_n = (pt + PS_h) \times N_h + (pt + PS_c) \times N_c + pt \quad (67)$$

$$Volume = L_h \times L_c \times L_n \quad (68)$$

where, pt is plate thickness and assumed as 1 mm.

5.3. Objective Function & Constraints

Objective functions and constraints are given in Table 10. Operating conditions are determined by using F-15 jet fighter data and are given previously in Section 5.1. Since pressure of the engine bleed air can reach up to 1.41 MPa (205 psi), it must be regulated

generally to 607-372 kPa (88-54 psi) [3]. Therefore, pressure drop is not a primary concern for hot bleed air side provided that it is not excessive (e.g. $\Delta P>138$ kPa or 20 psi). However, cold ram air pressure drop directly affects the aircraft drag force. Therefore, pressure drop for ram air side and bleed air side are chosen as 34.5 kPa (5 psi) and 68.9 kPa (10 psi), respectively. The detailed expressions of objective functions, operating conditions and constraints are given below in Table 10.

Table 10: Optimization Parameters

Multi - Objective Functions	Maximization of Heat Transfer	
	Minimization of Volume	
	Minimization of Ram Air Flow Rate	
Hot Side Operating Conditions:	0.6 kg/s at 479 kPa, 832 K	
Cold Side Operating Conditions (1.14Ma at Sea Level)	0.5-4 kg/s at 260 kPa, 393 K	
Constraints:	Minimum Heat Duty:	243 kW
	Maximum Volume:	0.05 m^3
	Max. Bleed Air Pres. Drop:	68.9 kPa (10 psi)
	Max. Ram Air Pres. Drop:	34.5 kPa (5 psi)
	Reynolds Number:	1000<Re<5000
	Local Mach Number:	<0.3

5.4. Determination of Design Space

Design space is determined by using Kays & London Compact Heat Exchanger Book [5]. In the book, experiments were conducted to get Colburn j factors and Fanning friction factors for 12 different offset-strip fins (OSF) and 3 different wavy fins (WF)

and the results are given in Table 11 and Table 12 for offset-strip fin and wavy fin, respectively.

Table 11: Different Offset-Strip Fin Designs [5]

OSF Type	**Fin per meter [1/m]**	**PS [mm]**	**Fl [mm]**	**Dh [mm]**	**t [mm]**	**Compactness**	**FA/TA**	**Max Re Number**
3/32-12.22	480	12.3	2.4	3.41	0.1	1115	0.86	10000
1/4(s)-11.1	437	6.35	6.35	3.08	0.15	1204	0.76	8000
1/8-13.95	549	9.53	3.18	2.68	0.25	1250	0.84	6000
1/8-15.2	598	10.5	3.18	2.65	0.15	1368	0.87	6000
1/8-15.61	615	6.35	3.18	2.38	0.1	1548	0.81	6000
1/9-22.68	893	7.65	2.8	1.74	0.1	2069	0.89	4000
1/8-19.86	782	2.49	3.18	1.54	0.1	2254	0.79	4000
1/9-25.01	985	5.08	2.8	1.5	0.1	2360	0.85	3000
1/10-19.35	762	1.91	2.54	1.4	0.1	2490	0.61	3000
1/9-24.12	950	1.91	2.8	1.21	0.1	2830	0.67	2000
1/10-27.03	1064	6.38	2.54	1.42	0.1	2466	0.89	3000
1/10-19.74	777	1.29	2.54	1.22	0.05	3028	0.51	3000
Min	437	1.29	2.4	1.21	0.05	1115	0.51	2000
Max	1064	12.3	6.35	3.41	0.25	3028	0.89	10000

Table 12: Different Wavy Fin Designs [5]

WF Type	**Fin Pitch [1/m]**	**PS [mm]**	**Wl [mm]**	**Dh [mm]**	**t [mm]**	**Amp [mm]**	**Com-pact-ness**	**FA/ TA**	**Re Max**
11.44-3/8W	450.4	10.49	9.53	3.23	0.15	1.97	1152	0.85	8000
11.5-3/8W	452.8	9.53	9.53	3.02	0.25	1.98	1138	0.82	10000
17.8-3/8W	700.8	10.49	9.53	2.12	0.15	1.97	1686	0.89	5000
Min	450.4	9.53	9.53	2.12	0.15	1.97	1138	0.82	5000
Max	700.8	10.49	9.53	3.23	0.25	1.98	1686	0.89	10000

By considering these tables, fin per meter value is converted to minimum flow spacing and convenient value interval is determined as 0.9-2.5 mm for both offset-strip fin and wavy fin.

Plate spacing varies between 1.29 and 12.3 mm for offset-strip fin which also covers wavy fin plate spacing interval. However, when fin inclination angle become close to 30^o, which is determined as the minimum fin inclination angle of offset-strip fin, compactness value of offset-strip fin decreases dramatically with increasing plate spacing value. Compact heat exchangers have compactness value greater than 700 m^2/m^3 [84]. A sensitivity analysis is done in order to evaluate the effects of fin parameters on compactness value. First of all, fin parameters are set to values which are the average of global maximum and global minimum values and then parameters are varied from global minimum to global maximum. The results are shown in Figure 35. It can be seen that when plate spacing is increased, compactness decreases dramatically. Therefore, plate spacing is the most effective parameter on compactness. After that, global minimum values for all parameters are selected to find critical plate spacing value that gives compactness value lower than 700 m^2/m^3. As a result of this, maximum offset-strip fin plate spacing value is determined as 5.4 mm which gives

minimum 700 m^2/m^3 compactness value for all design space. It is predicted that heat transfer may dramatically decrease below this compactness value (or above this plate spacing value). Therefore, there is no need to investigate this region. On the contrary, there is no similar restriction for wavy fin. As a result, plate spacing interval is determined for offset-strip fin as 1-5.4 mm and 1-10.5 mm for wavy fin.

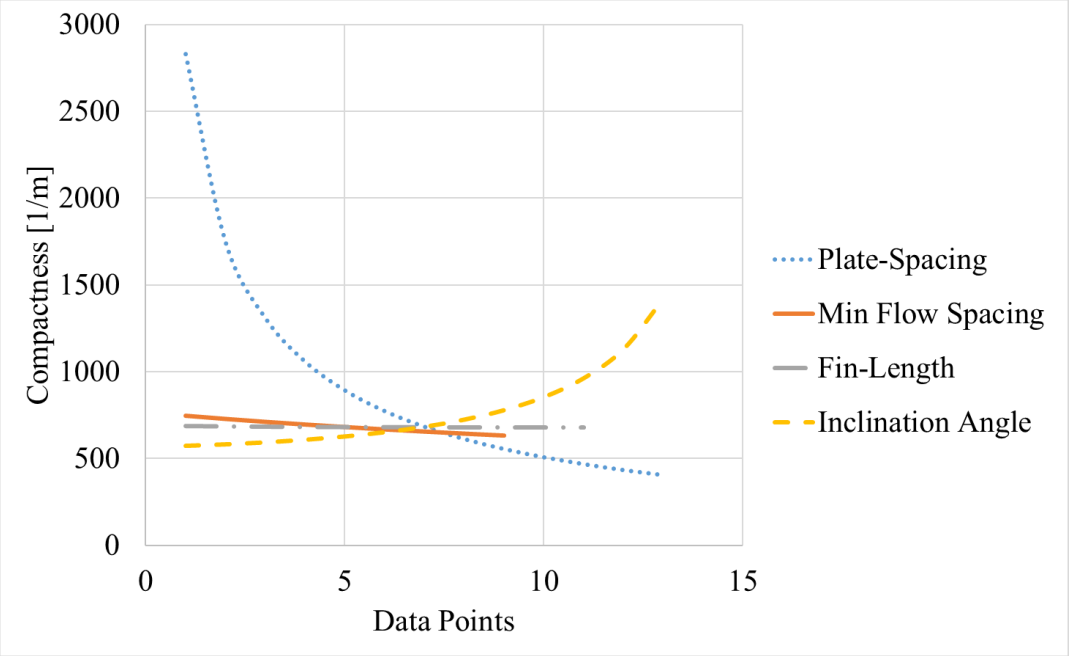

Figure 35: Offset-Strip Fin Compactness Sensitivity Analysis

Wavelength and amplitude values for wavy fin are determined as 8-11mm and 1-3mm, respectively. Additionally, fin length and fin inclination angle intervals are determined as 2-7 mm and 30-90º, respectively. Lastly, the Reynolds number interval is determined as 1000-5000 since the Reynolds number decreases with increasing compactness value. All in all, final design space is given in Table 13.

Table 13: Continuous Optimization Design Space

	MFS [mm]		PS [mm]		Wl [mm]	Fl [mm]	Amp [mm]	FIA [º]	Re	
	WF	**OSF**	**WF**	**OSF**	**WF**	**OSF**	**WF**	**OSF**	**WF**	**OSF**
MIN	0.9	0.9	1	1	8	2	1	30	1000	1000
MAX	2.5	2.5	10.5	5.4	11	7	3	90	5000	5000

5.5. Fanning Friction Factor & Colburn J Factor Prediction CFD Studies

5.5.1. Design of Experiments

Design of experiments concept is conducted for both wavy and offset-strip fin. Minimum flow spacing, plate spacing, wavelength, amplitude and the Reynolds number are selected as parameters for wavy fin and minimum flow spacing, plate spacing, offset-length, fin inclination angle and the Reynolds number are selected for offset-strip fin.

5.5.2. Wavy Fin f and j Prediction

Central composite design gives 43 runs for 5 wavy fin parameters according to formula at Table 1 by using the parameters given in Table 13. Before CFD runs, a mesh independence study is done first. The geometry is determined by considering the most severe condition (maximum air velocity, maximum wavy curve in the shortest distance) for the wavy fin which has MFS_{min}=0.9 mm, PS_{min}=1 mm, Wl_{min}=8 mm, Amp_{max}=3 mm and Re_{max}=5000. It is assumed that independent mesh settings found after this study can be applicable to all other wavy fin CFD simulations in the design space due to lower velocity and pressure gradients. Since the turbulence model and the wall function are previously determined from the wavy fin validation study, the same models, which are k-ε realizable turbulence model with enhanced wall function, are used in this part of the study. Meshes are constructed by considering $y^+<1$ requirement

due to enhanced wall function. One of the used mesh is shown in Figure 36. Edge sizing is used to refine mesh near walls. The mesh independence study is shown in Figure 37. As a result of this, mesh with 116000 elements is used since increasing the number of elements beyond this value changes the results by less than 1%.

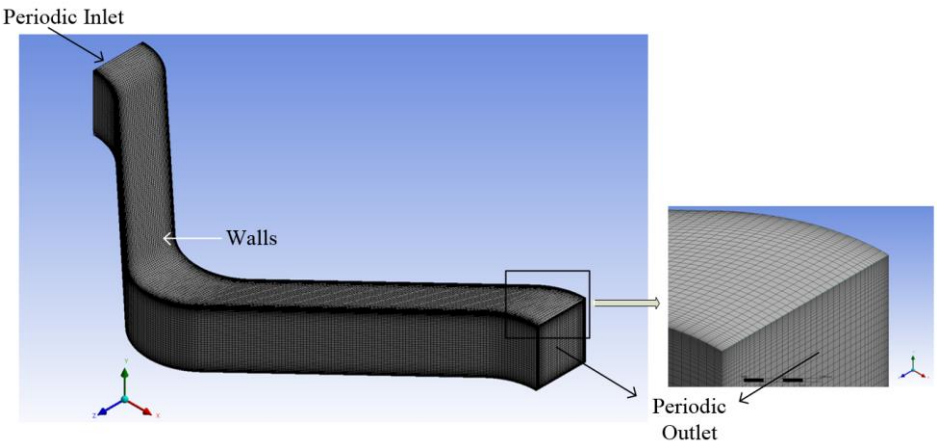

Figure 36: Wavy Fin Mesh

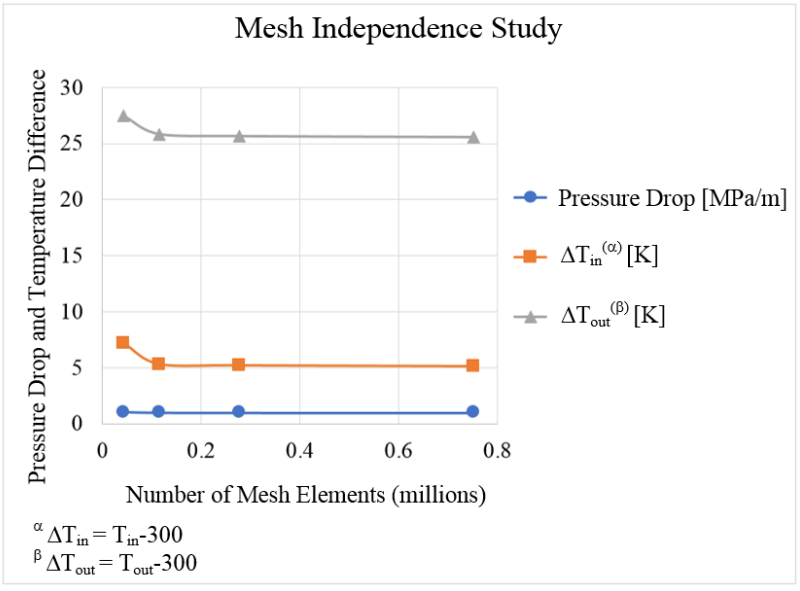

Figure 37: Wavy Fin Mesh Independence Study for Design Space

All 43 wavy fin design points (DPs) in the design space are constructed by using independent mesh settings and the results can be found in the first 43 rows of Appendix A. The first 43 runs of the results are put in the ModeFrontier software to generate a second order response surface equation. The equation is obtained and coefficients are given in Appendix B. Additionally, the correlated f factor versus numerical f factor and correlated j factor versus numerical j factor values error graphs are given in Figure 38 and Figure 39, respectively. The software gives second order response surface equations which have 34.7% average relative error with 0.860 adjusted R-square value for fanning friction factor and have 6.82% average relative error with 0.94 adjusted R-square value for Colburn j factor. As a result, adjusted R-square value is lower than 0.9 for f factor which is not good enough.

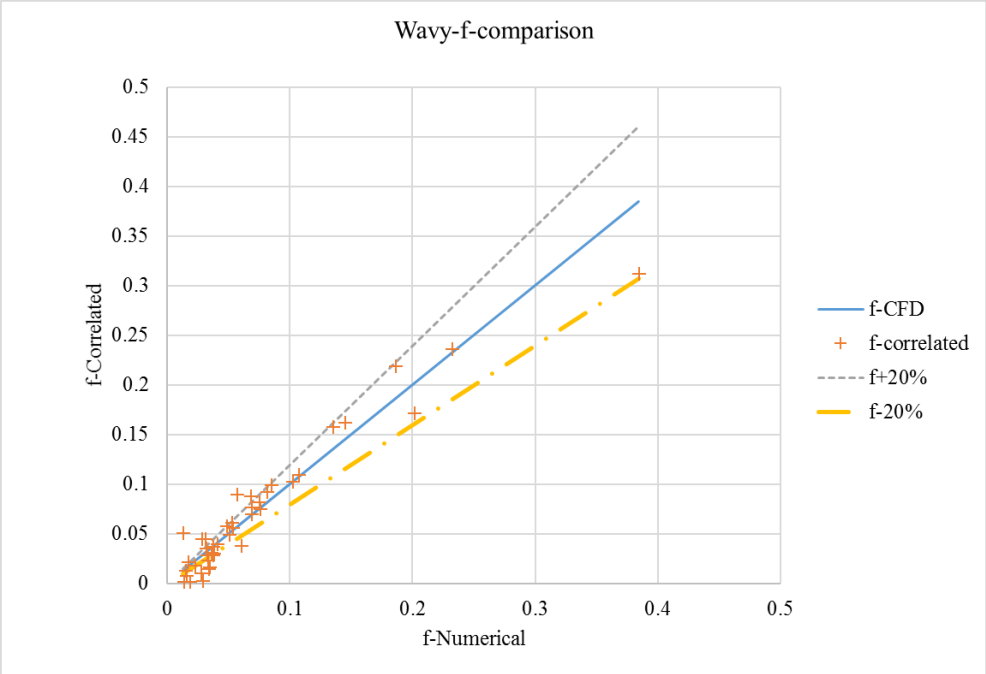

Figure 38: Wavy-fin Fanning Friction Factor Comparison for 43 Runs

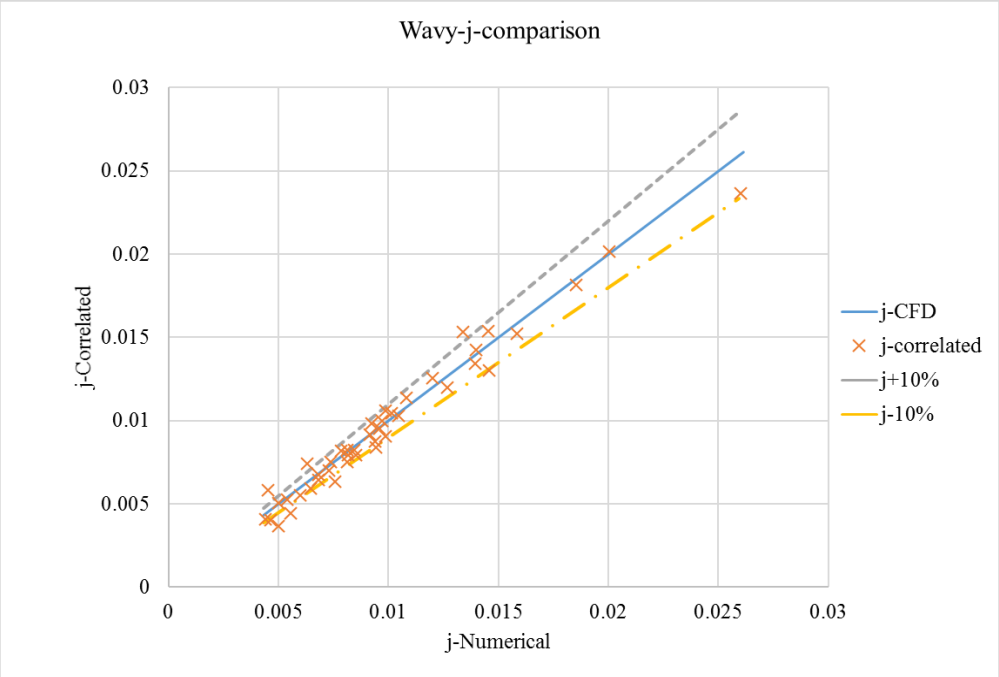

Figure 39: Wavy-fin Colburn j Factor Comparison for 43 Runs

In order to increase accuracy of the equation, 82 more CFD analysis are run (in total 125 CFD analysis) which can be found in the rows between 44 and 125 of Appendix A. In these additional runs, only Reynolds number is changed from 1000 to 5000 with 1000 increment since it is easy to change mass flow rates in the previously prepared analysis files. 125 analyses are done to generate third order response surface equations. The software gives much more accurate response surface equations which have 9.38% average relative error with 0.981 adjusted R-square value for fanning friction factor and have 2.23% average relative error with 0.988 adjusted R-square value for Colburn j factor. The correlated-numerical values error graphs are given in Figure 40 and Figure 41. It can be seen that almost all of the data points are within ± 20% error lines for fanning friction factor and within ± 10% error lines for Colburn j factor. The detailed inputs and outputs tables and correlations are given in Appendix A. Additionally, response surface equations for wavy fin is given in Appendix B.

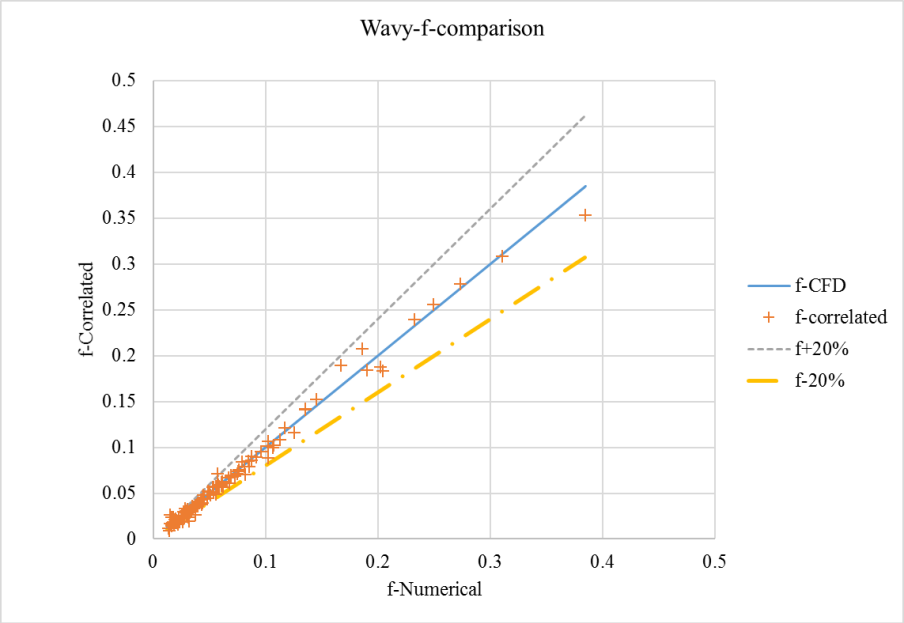

Figure 40: Wavy-fin Fanning Friction Factor Comparison for 125 Runs

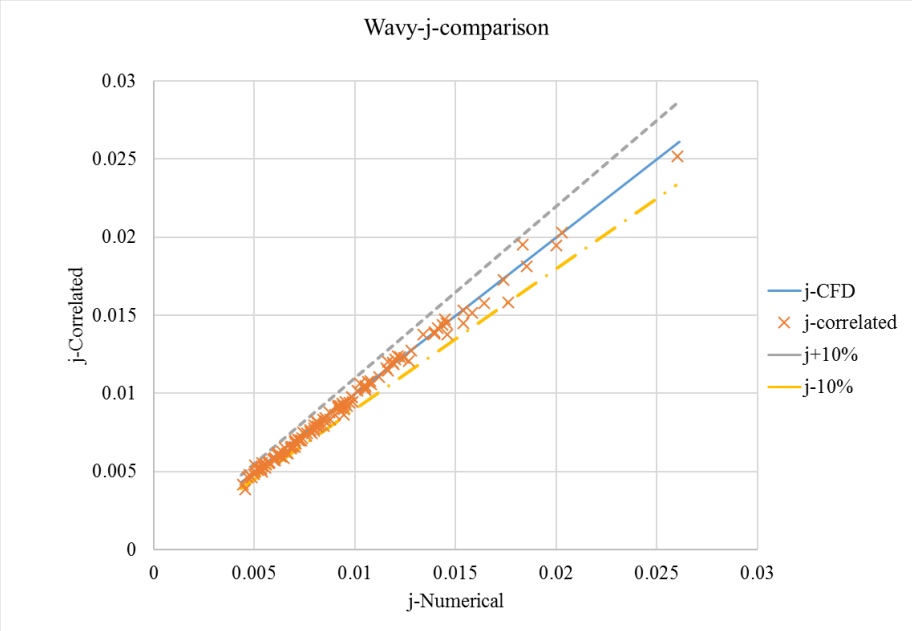

Figure 41: Wavy-fin Colburn j Factor Comparison for 125 Runs

After developing wavy fin f and Colburn j factor correlations, they are compared with the other studies from the literature. Comparison parameters are selected as the average of minimum and maximum values of Table 13. Two different wavy fin f and Colburn j factor correlations are found in literature [27, 85]. The results are shown in Figure 42 and Figure 43 for f and Colburn j factor, respectively. As it can be seen from the figures, developed correlations show good agreement with the study of Awad et al [85].

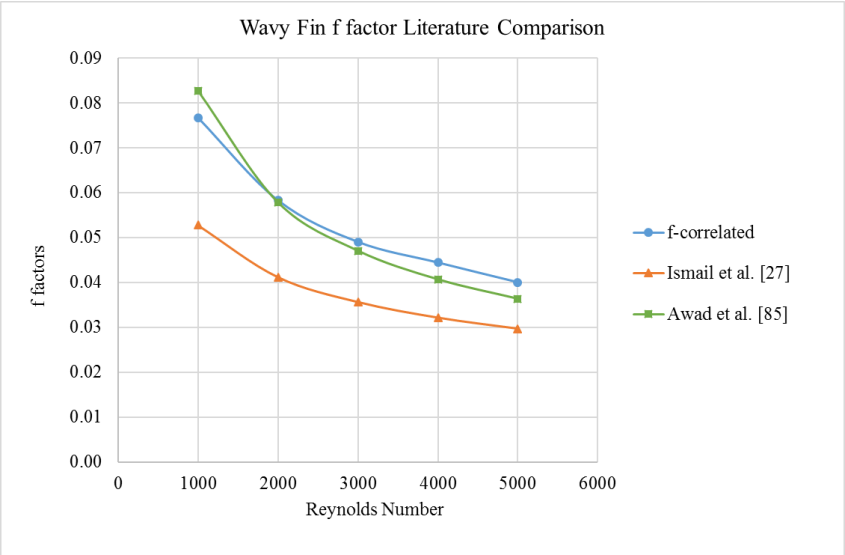

Figure 42: Comparison of developed wavy fin f factor correlation with literature

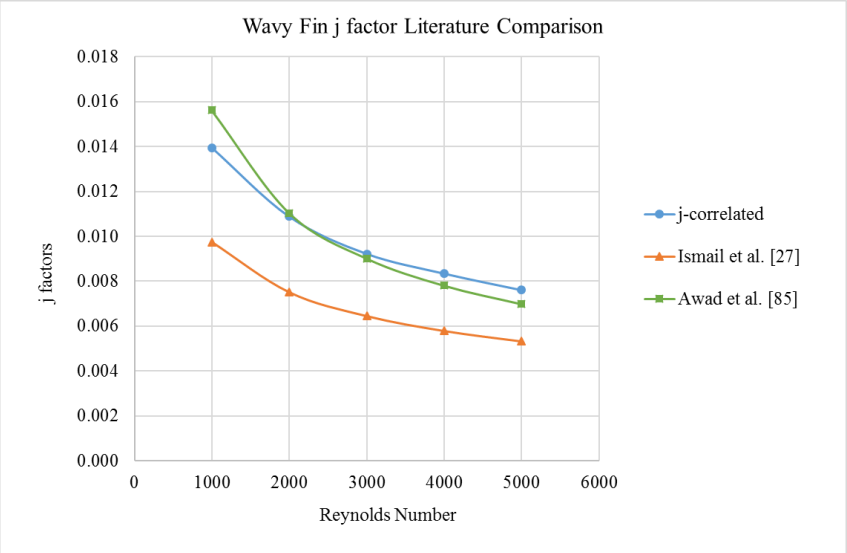

Figure 43: Comparison of developed wavy fin Colburn j factor correlation with literature

5.5.3. Offset-Strip Fin f and j Prediction

Central composite design gives 43 runs in total for 5 offset-strip fin parameters. Before CFD runs, again a mesh independence study is done first. Moreover, applying fin inclination angle as a geometrical optimization parameter creates non-periodicity in lateral direction. Therefore, inclined offset-strip fin geometries are made geometry independent by increasing number of inlet sections in lateral directions in order to get rid of wall effect at both lateral ends of the fin. The sample geometrical figures are shown Figure 44. Mesh independence study is implemented first on the two-section geometry to determine the independent mesh settings. As in the previous case, most severe condition for the offset-strip fin which has MFS=0.9 mm, PS=1 mm, Fl=2 mm, FIC=30 ^{o} and Re=5000 is selected for mesh independence study. Additionally, edge sizing is used to refine mesh near walls to keep y^{+} value below 1. The results are shown in Figure 45. It is clear that using the smallest number of elements will be beneficial because relative changes for all meshes are below 1%. However, 49500 elements mesh, which is shown in Figure 46, is selected because it is computationally affordable.

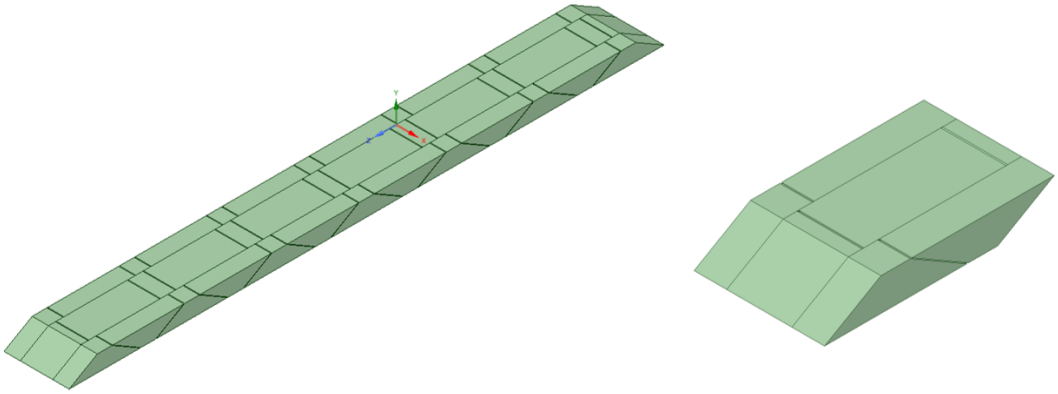

Figure 44: 13 Inlet Geometry (Left), 2 Inlet Geometry (Right)

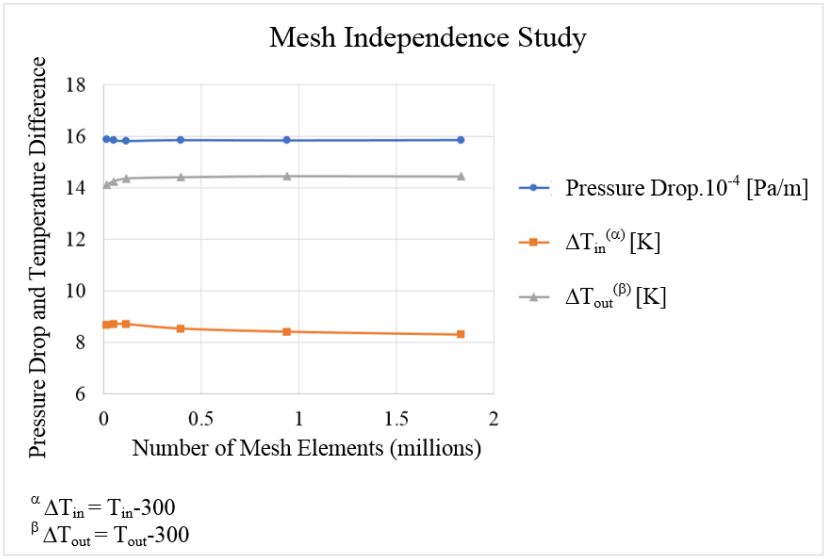

Figure 45: Offset-Strip Fin Mesh Independence Study

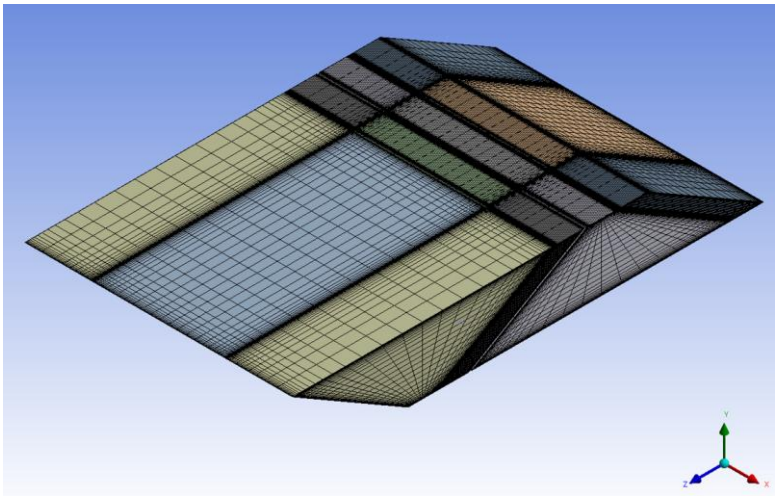

Figure 46: 2 Inlet Section Geometry Mesh

Geometry independence study is done by applying independent mesh settings. Number of inlet sections are increased from 2 to 13 to have a geometry independent solution. The results are shown in Figure 47. As a result of this, using 5 sections is determined as a geometry independent setting.

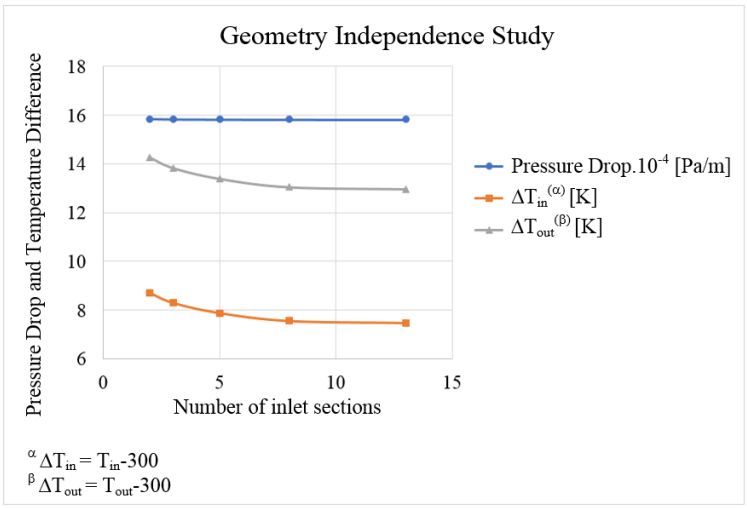

Figure 47: Offset-Strip Fin Geometry Independence Study

The same procedure is applied as in the case of wavy fin. All 43 wavy fin design points in the design space are constructed by using independent mesh settings and the results can be found in Appendix A. The first 43 runs of the results are put in the ModeFrontier software to generate a second order response surface equation. The equation is obtained and coefficients are given in Appendix B. Additionally, the correlated-numerical values error graphs for fanning friction factor and Colburn j factor are given in Figure 48 and Figure 49, respectively. The software gives second order response surface equations which have 8.32% average relative error with 0.92 adjusted R-square value for fanning friction factor and have 11.3% average relative error with 0.76 adjusted R-square value for Colburn j factor. As a result, adjusted R-square value is lower than 0.9 for Colburn j factor which lacks sufficient accuracy.

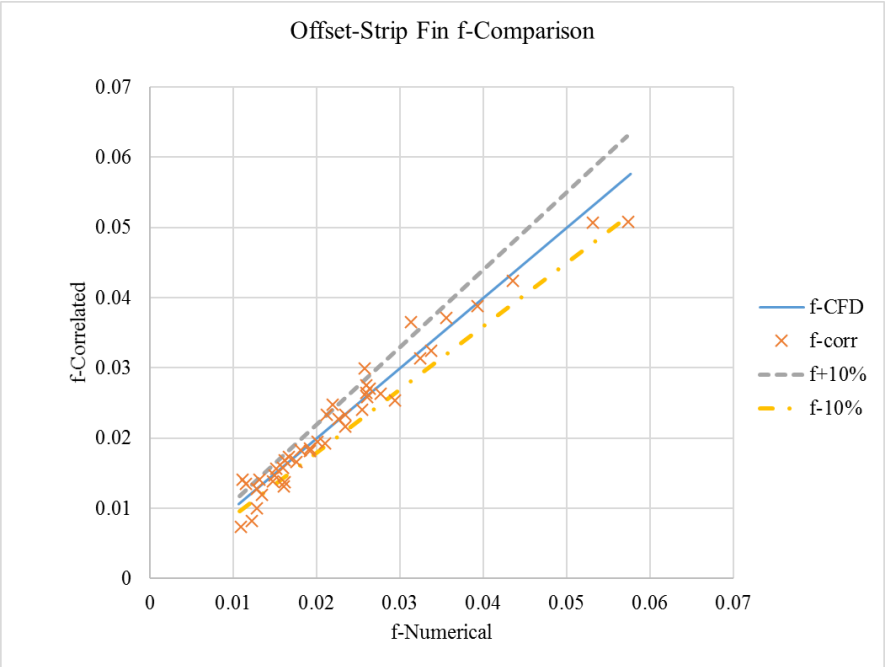

Figure 48: Offset-Strip Fin Fanning Friction Factor Comparison for 43 Runs

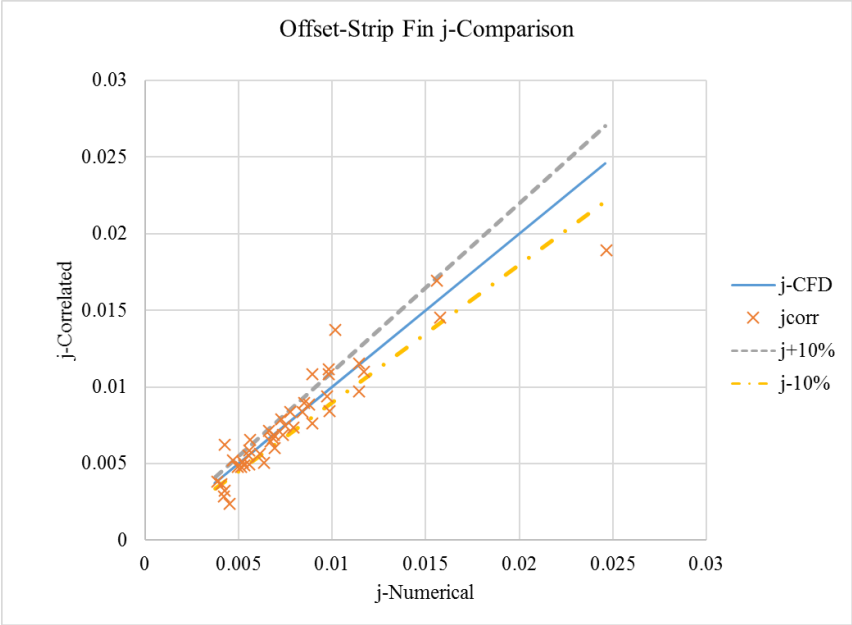

Figure 49: Offset-Strip Fin Colburn j Factor Comparison for 43 Runs

In order to increase accuracy of the equation, 82 more CFD analysis are run (in total 125 CFD analysis). In these additional runs, only Reynolds number is changed from 1000 to 5000 with 1000 increments since it is easy to implement. The results are used to generate third order response surface equations. The software gives response surface equations which have 2.47% average relative error with 0.988 adjusted R-square value for fanning friction factor and 5.04% maximum relative error with 0.936 adjusted R-square value for Colburn j factor. The correlated-numerical value graphs are given in Figure 50 for fanning friction factor and Figure 51 for Colburn j factor. It can be seen that almost all of the data points are within ±10% error lines for both the fanning friction factor and the Colburn j factor. Detailed input and output tables and correlations are given in Appendix A. Additionally, response surface equation for offset-strip fin is given in Appendix B.

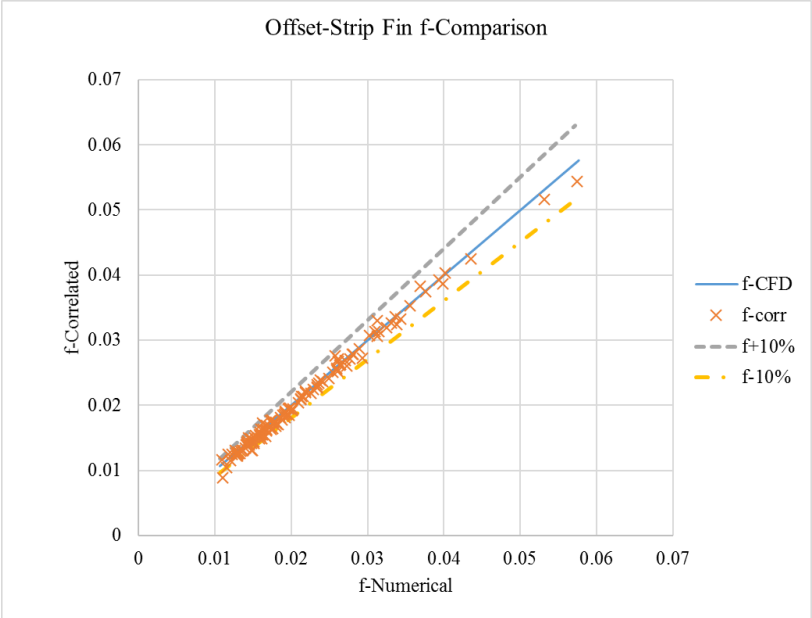

Figure 50: Offset-Strip Fin Fanning Friction Factor Comparison for 125 Runs

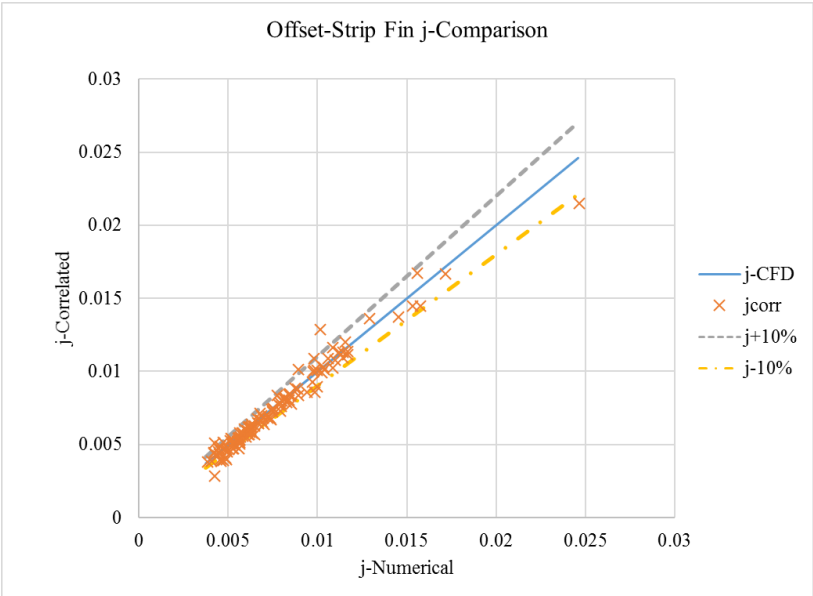

Figure 51: Offset-Strip Fin Colburn j Factor Comparison for 125 Runs

After developing offset-strip fin f and Colburn j factor correlations, they are compared with the other studies from the literature. Comparison parameters are selected as the average of minimum and maximum values of Table 13. Since the literature studies are only for vertical offset-strip fins, fin inclination angle is taken as 90°. Five different offset-strip fin f and Colburn j factor correlations are found in literature [86, 80, 87, 88, 89]. The results are shown in Figure 52 and Figure 53 for f and Colburn j factor, respectively. As it can be seen from the figures, developed correlations show good agreement with the study of Manglik et al [88]. for f factor and the study of Wieting [86] for Colburn j factor. Besides, these literature correlations do not investigate fin inclination angle parameter which is covered by this thesis.

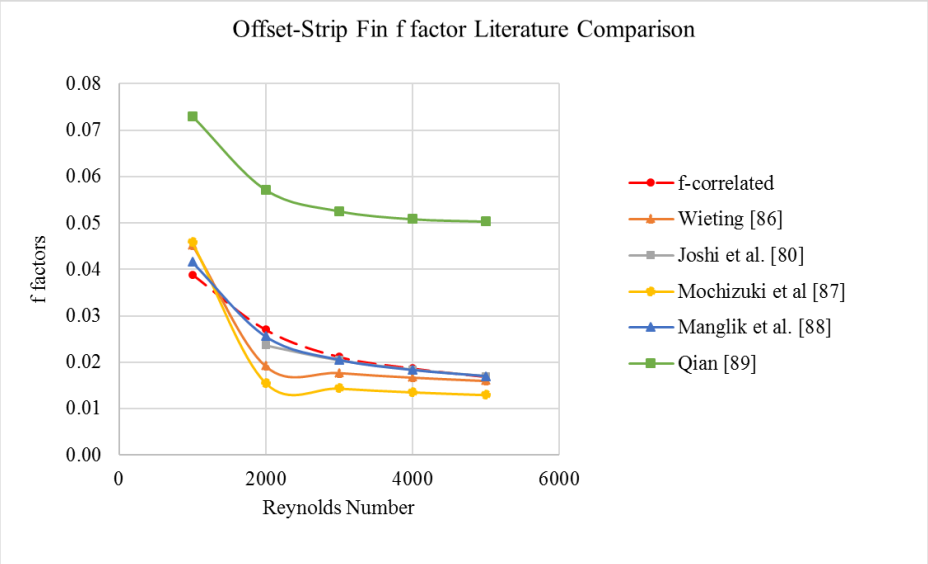

Figure 52: Comparison of developed offset-strip fin f factor correlation with the literature

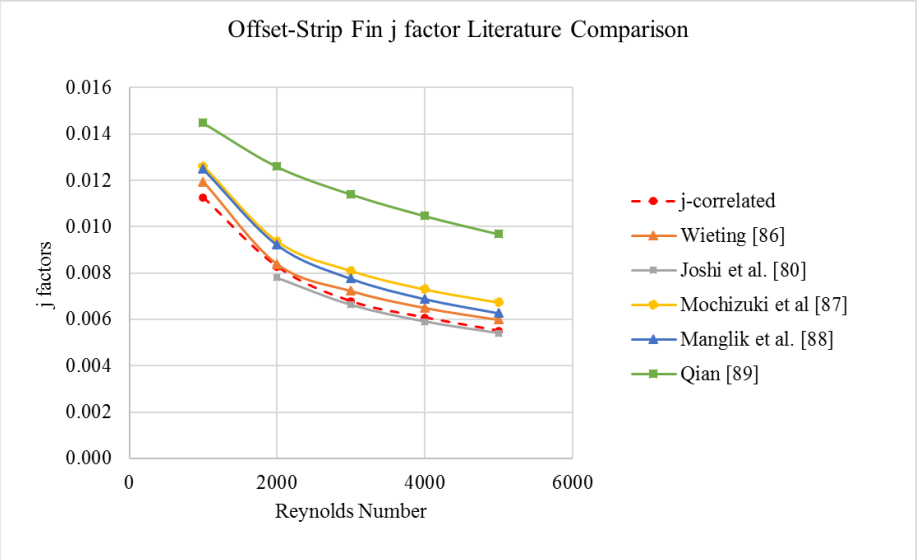

Figure 53: Comparison of developed offset-strip fin Colburn j factor correlation with the literature

5.6. Optimization Studies

5.6.1. Sensitivity Analysis

Sensitivity analysis is done in order to determine the effects of genetic algorithm parameters such as crossover probability (CP) on objective functions, which are selected only as maximizing the heat transfer and minimizing the volume for simplicity. Third objective function, minimizing the ram air mass flow rate, is not included. The purpose of this study is to investigate GA parameters on heat transfer and volume. GA parameters are taken from several literature studies which are shown in Table 14. CP is selected between 0.5 and 0.9 with 0.1 increment. Moreover, mutation probability (MP) is selected as 0.01, 0.05, 0.1, 0.3 and 0.5. Population size and number of generations are taken as constant for all analysis and the maximum value of the literature results are selected as 200 and 5000, respectively. Additionally, migration fraction and pareto fraction are chosen as 0.2 and 0.35 which are the default values. Likewise, tournament selection which are the only option for multi-objective optimization is selected with 2 elite individuals. Lastly, functional tolerance is selected as 1e-6 as a stopping criterion.

Table 14: Genetic Algorithm Parameters Literature Search Results

Reference	Crossover Probability	Mutation Probability	Population Size	Number of Generation
Maghsoudi et al. [90]	0.8	Not Given	200	5000
Hajabdollahi et al. [39]	0.9	0.035	100	150
Maghsoudi et al. [91]	0.8	Not Given	25	5000
Juan et al. [42]	0.7	0.5	200	500
Ozkol et al. [92]	0.7	0.01	150	Not Given
Najafi et al. [93]	0.8	0.01	110	Not Given
Sanaye et al. [94]	0.9	0.035	100	100
Hilbert et al. [40]	0.9	Not Given	100	30
Xie et al. [57]	0.5	0.005	50	1000
Sanaye et al. [95]	0.9	0.035	150	100

Crossover probability and mutation probability are the only parameters for sensitivity analysis. Since there are 5 crossover and 5 mutation probabilities, 25 analyses are required for each fin type. The results are shown in Figure 54 and Figure 55 for wavy fin and offset-strip fin, correspondingly. The curve on the bottom side of the figures gives lower volume for the same heat transfer value. Therefore, it is found that one of the best CP and MP values are found as 0.7 and 0.1 for wavy fin and 0.9 and 0.05 for offset-strip fin, respectively. Beyond this point, these values will be used for the optimization study.

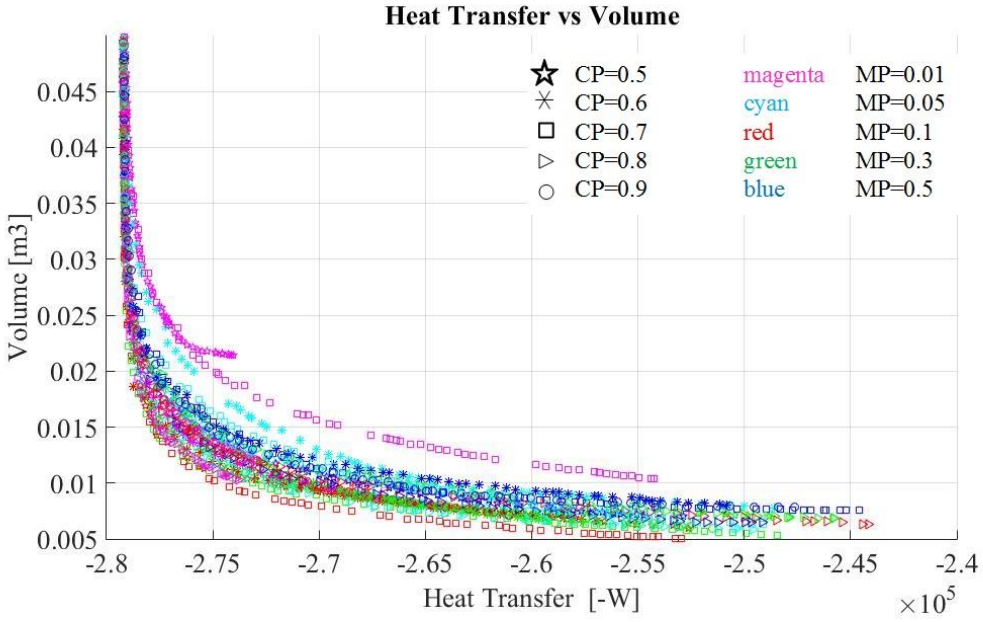

Figure 54: Wavy Fin Sensitivity Analysis Results (CP=Crossover Probability, MP=Mutation Probability)

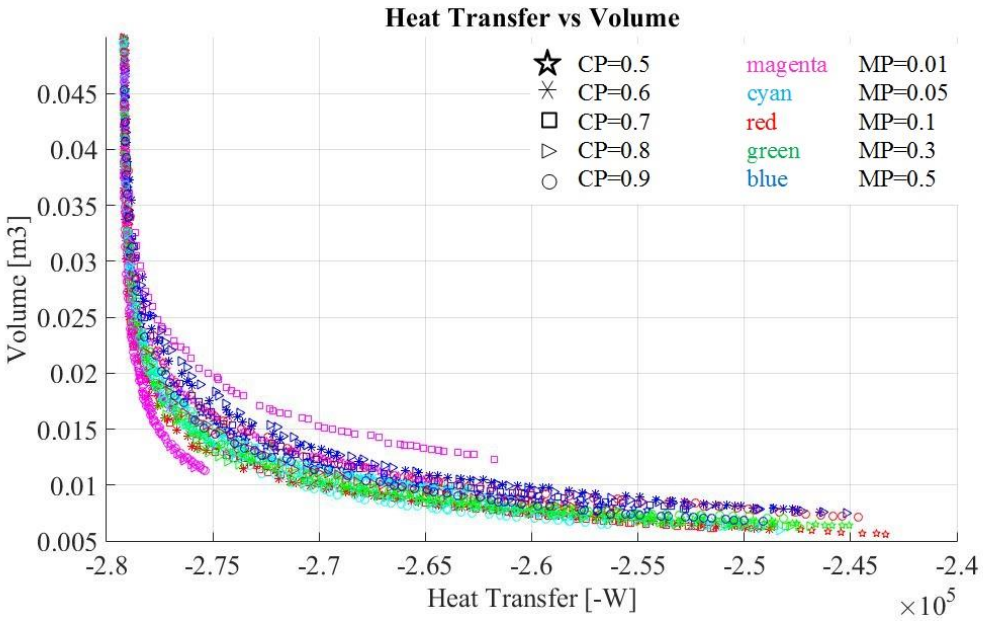

Figure 55: Offset-Strip Fin Sensitivity Analysis Results (CP=Crossover Probability, MP=Mutation Probability)

5.6.2. Multi-Objective Optimization & Results

Multi-objective optimization is done by considering three objective functions which are mentioned before. Since supplying conditioned air to systems for all phases of the flight envelope is the most critical duty for an aircraft air conditioning system, the most critical objective is selected as maximizing the heat transfer (HT). The second critical objective is selected as minimizing the volume (VOL) because minimizing equipment volume is beneficial for aircraft equipment integration. Lastly, minimizing the ram air mass flow rate (MFR) is considered the least critical objective function for an air conditioning engineer since this will affect aircraft intake design and reduce drag forces. The second and third objectives are aircraft level objectives which do not affect air conditioning system directly but they reduce air conditioning volume and drag penalty to aircraft. Consequently, the optimum design is selected by considering these situations. Multi-objective genetic algorithm is run and pareto fronts for three objectives are shown in Figure 56. In the figure, two surfaces are created from optimum wavy and offset-strip fin data. Moreover, these data points are imprinted to three 2-D surfaces. Wavy fin and offset-strip fin are represented by magenta and blue colors, respectively.

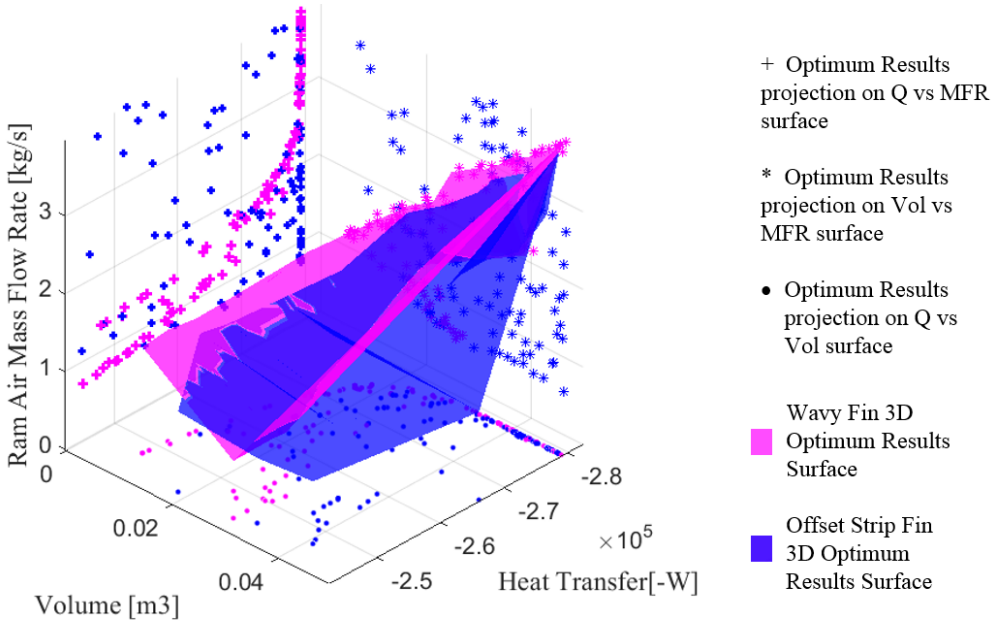

Figure 56: Pareto Front Results

Beyond this point, one suitable design must be selected for porous media analysis. Firstly, the heat exchanger heat duty is 243.3kW which is given before. 10% margin is added in order to suppress numerical and other errors. As a result of this, the design must provide at least 267.6 kW heat transfer. Moreover, minimum volume and ram air mass flow rate design are considered. The most optimum solution is found by using a rating function which is shown below:

$$\text{Optimum}_{\text{Result\_Function}} = C_1 * \frac{\text{HT}}{\text{HT}_{\text{Max}}} + C_2 * \frac{\text{VOL}_{Max}}{VOL} + C_3 * \frac{MFR_{Max}}{MFR} \quad (69)$$

$$C_1 + C_2 + C_3 = 1 \quad (70)$$

where C_1, C_2 and C_3 are coefficients, which are related to the importance of the objective functions HT_{max} (279.2 kW, theoretical maximum heat transfer), VOL_{max} (0.05 m^3), MFR_{max} (4 kg/s). Their values are between 0 and 1. In this study, C_1 is varied from 0.5 to 0.6, C_2 from 0.20 to 0.35, and C_3 from 0.25 to 0.1 with 0.05 change.

Using optimization results from Figure 56, rating functions are calculated for different values of C1, C2, and C3 and tabulated in Table 15. In the table every single row is a candidate optimum result. The results show that the first row of the table is the best for all optimum result columns. As it can be seen, in general wavy fins (WF) have superiority over offset-strip fins (OSF).

Table 15: Candidate Optimum Designs from Multi-Objective Optimization Results

Q [kW]	**Vol [l]**	**MFR [kg/s]**	**Optimum$_{Result_Function}$**						
			C_1=0.5 C_2=0.25 C_3=0.25	**C_1=0.5 C_2=0.3 C_3=0.2**	**C_1=0.5 C_2=0.35 C_3=0.15**	**C_1=0.6 C_2=0.2 C_3=0.2**	**C_1=0.6 C_2=0.25 C_3=0.15**	**C_1=0.6 C_2=0.3 C_3=0.1**	**Type**
268.3	13.5	1.71	1.99	2.06	2.12	1.78	1.85	1.92	WF
268.5	13.5	1.73	1.98	2.05	2.12	1.78	1.85	1.92	WF
269.3	13.4	1.81	1.97	2.04	2.12	1.77	1.84	1.92	WF
268.8	14.6	1.65	1.95	2.00	2.05	1.75	1.8	1.85	WF
269.0	14.4	1.68	1.94	2.00	2.05	1.75	1.8	1.86	WF
268.7	14.8	1.63	1.94	1.99	2.03	1.74	1.79	1.84	WF
269.0	14.7	1.66	1.94	1.99	2.04	1.74	1.79	1.84	WF
269.2	14.7	1.67	1.93	1.98	2.03	1.74	1.79	1.84	WF
268.1	16.2	1.48	1.93	1.95	1.97	1.73	1.75	1.77	WF
268.3	16.4	1.48	1.92	1.93	1.95	1.73	1.74	1.76	WF
268.4	15.3	1.63	1.91	1.96	2.00	1.72	1.76	1.81	OSF
269.9	15	1.7	1.91	1.96	2.01	1.72	1.77	1.82	WF
269.5	15.1	1.71	1.9	1.95	2.00	1.71	1.76	1.81	OSF
270.2	15.1	1.72	1.89	1.94	1.99	1.71	1.76	1.81	WF
271.0	14.2	1.9	1.89	1.96	2.03	1.71	1.78	1.85	WF

The optimum heat exchanger design on the first row of Table 15 has the highest rating function for all sets of coefficients, therefore, this design is selected as the optimized heat exchanger and will be considered for further calculations. Corresponding design parameters of this optimum heat exchanger are given below in Table 16.

Table 16: Optimum Wavy Fin Design Parameters

Hot Side Flow Length (L_h) [mm]	555.4	**Hot Side Plate Spacing (PS_h) [mm]**	1.75
Cold Side Flow Length (L_c) [mm]	140.8	**Cold Side Wavelength (Wl_c) [mm]**	8.77
Number of Hot Plates (N_h)	32	**Hot Side Wavelength (Wl_h) [mm]**	8.86
Cold Side Minimum Flow Spacing (MFS_c) [mm]	0.91	**Cold Side Amplitude (Amp_c) [mm]**	2.95
Hot Side Minimum Flow Spacing (MFS_h) [mm]	1.02	**Hot Side Amplitude (Amp_h) [mm]**	2.14
Cold Side Plate Spacing (PS_c) [mm]	1.54	**Cold Side Mass Flow Rate (MFR) [kg/s]**	1.71

Optimum solution is investigated according to effectiveness formula optimization which is given in Equation 63, Section 5.2. The optimum solution gives C*=0.36 and NTU=6.35 in thermal model. Corresponding effectiveness curve for the optimum design point is given in Figure 57. It can be concluded that beyond optimum solution there is no significant improvement with increasing NTU. Moreover, effectiveness can be increased by decreasing C* value. However, decreasing C* results increasing cold side (ram air) mass flow rate which is not intended in this study. Consequently, the optimum solution seems reasonable.

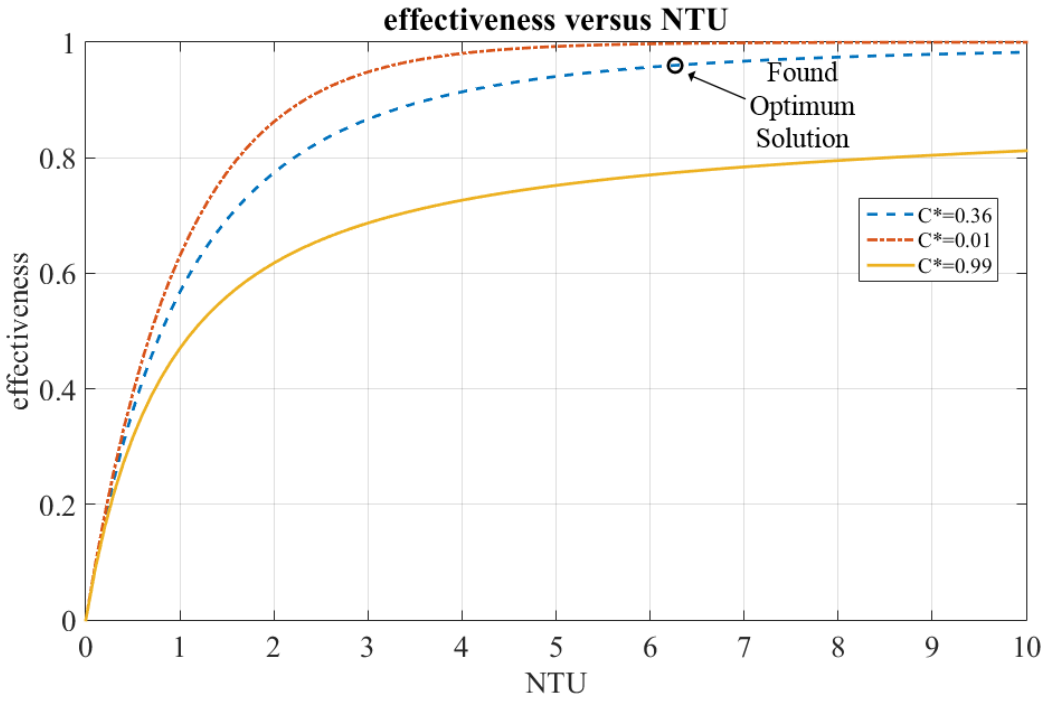

Figure 57: NTU versus effectiveness investigation on optimum solution

CHAPTER 6

POROUS MEDIA STUDIES

Compact heat exchanger CFD modelling with physical fins requires extremely fine mesh and solving this may not be efficient in terms of time and computational source. Porous media approach helps to overcome this difficulty by simplifying heat exchanger geometry. Therefore, number of CFD mesh elements can be reduced significantly with the help of porous media approach. In the following section, fully-detailed physical heat exchanger CFD analysis is done and compared with porous media approach.

6.1. Validation of Porous Media Approach With 3-D CFD Analysis

Porous media method is evaluated by modelling a small portion of the optimum heat exchanger configuration whose dimensions are previously given in Table 16. Modelled heat exchanger is shown in Figure 58. Only vertical fin walls are taken into consideration for simplicity. Horizontal fin walls, shown in Figure 32, are neglected. External size of the geometry is determined by considering the available computational resources in this study.

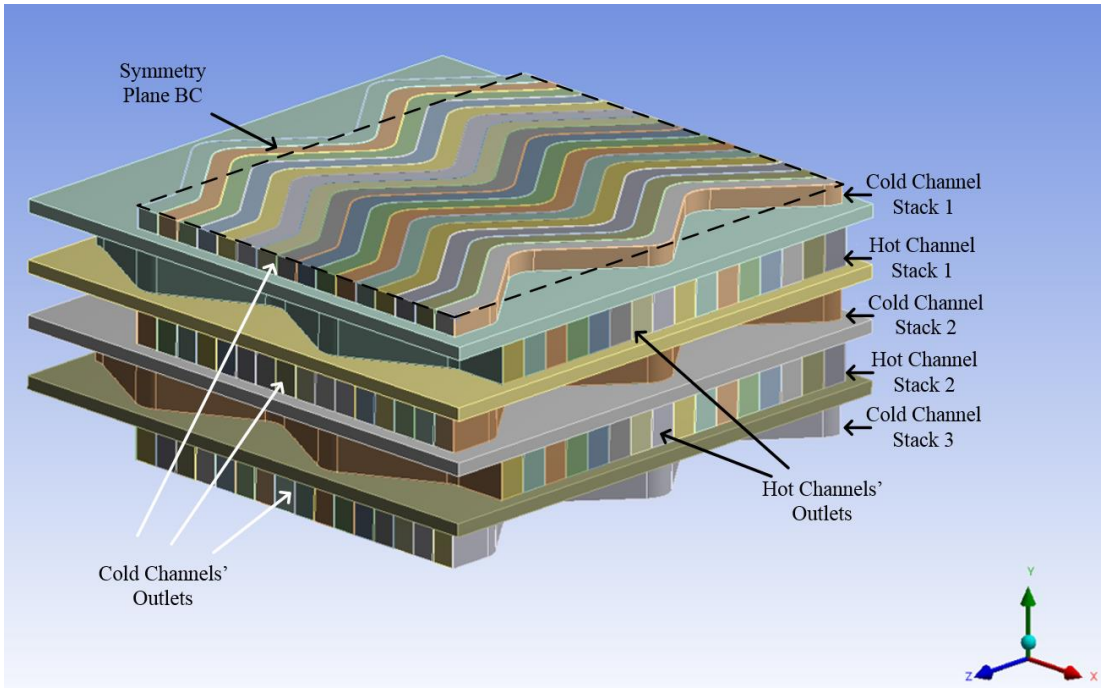

Figure 58: Modelled Small Portion of Optimum Heat Exchanger Geometry

6.1.1. Mesh Independence Study for the 3-D CFD Analysis of the Optimum Heat Exchanger Geometry

Mesh independence study is done in two steps. The first step is determining the independent mesh settings for only channels as shown in Figure 59. Since there are only two types of channels in total (cold and hot), there is no need to analyze all channels in order to decrease the computational effort. The second step is determining the independent mesh settings for whole heat exchanger including all channels and separation plates. This mesh independency approach with two steps is to find channel flow mesh settings (number of edge division, first layer thickness of the inflation layer etc.) and separation plate mesh settings (maximum cell size, body of influence cell size etc.), individually.

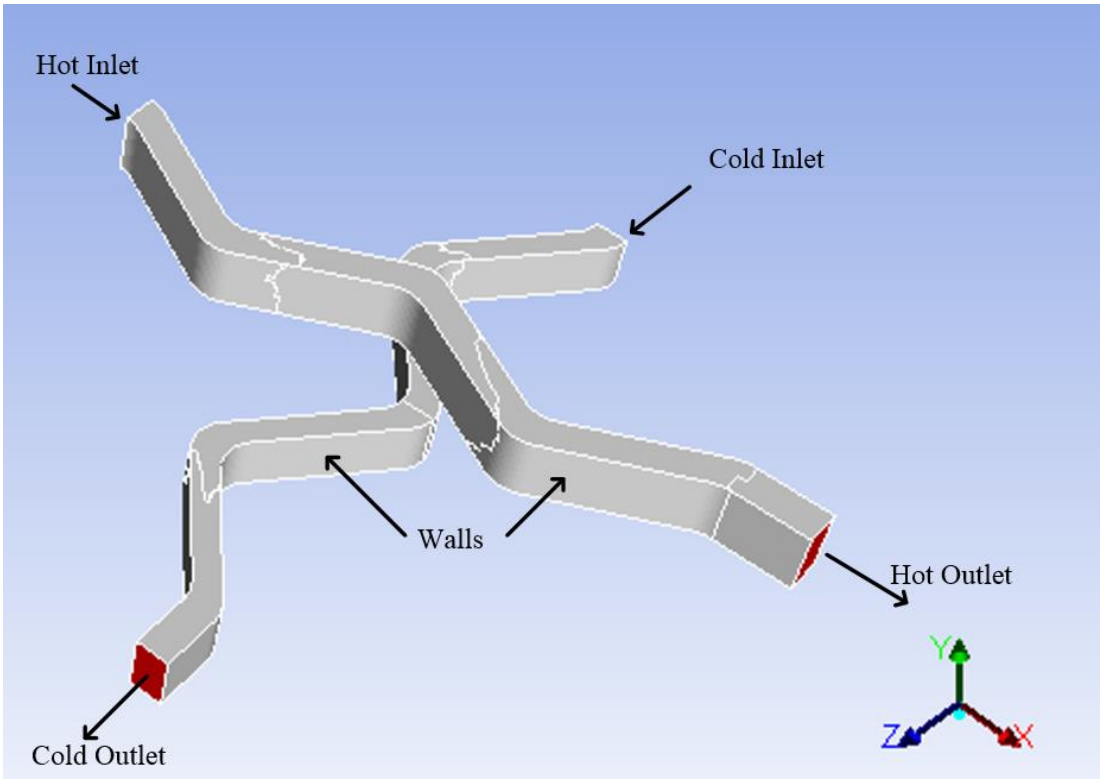

Figure 59: Hydrodynamic Mesh Independence Study Geometry

In the 3-D CFD simulation model, outlets of the flow channels are extended about 10% of the total channel length in order not to get backflow which affects both the pressure drop and the exit temperature of the flow. Channels inlet boundary conditions are set to 60 m/s constant velocity inlet which is the maximum value for porous media coefficients and the walls are set to 600 K constant temperature in order to get independent mesh settings both hydrodynamically and thermally. The results are shown in Figure 60. It is clear that using 189000 mesh elements setting is mesh independent.

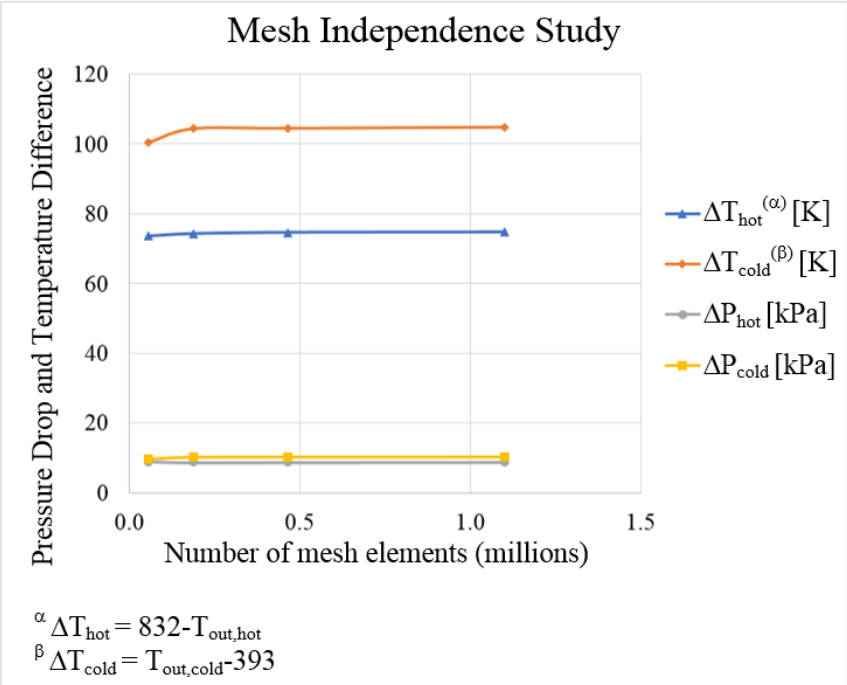

Figure 60: 3-D CFD Analysis Mesh Independence Study

In the 3-D CFD analysis, the size of the heat exchanger is found iteratively by considering the available computational resource. The selected geometry contains 4 separation plates and 4.5 stack of channels (2.5 cold stack of channels and 2 hot stack of channels) as shown in Figure 58. Every stack of channel contains 16 flow channels. Therefore, there are 80 (16×5) flow channels in total. Next, the mesh is created for the heat exchanger and shown below in Figure 61 and Figure 62. The created mesh contains conformal elements up to 63 million with 0.91 maximum (0.27 average) skewness. Skewed elements are mainly due to separation plate between hot and cold flow channels. Connecting two perpendicular wavy patterns in separation plates results in highly skewed cells and high number of mesh elements. Flow channel meshes and separation plate meshes are constructed by using hexahedral and tetrahedral meshes, respectively.

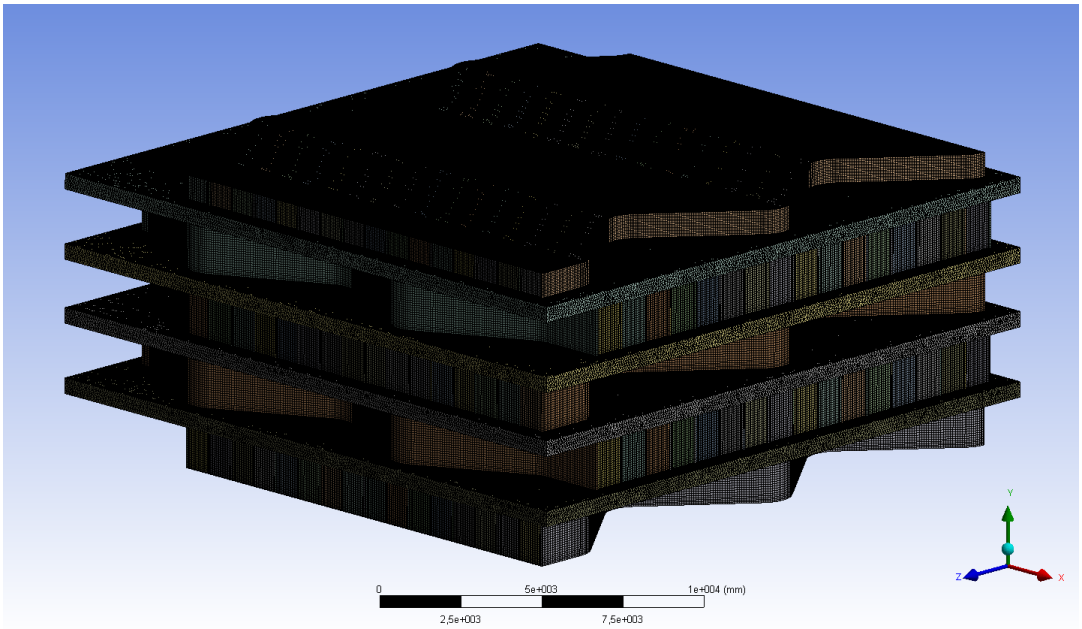

Figure 61: Whole Heat Exchanger Mesh

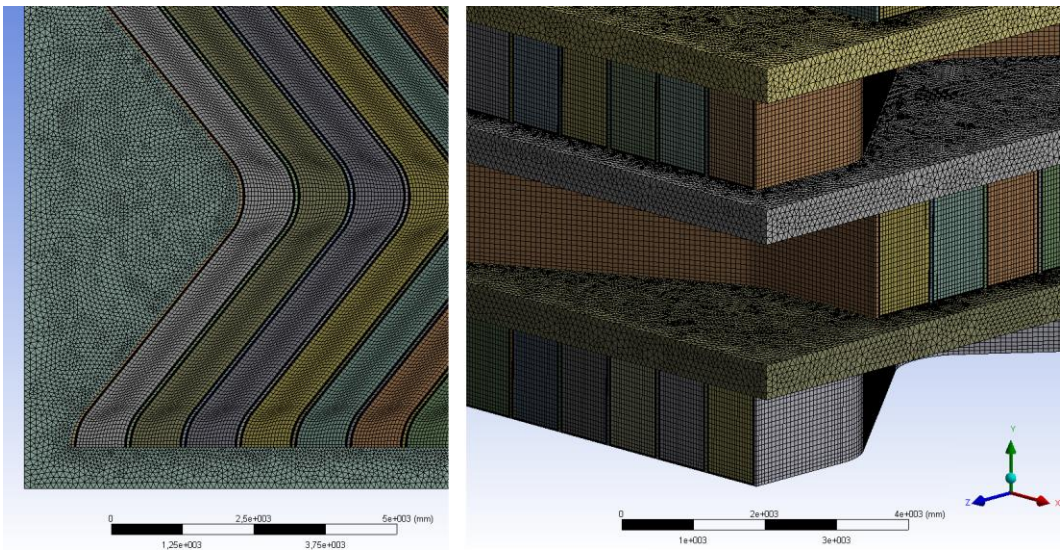

Figure 62: Top View (Left) and Isometric View (Right) of the Whole Heat Exchanger Mesh

Channels inlet boundary conditions are set to optimum values by considering the values in the Table 16. Corresponding inlet velocities are 28.8 m/s and 40.3 m/s for hot and cold flow, respectively. Inner walls are coupled and outer walls are isolated. Final mesh independence results are given in Figure 63. It is clear that using meshes higher than 42.6 million elements has almost no effect on the results.

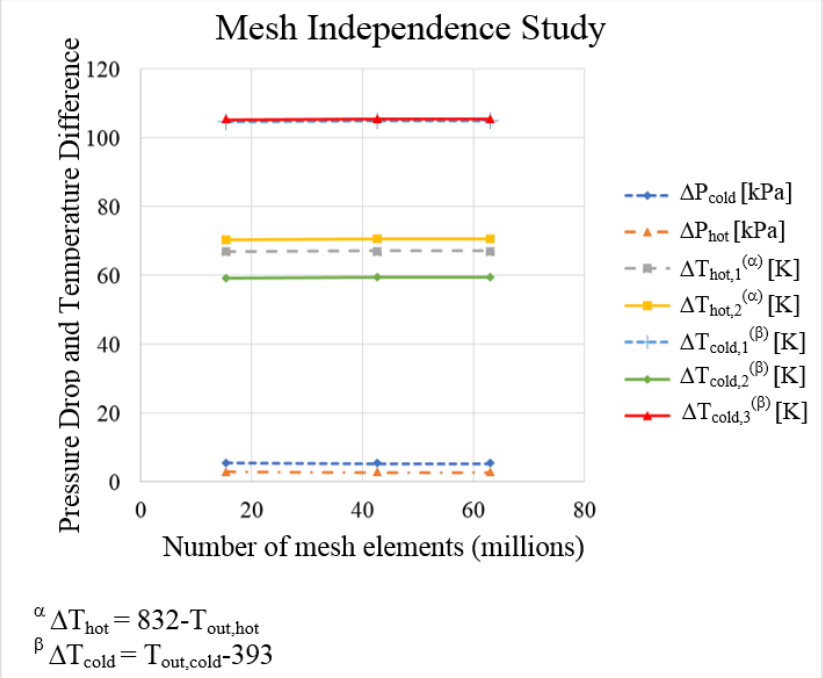

Figure 63: Whole Heat Exchanger Mesh Independence Study

The external geometry of this model has 9.35×20.59×20.98 mm^3 outer dimensions and it requires at least 42.6 million mesh elements. This model heat exchanger is much smaller than the half geometry of the optimum heat exchanger given in the Table 16, which has 555.4×140.8×86.44 mm^3 outer dimensions. (volume of the optimum heat exchanger is 1673 times larger than the modelled heat exchanger in this section.) By extrapolating the result, modelling of all details of the optimum heat exchanger requires 71.3 billion mesh elements which is computationally almost impossible with the available computer resources in this study.

A mesh independence study for the heat exchanger model used in the porous media analysis is also done and the results in Figure 64 show that the mesh independent porous media mesh has 1.2 million mesh elements, which is much less than the 43 million mesh elements for the model heat exchanger to be used in the 3-D CFD analysis.

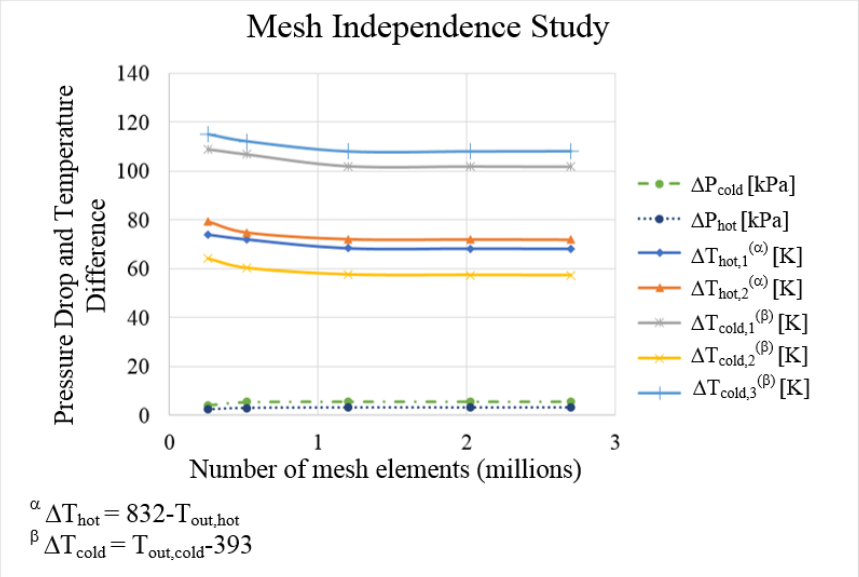

Figure 64: Mesh Independence Study for Porous Media

6.1.2. Determination of Porous Coefficients for the Porous Media Analysis of the Small-Sized Heat Exchanger

Porous coefficients are determined by using CFD results of physical fin simulation. Hydrodynamic porous coefficients can be determined via pressure drop against velocity data [74] as shown in Figure 65 and Figure 66 for hot and cold side, respectively. The velocities are taken from velocity=10 m/s to velocity=60 m/s with 10 m/s increments. According to fitted curve equations in these figures, viscous and inertial coefficients are calculated and shown in Table 17. Viscous coefficient is found by dividing the fitted equation second term coefficient on the right-hand side of Figure 65 to viscosity and flow length for hot flow. Additionally, inertial coefficient is found by dividing the fitted equation first term coefficient of Figure 65 to 0.5×density and

flow length for hot flow. Moreover, necessary parameters such as Interfacial Area Density (IAD), the ratio of the area of the fluid / solid interface and the volume of the porous zone, are given in the same table. Furthermore, porosity, which is the volume fraction of fluid within the porous region, is calculated by considering only vertical walls of the fin. Heat transfer coefficients are obtained by using log-mean temperature difference method [96].

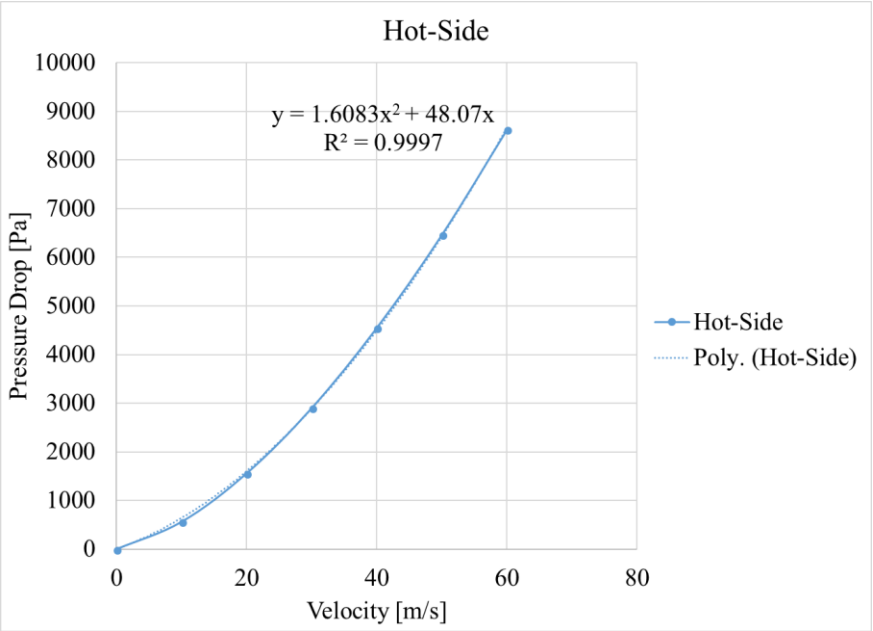

Figure 65: Hot Side Pressure Drop versus Velocity Graph and Fitted Polyline

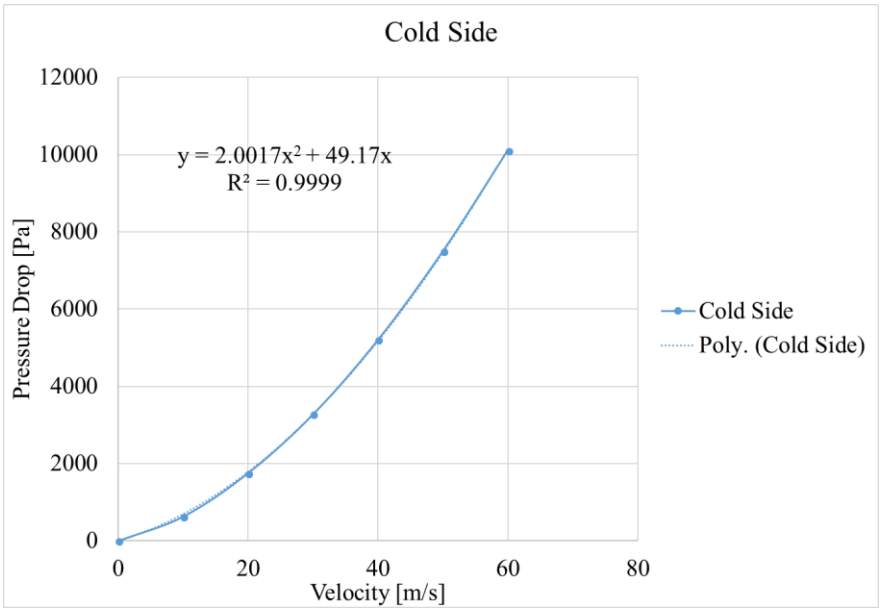

Figure 66: Cold Side Pressure Drop versus Velocity Graph and Fitted Polyline

Table 17: Physical Heat Exchanger Porous Media Coefficients

Channel Number	**Viscous Coefficients**	**Inertial Coefficients**	**IAD [1/m]**	**Porosity**	**HTC [W/m²K]**
Hot Channels 1	7.598E+07	5.689E+01	2188	0.949	1218.2
Hot Channels 2	7.598E+07	5.689E+01	2188	0.949	1216.8
Cold Channel 1 (Half Channels)	1.022E+08	1.268E+02	2652	0.944	1275.0
Cold Channels 2	1.022E+08	1.268E+02	2652	0.944	1273.3
Cold Channels 3	1.022E+08	1.268E+02	2652	0.944	1175.9

6.1.3. Results of the Porous Media Approach and the 3-D CFD Analysis for the Small-Sized Heat Exchanger

Porous media analyses are run with k-ε realizable turbulence model with enhanced wall function and k-ω shear stress transport turbulence model. It is seen that k-ω turbulence model gives slightly better results than k-ε turbulence model and only the former results are given in Table 18. Moreover, temperature and pressure contours of the full heat exchanger are shown in Figure 67 and Figure 68.

Table 18: 3-D CFD Analysis versus Porous Media Results for the Small-Sized Heat Exchanger

Channel	**3-D CFD Temp Outlet [K]**	**Porous Media Outlet Temp [K]**	**3-D CFD Pressure Drop [kPa]**	**Porous Media Pressure Drop [kPa]**	**Temp Error [%]**	**Pressure Error [%]**
Hot Channel 1	765.0	763.6	2.80	3.12	0.18	9.04
Hot Channel 2	761.4	759.9	2.80	3.12	0.19	9.04
Cold Channel 1	497.9	495.1	5.35	5.60	0.56	4.81
Cold Channel 2	452.4	450.6	5.35	5.60	0.40	4.81
Cold Channel 3	498.4	501.1	5.35	5.60	0.53	4.81

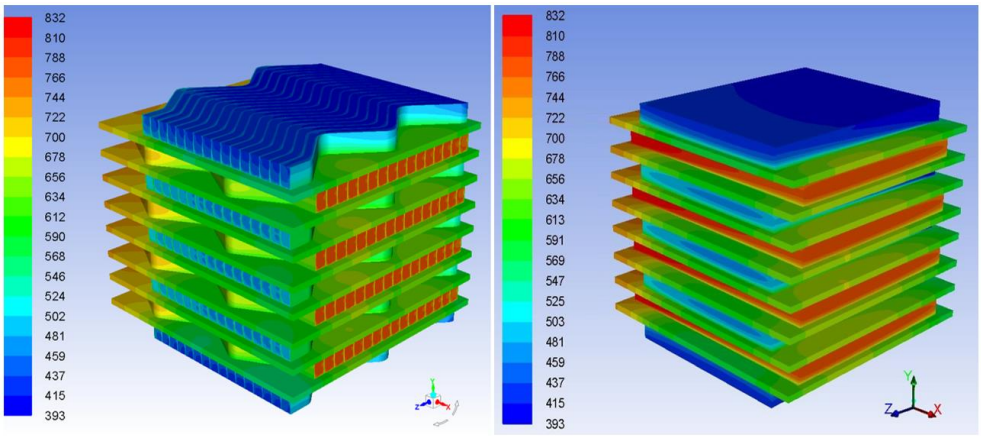

Figure 67: Temperature Contours of 3-D CFD Simulation (Left) and Porous Media Analysis (Right) [K]

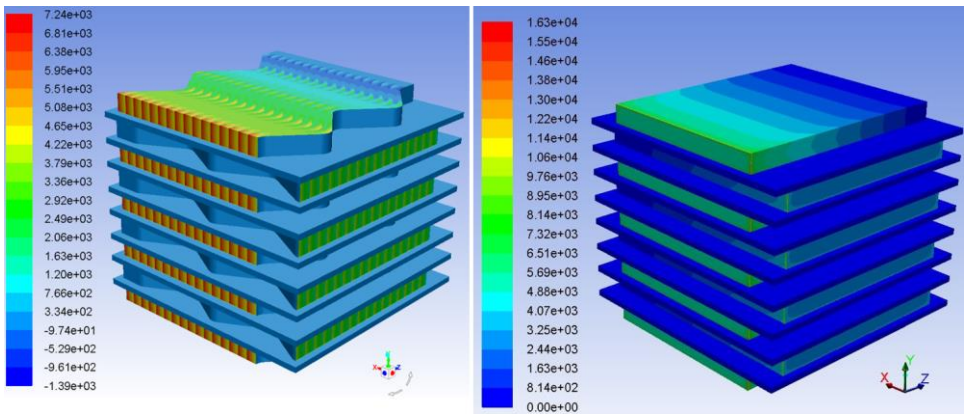

Figure 68: Pressure Drop Contours of 3-D CFD Simulation (Left) and Porous Media Analysis (Right) [Pascal]

It can be seen from the table that there is a perfect match between outlet temperatures. However, relative error of pressure drops reaches above 9%. This error may be resulted from the fact that 63 M mesh elements 3-D CFD simulations are done by using high performance computing machine with Intel Xeon CPU (1360 physical cores) and 1.2 M mesh elements porous media analysis is done by using an ordinary laptop with Intel

i7 CPU (8 physical cores). This causes unequal parallel partitioning and increases numerical error.

6.2. Porous Media Analysis of the Full-Scale Optimum Heat Exchanger

Having validated the porous media approach with 3-D CFD analysis, porous media analysis is conducted on the full-scale optimized cross flow heat exchanger with the dimensions given in Table 16 to validate its design. From the table, the optimized design has 32 hot plates. This means that there are 33 cold plates. Consequently, there are 65 plates in total.

6.2.1. Mesh Independence Study

Mesh independence study is done by taking one full hot plate and two half cold plates as shown in Figure 69. Top and bottom faces of the model are taken as symmetric boundary conditions. After determining the independent mesh settings, the same ones will be applied to 65 plate full heat exchanger. Since the superiority of the k-ε turbulence model with enhanced wall function is proven before, it is also used in this porous media analysis. Since enhanced wall function requires y^+ value is less than one, thin inflation layer is applied to mesh.

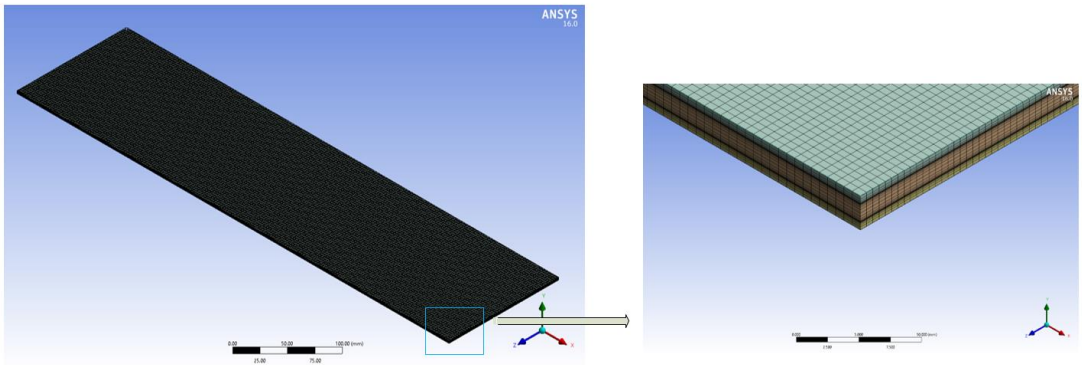

Figure 69: Porous Media Mesh Independence Study

The mesh independence results are given in Figure 70. In order to observe independency, outlet temperatures and pressure drops are investigated. As seen in the table, there is no significant change when the mesh elements number increased to 48000 for two half cold plates and one hot plate. As a result of this, this mesh settings will be applied beyond this point.

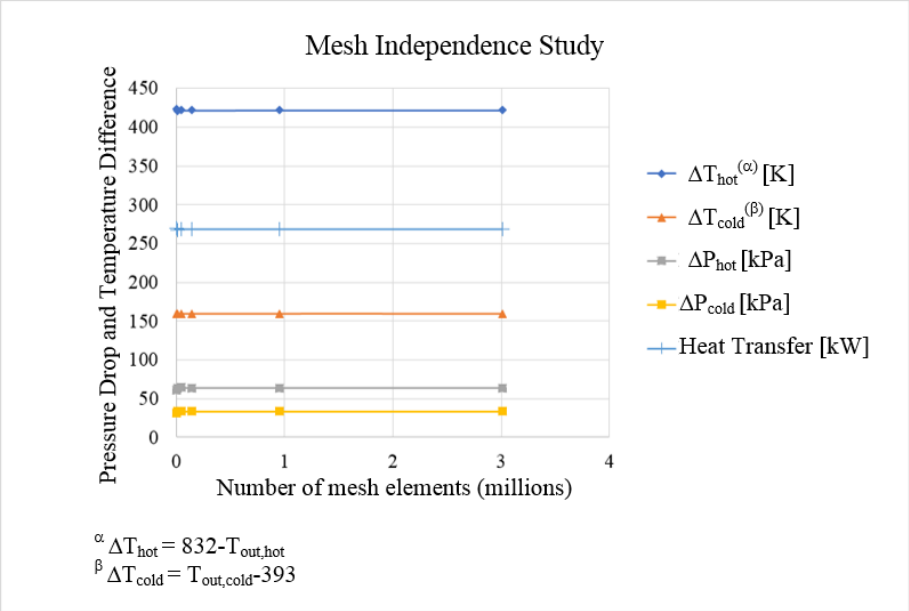

Figure 70: Porous Media Mesh Independence Study

6.2.2. Determination of Porous Coefficients for the Full-Sized Optimum Heat Exchanger

Hydrodynamic porous coefficients are determined by using the generated f factor response surface equation. Pressure drop versus velocity graphs are generated by using Equation (63) and shown in Figure 71 and Figure 72 for the hot side and cold side, respectively. The velocities in these graphs correspond to Re=1000 to Re=5000 with 1000 increment. Viscous and inertial coefficients are calculated according to the procedure explained in Section 6.1.2 and shown in Table 19 . Although used fins are the same compared to previous section, IAD and porosity are different due to an extra

horizontal fin face shown in Figure 32. As a result of this, IAD is slightly higher and porosity is slightly lower than the previous ones.

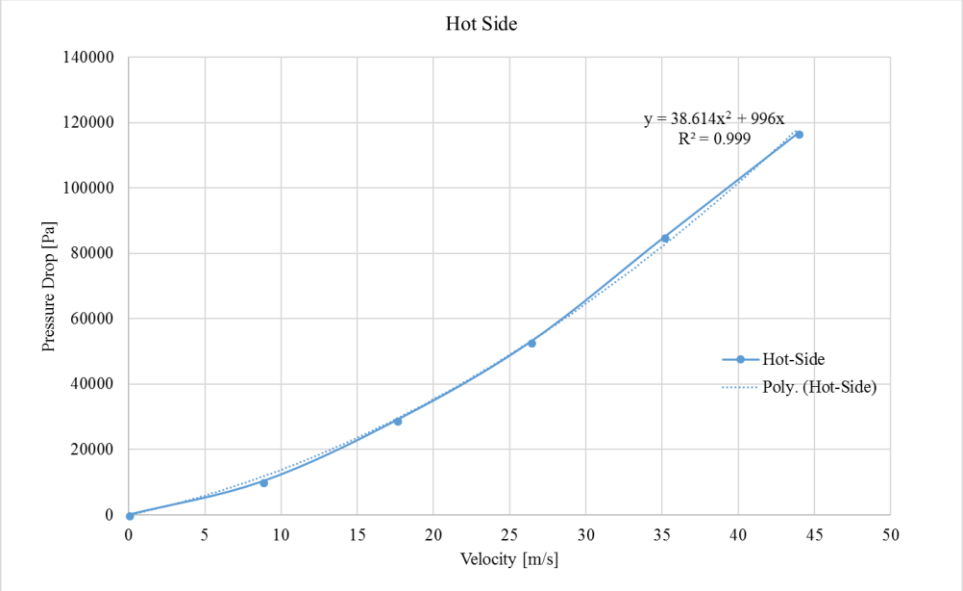

Figure 71: Hot Side Pressure Drop versus Velocity Graph and Fitted Polyline

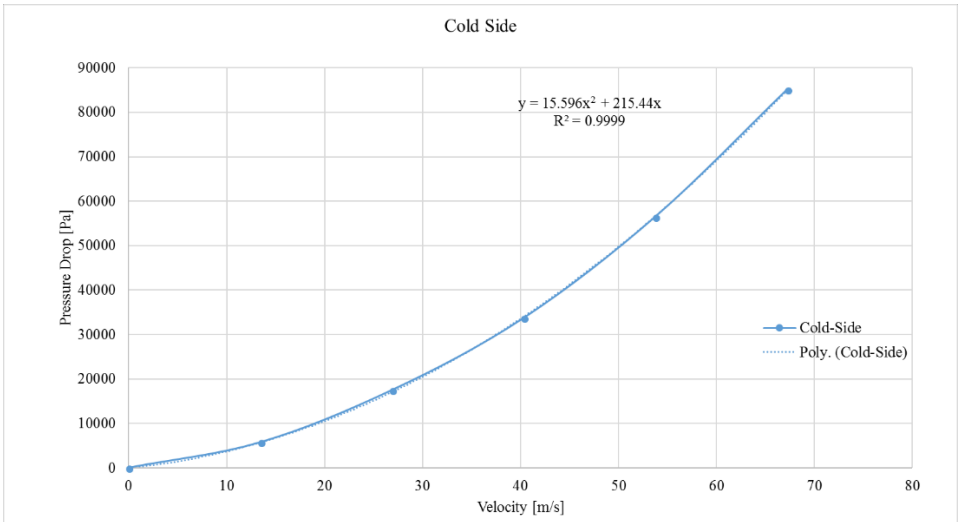

Figure 72: Cold Side Pressure Drop versus Velocity Graph and Fitted Polyline

Table 19: Full Scale Heat Exchanger Porous Media Coefficients

Channel	Viscous Coefficients	Inertial Coefficients	IAD [1/m]	Porosity	HTC [W/m^{2}K]
Hot Channels	5.60E+07	4.86E+01	2642.6	0.926	850.6
Cold Channels	6.12E+07	1.35E+02	3209.6	0.917	1039.3

6.2.3. Results of the Porous Media Analysis of the Full-Scale Optimum Heat Exchanger

Full scale porous media analysis is done by utilizing the symmetry of the heat exchanger. Instead of meshing 65 plates in total, half of the heat exchanger (16.5 hot and 16 cold plates) is analyzed. Symmetric boundary condition is applied to half cold plate wall as shown in Figure 73. In the figure, azure face, red faces and other faces indicate symmetric boundary condition, pressure outlet and walls, separately. Thanks to this, 780000 elements mesh is used for 32.5 plate half heat exchanger which can be solved by ordinary computers.

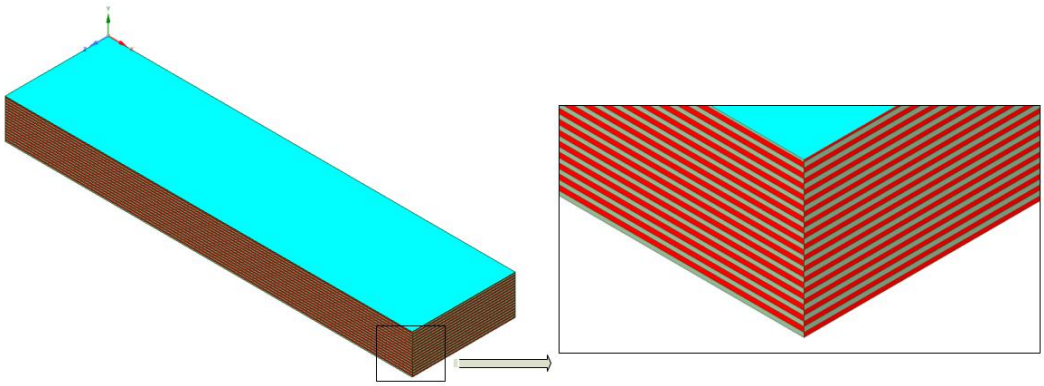

Figure 73: Full-Size Heat Exchanger Porous Media Geometry

Porous analysis pressure and temperature contours are shown in Figure 74 and Figure 75. It can be seen that temperature gradients from +Y axis to -Y axis do not change after first six or seven plates. Additionally, pressure gradients are the same for all plates as expected. The detailed comparison between the two methods can be made using Table 20. As it can be seen, the results are quite close to each other except hot side pressure drop. Besides, modelling 65 channels gives total heat transfer 268.9 kW in the Table 20 and modelling one full hot plate and two half cold plates by using symmetry boundary conditions gives total heat transfer 268.6 kW. The results are very close to each other. As a result of this, modelling full heat exchanger via porous media can be done by using the method explained in Section 6.2.1 in order to decrease computational effort.

In aircrafts, there are numerous fluid pipes that can contain fuel or other flammable fluids. These pipes may be located near hot zones such as heat exchangers. Therefore, determination of the temperature distribution in the heat exchanger is useful for designing the aircraft piping. Additionally, fire suppression systems may be located near hot zones. Temperature and pressure variation in the heat exchanger are observed which may be critical for fireworthiness of the aircraft.

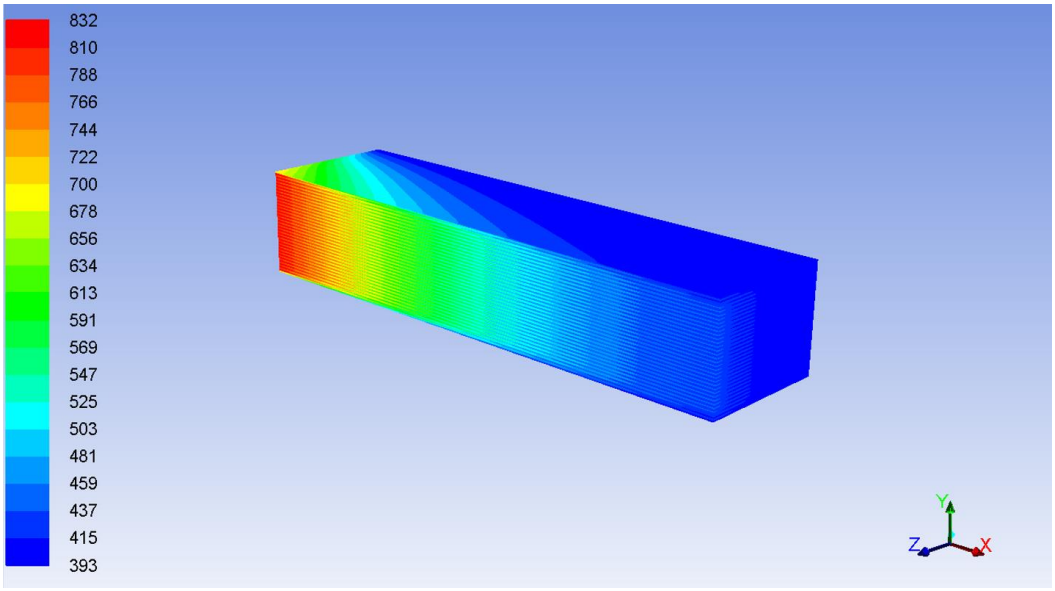

Figure 74: Porous Media Temperature Distribution [K]

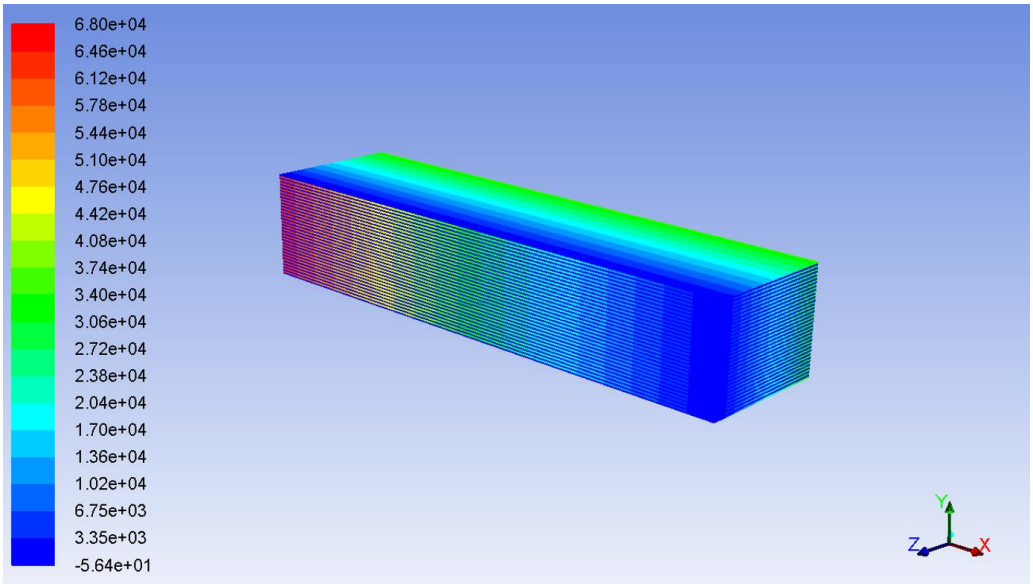

Figure 75: Porous Media Pressure Distribution [Pascal]

Table 20: ε-NTU and CFD Results Comparison

CFD Q [kW]	**CFD DPh [kPa]**	**CFD DPc [kPa]**	**ε-NTU Q [kW]**	**ε-NTU DPh [kPa]**	**ε-NTU DPc [kPa]**	**Error Q [%]**	**Error DPh [%]**	**Error DPc [%]**
268.9	63.94	33.53	268.3	60.73	33.60	0.22	5.29	0.22

6.2.4. Concluding Remarks

Design and optimization analysis of a full-sized air to air crossflow heat exchanger (with a minimum 243 kW and a nominal 268.9 kW heat load) for a fighter aircraft ECS was performed and the results (heat transfer and pressure drop values of both sides) were obtained. Porous media CFD analysis was done to validate the results obtained using ε-NTU method by considering a horizontal symmetry plate at the middle section.

For the optimized heat exchanger, the ε-NTU method provides a heat duty of 268.3 kW , while the porous media CFD approach accomplishes a 268.9 kW of heat duty. Moreover, ε-NTU method and porous media cold side pressure drops are calculated as 33.60 kPa and 33.53 kPa (Max. Ram Air Pressure Drop=34.5 kPa), respectively. These results are in good agreement. However, ε-NTU method hot side pressure drop value is slightly higher than that of porous media which are 60.73 kPa and 63.94 kPa (Max. Bleed Air Pressure Drop=68.9 kPa), correspondingly. This discrepancy may result from the fact that the hot side channel length is nearly 4 times larger than that of the cold side. Therefore, numerical errors may cause this deviation due to higher mesh elements in the flow direction.

CHAPTER 7

CONCLUSION & FUTURE WORK

7.1. General

In this study, air to air cross flow heat exchanger optimization study is performed under given conditions which is taken from F-15 aircraft [3]. The most critical thermal design condition for a fighter aircraft ECS system is found as high-speed flight at sea level. Most suitable heat exchanger type for ECS air to air heat exchangers is found as compact plate-fin heat exchanger. Several fin types of plate-fin heat exchanger are evaluated to find most suitable fin types for specified application. As a result of this, offset-strip fin and wavy fin are found as the most promising plate-fin heat exchanger fin types due to high heat transfer characteristics.

Fin CFD analyses are done by using periodic flow approach as described by Patankar et al [78]. This approach is found to be successful in predicting thermo-hydraulic characteristics of offset-strip and wavy fins compared to experimental data. Since compact heat exchanger fins have very small hydraulic diameters, it is predicted that near wall treatment may give better results than other models. Therefore, enhanced wall function model is found to be the most suitable wall function when k-ε turbulence model is applied as expected. Moreover, k-ω shear stress transport model is found to be suitable for near wall treatment of porous media CFD analyses and it slightly differs from k-ε realizable model.

Stochastic optimization methods are found to be more suitable optimization method than others due to the fact that it searches all design domain and it is very successful at highly non-linear problems such as ε-NTU heat exchanger design method. Among these methods, multi-objective genetic algorithm is selected to find a set of optimal solutions. GA optimization parameters such as crossover probability are found as case

dependent and they are found by sensitivity analysis. Consequently, three objective optimization is run and wavy fin is found to be an optimum solution.

A comparison between 3-D CFD analysis of the heat exchanger with fins and porous media approach is done. It is found that k-ω shear stress transport turbulence model gives slightly more accurate solution then k-ε realizable turbulence model with enhanced wall function. As a result of this, it is concluded that considerable amount of computational source can be saved by using porous media approach. For example, 3-D CFD simulations with 63 million mesh elements gives very close results to the porous media approach having 1.2 million mesh elements. Moreover, another comparison between analytical ε-NTU method and porous media analysis is also made. Porous coefficients are obtained from f and j factor correlations which were previously generated by using periodic flow approach of CFD and DOE. Consequently, there is a good match between analytical and porous media approach which means porous media approach is good enough for modelling compact heat exchangers. Additionally, using symmetry boundary conditions (as shown in Figure 69) in porous media analysis of compact heat exchangers also shows good match with the analytical results and number of used mesh elements can significantly be decreased by using this instead of modelling all plates.

7.2. Discussion and Recommendations for Future Work

In this thesis study, air to air crossflow heat exchanger is optimized and analyzed numerically. There are numerous assumptions made during the calculations that can be improved by further studies. First of all, fluid properties are taken as constant due to periodic flow constraint of commercial software Fluent 16.0. Users are warned not to use temperature dependent properties when periodic flow problems are solved [74]. Therefore, all CFD analyses are done by keeping fluid properties constant for consistency including porous media analyses. Results may be improved if periodic flow problems are solved with temperature dependent fluid properties. Moreover, cold side mass flow rate is initially assumed as 2.45 kg/s which gives average temperatures of inlet and outlet as 640 K and 445 K for hot and cold sides. Thermal properties of air

are calculated initially by using these average temperatures. However, cold side mass flow rate is found as 1.71 kg/s which gives 621 K and 470 K average temperatures for hot and cold sides, respectively. Therefore, the assumption is acceptable for air thermo-physical properties.

Although ε-NTU method is a widely-used heat exchanger rating method, it is only a global perspective method and provides no information concerning conditions within the heat exchanger [83]. For example, Bell-Delaware method is a complex method for shell and tube heat exchangers which is used to predict thermal and hydrodynamic characteristics of shell side. Similar detailed methods can be used for cross flow plate fin heat exchanger to improve the results.

Numerical modelling of periodic fin flows can also be improved and made parametric if Ansys Fluent 16.0 is improved. Periodic flow can only be solved in the software by writing some special text user interface codes which asks periodic zone, shadow zone etc. As a result of this, periodic mass flow rate input could not be made a parameter and considerable amount of time is spent to prepare analysis cases. Additionally, porous media analysis must be done by defining surface interfaces manually. Using non-equilibrium thermal model in porous media analysis of Fluent 16.0 creates exactly the same coincident surfaces for unequal porous solid temperature. Therefore, these extra surfaces must be connected by defining manual interfaces which is also a time-consuming process.

The design of experiments method presented in this thesis uses Central Composite Design to generate response surface equations for f and j factors. The accuracy of the equations can be increased by increasing the number of experiments which were 125 per fin type and 250 in total due to computationally available sources.

Lastly, actual experiments can be done for further studies to validate all theory mentioned in this thesis. CFD simulations are generally supported with experimental results and a straightforward methodology is derived for the same kind of design activities by comparing experimental results and CFD results.

REFERENCES

[1] SAE International, "AIR1957A: Heat Sinks for Airborne Vehicles," 2015. [Online]. Available: https://doi.org/10.4271/AIR1957A.

[2] C. J. Forster and P. Lemiuex, "Development of an Air-Cycle Environmental Control System for Automotive Applications," California Polytechnic State University, California, 2011.

[3] D. Matullch, "High-Temperature Bootstrap Compared with F-15 Growth Air Cycle Air Conditioning System," in *19th Intersociety Conference on Environmental Systems*, San Diego, California, 1989.

[4] C. W. Lui, C. K. Lee and E. Schwan, "Integrated Environmental Control System and Liquid Cooling System for F/A-18 E/F Aircraft," in *SAE Aerospace Atlantic Conference & Exposition*, Dayton, Ohb, 1995 .

[5] W. M. Kays and A. L. London, Compact Heat Exchangers-Third Edition, Florida: McGraw-Hill, Inc., 1998.

[6] "Cooling of Military Avionic Equipment," SAE International, 2015.

[7] T. A. Cowell, "A General Method for the Comparison of Compact Heat Transfer Surfaces," *J. Heat Transfer,* vol. 112, pp. 288-294, 1990.

[8] M. Picon-Nunez, G. T. Polley, E. Torres-Reyes and A. Gallegos-Munoz, "Surface selection and design of plate-fin heat exchangers," *Applied Thermal Engineering,* vol. 19, pp. 917-931, 1999.

[9] G. Hall and J. Marthinuss Jr., "Air Cooled Compact Heat Exchanger Design For Avionics Thermal Management Using Published Test Data," *International Electronic Packaging Technical Conference and Exhibition,* vol. 2, pp. 705-711, 2003.

[10] SAE International, "AIR 1277B: Cooling of Military Avionic Equipment," 2015. [Online]. Available: https://doi.org/10.4271/AIR1277B.

[11] E. H. Hunt, D. H. Reid, D. R. Space and F. E. Tilton, "Commercial Airliner Environmental Control System," Aerospace Medical Association, California, 1995.

[12] Boeing, "Inside the 747-8 New Environmental Control System," *AERO Magazine,* pp. 19-26, 2012.

[13] M. Sinnett, "787 No-Bleed Systems: Saving Fuel and Enhancing Operational Efficiencies," *Boeing Aero Magazine,* vol. 4, pp. 6-11, 2007.

[14] R. Ashford and S. Brown, "F-22 Environmental Control System/Thermal Management System (ECS/TMS) Flight Test Program - Downloadable Constants, an Innovative Approach," *SAE Technical Paper Series,* 2000.

[15] S. Yu and E. Ganev, "Next Generation Power and Thermal Management System," *SAE International,* vol. 1, no. 1, pp. 1107-1121, 2009.

[16] G. Starace, M. Fiorentino, M. P. Longo and E. Carluccio, "A hybrid method for the cross flow compact heat exchangers design," *Applied Thermal Engineering,* vol. 111, p. 1129–1142, 2017.

[17] S. B. Saad, C. Gentric, J.-F. Fourmigué, P. Clément and J.-P. Leclerc, "CFD and experimental investigation of the gas–liquid flow in the distributor of a compact heat exchanger," *Chemical EngineeringResearchandDesign,* vol. 92, p. 2361–2370, 2014.

[18] R. Camilleri, D. A. Howey and M. D. McCulloch, "Predicting the flow distribution in compact parallel flow heat exchangers," *Applied Thermal Engineering,* vol. 90, pp. 551-558, 2015.

[19] C. Sert, "ME 485 Lecture Notes," METU, Ankara, 2015.

[20] W. Yaïci, M. Ghorab and E. Entchev, "3D CFD study of the effect of inlet air flow maldistribution on plate-fin-tube heat exchanger design and thermal–hydraulic performance," *International Journal of Heat and Mass Transfer,* no. 101, p. 527–541, 2016.

[21] E. Özden and İ. Tarı, "Shell side CFD analysis of a small shell-and-tube heat exchanger," *Energy Conversion and Management,* vol. 51, pp. 1004-1014, 2010.

[22] U. U. Rehman, "Heat Transfer Optimization of Shell-and-Tube Heat Exchanger through CFD Studies," Chalmers University of Technology, Göteborg, 2011.

[23] C. Pan, T. Zhanga, J. Wang and Y. Zhou, "CFD study of heat transfer and pressure drop for oscillating flow in helical rectangular channel heat exchanger," *International Journal of Thermal Sciences,* vol. 129, pp. 106-114, 2018.

[24] E. Y. Rios-Iribe, M. E. Cervantes-Gaxiola, E. Rubio-Castro and O. M. Hernández-Calderón, "Heat transfer analysis of a non-Newtonian fluid flowing through a Plate Heat Exchanger using CFD," *Applied Thermal Engineering,* vol. 101, p. 262–272, 2016.

[25] Ł. Amanowicz and J. Wojtkowiak, "Validation of CFD model for simulation of multi-pipe earth-to-air heat exchangers (EAHEs) flow performance," *Thermal Science and Engineering Progress,* vol. 5, pp. 44-49, 2018.

[26] S. B. Hosseini, R. H. Khoshkhoo and M. Javadi, "Experimental and Numerical Investigation on Particle Deposition in a Compact Heat Exchanger," *Applied Thermal Engineering,* vol. 115, pp. 406-417, 2017.

[27] S. Ismail and R. Velraj, "Studies on Fanning Friction (F) And Colburn (J) Factors of Offset And Wavy Fins Compact Plate Fin Heat Exchanger–A CFD Approach," *Numerical Heat Transfer,* vol. 56, pp. 987-1005, 2009.

[28] R. B. S. Rao, G. Ranganath and C. Ranganayakulu, "Development of colburn ‘j’ factor and fanning friction factor ‘f’ correlations for compact heat exchanger plain fins by using CFD," *Heat Mass Transfer,* vol. 49, pp. 991-1000, 2013.

[29] S. Girgin, "An Investigation of Heat Transfer Performance of Rectangular Channel by Using Vortex Generators," İstanbul Technical University, İstanbul, 2017.

[30] K. G. Güler, "Computational Modeling of Fin-And-Tube Type Vehicle Radiators Based on Porous Medium Approach," METU, Ankara, 2014.

[31] M. Musto, N. Bianco, G. Rotondo and F. Toscano, "A simplified methodology to simulate a heat exchanger in an aircraft’s oil cooler by means of a Porous Media model," *Applied Thermal Engineering,* vol. 94, pp. 836-845, 2016.

[32] W. Wang, J. Guo, S. Zhang, J. Yang, X. Ding and X. Zhan, "Numerical study on hydrodynamic characteristics of plate-fin heat exchanger using porous media approach," *Computers and Chemical Engineering,* vol. 61, pp. 30-37, 2014.

[33] S. Mao, C. Cheng, X. Li and E. E. Michaelides, "Thermal/structural analysis of radiators for heavy-duty trucks," *Applied Thermal Engineering,* vol. 30, pp. 1438-1446, 2010.

[34] A. M. Hayes, J. A. Khan, A. H. Shaaban and I. G. Spearing, "The thermal modeling of a matrix heat exchanger using a porous medium and the thermal non-equilibrium model," *International Journal of Thermal Sciences,* vol. 47, pp. 1306-1315, 2008.

[35] X. Zhang, P. Tseng, M. Saeed and J. Yu, "A CFD-based simulation of fluid flow and heat transfer in the Intermediate Heat Exchanger of sodium-cooled fast reactor," *Annals of Nuclear Energy,* vol. 109, pp. 529-537, 2017.

[36] A. Hadidi, "A robust approach for optimal design of plate fin heat exchangers using biogeography based optimization (BBO) algorithm," *Applied Energy*, vol. 150, pp. 196-210, 2015.

[37] A. R. Doodman, M. Fesanghary and R. Hosseini, "A robust stochastic approach for design optimization of air cooled heat exchangers," *Applied Energy,* pp. 1240-1245, 2009.

[38] S. Fettaka, J. Thibault and Y. Gupta, "Design of shell-and-tube heat exchangers using multiobjective optimization," *International Journal of Heat and Mass Transfer,* vol. 60, p. 343–354, 2013.

[39] H. Hajabdollahi, M. Tahani and S. Fard, "CFD modeling and multi-objective optimization of compact heat exchanger using CAN method," *Applied Thermal Engineering*, pp. 2597-2604, 2011.

[40] R. Hilbert, G. Janiga, R. Baron and D. Thevenin, "Multi-objective shape optimization of a heat exchanger using parallel genetic algorithms," *International Journal of Heat and Mass Transfer,* pp. 2567-2577, 2006.

[41] M. Imran, N. A. Pambudi and M. Farooq, "Thermal and hydraulic optimization of plate heat exchanger using multi objective genetic algorithm," *Case Studies in Thermal Engineering,* vol. 10, pp. 570-578, 2017.

[42] D. Juan, Y. Man-Ni and Y. Shi-Fang, "Correlations and optimization of a heat exchanger with offset fins by genetic algorithm combining orthogonal design," *Applied Thermal Engineering,* pp. 1091-1103, 2016.

[43] W. Zalewski, B. Niezgoda-Zelasko and M. Litwin, "Optimization of evaporative fluid coolers," *International Journal of Refrigeration,* vol. 23, pp. 553-565, 2000.

[44] M. T. Gonzalez, N. C. Petracci and M. J. Urbician, "Air-Cooled Heat Exchanger Design Using Successive Quadratic Programming (SQP)," *HeatTransfer Engineering,* vol. 22, pp. 11-16, 2001.

[45] S. W. Stewart, S. V. Shelton and K. A. Aspelund, "Finned Tube Heat Exchanger Optimization," in *2nd International Conference on Heat Transfer, Fluid Mechanics and Thermodynamics*, Victoria Falls, 2003.

[46] H. Zarea, F. M. Kashkooli, A. M. Mehryan, M. R. Saffarian and E. N. Beherghani, "Optimal design of plate-fin heat exchangers by a Bees Algorithm," *Applied Thermal Engineering,* vol. 69, pp. 267-277, 2014.

[47] S.-Y. Zhao and Q. Chen, "A thermal circuit method for analysis and optimization of heat exchangers with consideration of fluid property variation," *International Journal of Heat and Mass Transfer,* vol. 99, pp. 209-218, 2016.

[48] J. V. Vargas and A. Bejan, "Thermodynamic Optimization of Finned Crossflow Heat Exchangers for Aircraft Environmental Control Systems," *International Journal of Heat and Fluid Flow,* vol. 22, pp. 657-665, 2001.

[49] T. Bello-Ochende, E. M. Simasiku and J. Baloyi, "Optimum Design Of Heat Exchanger For Environmental Control System of An Aircraft Using Entropy Generation Minimization (EGM) Technique," in *12th International Conference on Heat Transfer*, Malaga, 2016.

[50] R. V. Rao, A. Saroj, P. Ocloń, J. Taler and D. Taler, "Single- and Multi-Objective Design Optimization of Plate-Fin Heat Exchangers Using Jaya Algorithm," *Heat Transfer Engineering,* vol. 39, pp. 1201-1216, 2018.

[51] B. D. Raja, R. L. Jhala and V. Patel, "Many-objective optimization of cross-flow plate-fin heat exchanger," *International Journal of Thermal Sciences,* vol. 118, pp. 320-339, 2017.

[52] S. Bari and S. N. Hossain, "Design and Optimization of Compact Heat Exchangers to be Retrofitted into a Vehicle for Heat Recovery from a Diesel Engine," *Procedia Engineering,* vol. 105, pp. 472-479, 2015.

[53] H. Najafi and B. Najafi, "Multi-objective optimization of a plate and frame heat exchanger via genetic algorithm," *Heat Mass Transfer,* vol. 46, p. 639–647, 2010.

[54] H. Sadeghzadeh, M. Aliehyaei and M. A. Rosen, "Optimization of a Finned Shell and Tube Heat Exchanger Using a Multi-Objective Optimization Genetic Algorithm," *Sustainability,* vol. 7, no. 9, pp. 11679-11695, 2015.

[55] H. Hajabdollahi, P. Ahmadi and I. Dincer, "Thermoeconomic optimization of a shell and tube condenser using both genetic algorithm and particle swarm," *International Journal ofRefrigeration,* vol. 34, no. 4, pp. 1066-1076, 2011.

[56] M. S. Yadav, S. A. Giri and V. C. Momale, "Sizing analysis of louvered fin flat tube compact heat exchanger by genetic algorithm," *Applied Thermal Engineering,* vol. 125, p. 1426–1436, 2017.

[57] G. Xie, B. Sunden and Q. Wang, "Optimization of compact heat exchangers by a genetic algorithm," *Applied Thermal Engineering,* pp. 895-906, 2008.

[58] M. Mishra, P. K. Das and S. Sarangi, "Second law based optimisation of crossflow plate-fin heat exchanger design using genetic algorithm," *Applied Thermal Engineering,* vol. 29, p. 2983–2989, 2009.

[59] R. Selbas, Ö. Kızılkan and M. Reppich, "A new design approach for shell-and-tube heat exchangers using genetic algorithms from economic point of view," *Chemical Engineering and Processing,* vol. 45, p. 268–275, 2006.

[60] S. Sanaye and H. Hajabdollahi, "Multi-objective optimization of shell and tube heat exchangers," *Applied Thermal Engineering,* vol. 30, pp. 1937-1945, 2010.

[61] D. Geb, F. Zhou, G. DeMoulin and I. Catton, "Genetic Algorithm Optimization of a Finned-Tube Heat Exchanger Modeled With Volume-Averaging Theory," *Journal of Heat Transfer,* vol. 135, pp. 082602-1-082602-9, 2013.

[62] T. Selleri, B. Najafi, F. Rinaldi and G. Colombo, "Mathematical Modeling and Multi-Objective Optimization of a Mini-Channel Heat Exchanger Via Genetic Algorithm," *Journal of Thermal Science and Engineering Applications,* vol. 5, pp. 031013-1-031013-10, 2013.

[63] H. Peng and X. Ling, "Optimal design approach for the plate-fin heat exchangers using neural networks cooperated with genetic algorithms," *Applied Thermal Engineering,* vol. 28, pp. 642-650, 2008.

[64] A. V. Azad and M. Amidpour, "Economic optimization of shell and tube heat exchanger based on constructal theory," *Energy,* vol. 36, pp. 1087-1096, 2011.

[65] M. Cavazzuti, Optimization Methods: From Theory to Design, Springer-Verlag Berlin Heidelberg, 2013.

[66] P. Kumar and K.-H. Lee, "Optimum Design of Finned Tube Heat Exchanger Using DOE," *Springer International Publishing,* pp. 569-576, 2015.

[67] B. Sahin, K. Yakut, I. Kotcioglu and C. Celik, "Optimum design parameters of a heat exchanger," *Applied Energy,* vol. 82, pp. 90-106, 2005.

[68] M.-S. Kim, J. Lee, S.-J. Yook and K.-S. Lee, "Correlations and optimization of a heat exchanger with offset-strip fins," *International Journal of Heat and Mass Transfer,* vol. 54, pp. 2073-2079, 2011.

[69] C. Liu, W. Bu and D. Xu, "Multi-objective shape optimization of a plate-fin heat exchanger using CFD and multi-objective genetic algorithm," *International Journal of Heat and Mass Transfer,* no. 111, pp. 65-82, 2017.

[70] A. Ceylanoğlu, "An Accelerated Aerodynamic Optimization Approach for A Small Turbojet Engine Centrifugal Compressor," MSc. Thesis, Middle East Technical University, Ankara, 2009.

[71] S. Wang, J. Xiao, J. Wang, G. Jian, J. Wen and Z. Zhang, "Application of response surface method and multi-objective genetic algorithm to configuration optimization of Shell-and-tube heat exchanger with fold helical baffles," *Applied Thermal Engineering,* vol. 129, pp. 512-521, 2007.

[72] C. Liu, X. Y. Deng, X. Liu, Y. P. Wang and C. Q. Su, "Multi-objective optimization of heat exchanger in an automotive exhaust thermoelectric generator," *Applied Thermal Engineering,* vol. 108, pp. 916-926, 2016.

[73] K. M. Shirvan, R. Ellahi, S. Mirzakhanlari and M. Mamourian, "Enhancement of heat transfer and heat exchanger effectiveness in a double pipe heat exchanger filled with porous media: Numerical simulation and sensitivity analysis of turbulent fluid flow," *Applied Thermal Engineering,* vol. 109, pp. 761-774, 2016.

[74] Ansys, Inc., "ANSYS Fluent User's Guide 16.1," Canonsburg, 2015.

[75] The MathWorks, Inc., Global Optimization Toolbox User's Guide, Natick, MA, 2017.

[76] Ansys, Inc., "DesignXplorer Design of Experiments," 2016.

[77] ESTECO, "modeFRONTIER," [Online]. Available: https://www.esteco.com/modefrontier. [Accessed 15 8 2018].

[78] S. V. Patankar, C. H. Liu and E. M. Sparrow, "Fully Developed Flow and Heat Transfer in Ducts Having Streamwise-Periodic Variations of Cross-Sectional Area," ASME, Minnesota, 1977.

[79] "ANSYS Fluent Theory Guide 16.0," ANSYS, Inc., Canonsburg, 2015.

[80] H. M. Joshi and R. L. Webb, "Heat transfer and friction in the offset strip-fin heat exchanger," *International Journal of Heat and Mass Transfer,* vol. 30, no. 1, pp. 69-84, 1987.

[81] Department of Defense Handbook, "MIL-HDBK-310C-Global Climatic Data for Developing Military Products," 1997.

[82] Aerospace Information Report, "Aerothermodynamic Systems Engineering and Design," Sae International, 2004.

[83] F. P. Incropera, D. P. Dewitt, T. Bergman and A. Lavine, Fundamentals of Heat and Mass Transfer, 7th edition, John Wiley & Sons, 2011.

[84] R. K. Shah and D. P. Sekulic, Fundamentals of Heat Exchanger Design, John Wiley & Sons, Inc., 2003.

[85] M. M. Awad and Y. S. Muzychka, "Models for Pressure Drop and Heat Transfer in Air Cooled Wavy Fin Heat Exchangers," *Journal of Enhanced Heat Transfer,* vol. 3, no. 18, pp. 191-207, 2011.

[86] A. R. Wieting, "Empirical correlations for heat transfer and flow friction characteristics of rectangular offset-fin plate-fin heat exchangers," *Journal of Heat Transfer,* vol. 3, no. 97, pp. 488-490, 1975.

[87] S. Mochizuki, Y. Yagi and W. J. Yang, "Transport Phenomena in Stacks of Interrupted Parallel-Plate Surfaces," *Experimental Heat Transfer,* vol. 1, no. 2, pp. 127-140, 1987.

[88] R. M. Manglik and A. E. Bergles , "Heat transfer and pressure drop correlations for the rectangular offset strip fin compact heat exchanger," *Experimental Thermal and Fluid Science,* vol. 10, no. 2, pp. 171-180, 1995.

[89] S. W. Qian, Heat Exchanger Design Handbook, Beijing: 2002, 2002.

[90] P. Maghsoudi, S. Sadeghi, H. Khanjarpanah and H. H. Gorgani, "A comprehensive thermo-economic analysis, optimization and ranking of different microturbine plate-fin recuperators designs employing similar and dissimilar fins on hot and cold sides with NSGA-II algorithm and DEA model," *Applied Thermal Engineering,* vol. 130, pp. 1090-1104, 2018.

[91] P. Maghsoudi, S. Sadeghi and H. H. Gorgani, "Comparative study and multi-objective optimization of plate-fin recuperators applied in 200 kW microturbines based on non-dominated sorting and normalization method considering recuperator effectiveness, exergy efficiency and total cost," *International Journal of Thermal Sciences,* vol. 124, pp. 50-67, 2018.

[92] I. Ozkol and G. Komurgoz, "Determination of The Optimum Geometry of The Heat Exchanger Body via A Genetic Algorithm," *Numerical Heat Transfer*, vol. 48, p. 283–296, 2005.

[93] H. Najafi, B. Najafi and P. Hoseinpoori, "Energy and cost optimization of a plate and fin heat exchanger using genetic algorithm," *Applied Thermal Engineering*, pp. 1839-1847, 2011.

[94] S. Sanaye and H. Hajabdollahi, "Multi-objective optimization of rotary regenerator using genetic algorithm," *International Journal of Thermal Sciences*, vol. 48, pp. 1967-1977, 2009.

[95] S. Sanaye and H. Hajabdollahi, "Thermal-economic multi-objective optimization of plate fin heat exchanger using genetic algorithm," *Applied Energy*, pp. 1893-1902, 2010.

[96] M. J. de Lemos, "Modeling of Thermal Non-equilibrium," in *Thermal Non-Equilibrium in Heterogeneous Media*, Springer, 2016, pp. 9-41.

APPENDICES

9.1. APPENDIX A

Table A-1:Wavy Fin Design Inputs & Outputs

DPs	MFS [mm]	PS [mm]	Wl [mm]	Amp [mm]	Re	f CFD	j CFD	f corr	j corr
1	0.9	1	8	1	1000	3.44E-02	9.33E-03	3.66E-02	9.29E-03
2	2.5	1	8	1	1000	3.66E-02	8.06E-03	2.70E-02	7.97E-03
3	0.9	10.5	8	1	1000	3.76E-02	1.01E-02	3.74E-02	1.03E-02
4	2.5	10.5	8	1	1000	5.77E-02	1.19E-02	7.04E-02	1.23E-02
5	0.9	1	11	1	1000	2.76E-02	8.05E-03	3.39E-02	8.24E-03
6	2.5	1	11	1	1000	2.86E-02	7.51E-03	2.98E-02	7.41E-03
7	0.9	10.5	11	1	1000	3.13E-02	9.36E-03	2.01E-02	8.76E-03
8	2.5	10.5	11	1	1000	3.56E-02	9.14E-03	3.58E-02	9.31E-03
9	0.9	1	8	3	1000	1.02E-01	1.58E-02	8.90E-02	1.53E-02
10	2.5	1	8	3	1000	1.86E-01	1.33E-02	2.08E-01	1.39E-02
11	0.9	10.5	8	3	1000	1.35E-01	1.99E-02	1.42E-01	1.96E-02
12	2.5	10.5	8	3	1000	3.84E-01	2.59E-02	3.54E-01	2.53E-02
13	0.9	1	11	3	1000	5.99E-02	1.26E-02	5.87E-02	1.22E-02
14	2.5	1	11	3	1000	8.12E-02	1.07E-02	7.15E-02	1.07E-02
15	0.9	10.5	11	3	1000	6.85E-02	1.45E-02	6.99E-02	1.46E-02
16	2.5	10.5	11	3	1000	1.44E-01	1.85E-02	1.53E-01	1.83E-02
17	0.9	1	8	1	5000	1.56E-02	4.90E-03	1.51E-02	4.93E-03
18	2.5	1	8	1	5000	1.69E-02	4.57E-03	2.42E-02	4.71E-03
19	0.9	10.5	8	1	5000	1.85E-02	5.49E-03	1.83E-02	5.56E-03
20	2.5	10.5	8	1	5000	3.09E-02	6.74E-03	2.47E-02	6.59E-03
21	0.9	1	11	1	5000	1.25E-02	4.46E-03	-1.39E-03	3.98E-03
22	2.5	1	11	1	5000	1.31E-02	4.33E-03	1.24E-02	4.25E-03
23	0.9	10.5	11	1	5000	1.43E-02	4.93E-03	2.74E-02	5.49E-03
24	2.5	10.5	11	1	5000	1.79E-02	5.31E-03	1.57E-02	5.07E-03
25	0.9	1	8	3	5000	5.22E-02	8.45E-03	5.76E-02	8.54E-03
26	2.5	1	8	3	5000	2.01E-01	8.37E-03	1.88E-01	7.99E-03
27	0.9	10.5	8	3	5000	6.74E-02	9.80E-03	6.19E-02	9.54E-03

Table A-1 Continued: Wavy Fin Design Inputs & Outputs

28	2.5	10.5	8	3	5000	2.32E-01	1.39E-02	2.40E-01	1.40E-02
29	0.9	1	11	3	5000	2.71E-02	6.40E-03	2.95E-02	6.63E-03
30	2.5	1	11	3	5000	4.84E-02	5.93E-03	5.30E-02	5.96E-03
31	0.9	10.5	11	3	5000	3.35E-02	7.22E-03	3.20E-02	7.09E-03
32	2.5	10.5	11	3	5000	8.47E-02	9.65E-03	8.02E-02	9.50E-03
33	0.9	5.75	9.5	2	3000	3.29E-02	7.76E-03	3.20E-02	7.57E-03
34	2.5	5.75	9.5	2	3000	6.84E-02	9.78E-03	6.89E-02	9.87E-03
35	1.7	1	9.5	2	3000	3.24E-02	6.75E-03	3.25E-02	6.66E-03
36	1.7	10.5	9.5	2	3000	5.33E-02	9.51E-03	5.10E-02	9.29E-03
37	1.7	5.75	8	2	3000	7.47E-02	1.04E-02	7.43E-02	1.04E-02
38	1.7	5.75	11	2	3000	3.72E-02	8.09E-03	3.66E-02	7.99E-03
39	1.7	5.75	9.5	1	3000	2.22E-02	6.23E-03	2.19E-02	6.09E-03
40	1.7	5.75	9.5	3	3000	1.07E-01	1.45E-02	1.03E-01	1.39E-02
41	1.7	5.75	9.5	2	1000	7.54E-02	1.39E-02	7.67E-02	1.39E-02
42	1.7	5.75	9.5	2	5000	4.03E-02	7.31E-03	4.00E-02	7.60E-03
43	1.7	5.75	9.5	2	3000	4.99E-02	9.07E-03	4.90E-02	9.22E-03
44	0.9	1	8	1	2000	2.39E-02	6.94E-03	2.57E-02	6.99E-03
45	2.5	1	8	1	2000	2.59E-02	6.31E-03	1.92E-02	6.09E-03
46	0.9	10.5	8	1	2000	2.67E-02	7.55E-03	2.40E-02	7.53E-03
47	2.5	10.5	8	1	2000	4.39E-02	9.31E-03	4.88E-02	9.44E-03
48	0.9	1	11	1	2000	1.90E-02	6.10E-03	2.27E-02	6.25E-03
49	2.5	1	11	1	2000	1.97E-02	5.84E-03	2.15E-02	5.84E-03
50	0.9	10.5	11	1	2000	2.13E-02	6.82E-03	1.64E-02	6.67E-03
51	2.5	10.5	11	1	2000	2.57E-02	7.10E-03	2.37E-02	7.13E-03
52	0.9	1	8	3	2000	7.23E-02	1.15E-02	6.97E-02	1.17E-02
53	2.5	1	8	3	2000	1.66E-01	1.02E-02	1.90E-01	1.07E-02
54	0.9	10.5	8	3	2000	1.01E-01	1.44E-02	1.08E-01	1.49E-02
55	2.5	10.5	8	3	2000	3.10E-01	2.02E-02	3.10E-01	2.04E-02
56	0.9	1	11	3	2000	4.16E-02	9.08E-03	4.31E-02	9.23E-03
57	2.5	1	11	3	2000	6.12E-02	8.17E-03	5.70E-02	8.10E-03
58	0.9	10.5	11	3	2000	5.02E-02	1.06E-02	4.90E-02	1.08E-02
59	2.5	10.5	11	3	2000	1.17E-01	1.40E-02	1.22E-01	1.43E-02
60	0.9	1	8	1	3000	1.96E-02	5.91E-03	2.14E-02	5.92E-03
61	2.5	1	8	1	3000	2.13E-02	5.47E-03	1.91E-02	5.34E-03

Table A-1 Continued: Wavy Fin Design Inputs & Outputs

62	0.9	10.5	8	1	3000	2.25E-02	6.54E-03	1.93E-02	6.26E-03
63	2.5	10.5	8	1	3000	3.75E-02	8.06E-03	3.69E-02	7.97E-03
64	0.9	1	11	1	3000	1.56E-02	5.27E-03	1.61E-02	5.30E-03
65	2.5	1	11	1	3000	1.63E-02	5.11E-03	1.88E-02	5.22E-03
66	0.9	10.5	11	1	3000	1.76E-02	5.85E-03	1.94E-02	5.85E-03
67	2.5	10.5	11	1	3000	2.17E-02	6.18E-03	1.93E-02	6.11E-03
68	0.9	1	8	3	3000	6.03E-02	9.76E-03	6.10E-02	9.87E-03
69	2.5	1	8	3	3000	2.04E-01	9.37E-03	1.84E-01	9.11E-03
70	0.9	10.5	8	3	3000	8.40E-02	1.18E-02	8.56E-02	1.21E-02
71	2.5	10.5	8	3	3000	2.73E-01	1.73E-02	2.79E-01	1.73E-02
72	0.9	1	11	3	3000	3.41E-02	7.70E-03	3.60E-02	7.75E-03
73	2.5	1	11	3	3000	5.34E-02	6.98E-03	5.21E-02	6.87E-03
74	0.9	10.5	11	3	3000	4.24E-02	8.94E-03	3.87E-02	8.73E-03
75	2.5	10.5	11	3	3000	1.02E-01	1.18E-02	1.02E-01	1.20E-02
76	0.9	1	8	1	4000	1.72E-02	5.31E-03	1.94E-02	5.45E-03
77	2.5	1	8	1	4000	1.86E-02	4.93E-03	2.23E-02	5.09E-03
78	0.9	10.5	8	1	4000	2.01E-02	5.93E-03	1.89E-02	5.81E-03
79	2.5	10.5	8	1	4000	3.36E-02	7.29E-03	3.04E-02	7.23E-03
80	0.9	1	11	1	4000	1.38E-02	4.79E-03	9.52E-03	4.75E-03
81	2.5	1	11	1	4000	1.43E-02	4.65E-03	1.72E-02	4.90E-03
82	0.9	10.5	11	1	4000	1.57E-02	5.30E-03	2.46E-02	5.67E-03
83	2.5	10.5	11	1	4000	1.94E-02	5.67E-03	1.81E-02	5.64E-03
84	0.9	1	8	3	4000	5.68E-02	9.16E-03	5.85E-02	9.01E-03
85	2.5	1	8	3	4000	1.90E-01	8.69E-03	1.85E-01	8.41E-03
86	0.9	10.5	8	3	4000	7.41E-02	1.04E-02	7.19E-02	1.05E-02
87	2.5	10.5	8	3	4000	2.49E-01	1.53E-02	2.57E-01	1.54E-02
88	0.9	1	11	3	4000	2.99E-02	6.92E-03	3.30E-02	7.09E-03
89	2.5	1	11	3	4000	4.95E-02	6.30E-03	5.23E-02	6.37E-03
90	0.9	10.5	11	3	4000	3.71E-02	7.90E-03	3.45E-02	7.70E-03
91	2.5	10.5	11	3	4000	9.13E-02	1.04E-02	8.98E-02	1.06E-02
92	0.9	5.75	9.5	2	1000	5.33E-02	1.20E-02	5.76E-02	1.25E-02
93	2.5	5.75	9.5	2	1000	1.06E-01	1.53E-02	1.01E-01	1.46E-02
94	1.7	1	9.5	2	1000	5.49E-02	1.05E-02	4.92E-02	1.03E-02
95	1.7	10.5	9.5	2	1000	7.81E-02	1.43E-02	8.48E-02	1.45E-02

Table A-1 Continued: Wavy Fin Design Inputs & Outputs

96	1.7	5.75	8	2	1000	1.12E-01	1.63E-02	1.09E-01	1.59E-02
97	1.7	5.75	11	2	1000	5.74E-02	1.22E-02	6.00E-02	1.24E-02
98	1.7	5.75	9.5	1	1000	3.66E-02	9.16E-03	3.72E-02	9.25E-03
99	1.7	5.75	9.5	3	1000	1.35E-01	1.82E-02	1.42E-01	1.96E-02
100	0.9	5.75	9.5	2	2000	3.89E-02	9.09E-03	4.05E-02	9.29E-03
101	2.5	5.75	9.5	2	2000	8.03E-02	1.15E-02	7.99E-02	1.16E-02
102	1.7	1	9.5	2	2000	3.91E-02	7.90E-03	3.68E-02	7.84E-03
103	1.7	10.5	9.5	2	2000	6.11E-02	1.11E-02	6.28E-02	1.11E-02
104	1.7	5.75	8	2	2000	8.71E-02	1.23E-02	8.65E-02	1.24E-02
105	1.7	5.75	11	2	2000	4.34E-02	9.47E-03	4.43E-02	9.55E-03
106	1.7	5.75	9.5	1	2000	2.63E-02	7.13E-03	2.60E-02	7.07E-03
107	1.7	5.75	9.5	3	2000	1.25E-01	1.75E-02	1.17E-01	1.59E-02
108	0.9	5.75	9.5	2	4000	2.92E-02	6.93E-03	2.77E-02	6.68E-03
109	2.5	5.75	9.5	2	4000	6.05E-02	8.65E-03	6.31E-02	8.91E-03
110	1.7	1	9.5	2	4000	2.85E-02	6.06E-03	3.19E-02	6.15E-03
111	1.7	10.5	9.5	2	4000	4.78E-02	8.47E-03	4.49E-02	8.34E-03
112	1.7	5.75	8	2	4000	6.63E-02	9.16E-03	6.78E-02	9.29E-03
113	1.7	5.75	11	2	4000	3.31E-02	7.24E-03	3.26E-02	7.11E-03
114	1.7	5.75	9.5	1	4000	1.98E-02	5.67E-03	2.05E-02	5.68E-03
115	1.7	5.75	9.5	3	4000	9.49E-02	1.27E-02	9.58E-02	1.28E-02
116	0.9	5.75	9.5	2	5000	2.64E-02	6.36E-03	2.30E-02	5.98E-03
117	2.5	5.75	9.5	2	5000	5.54E-02	7.89E-03	5.81E-02	8.05E-03
118	1.7	1	9.5	2	5000	2.60E-02	5.63E-03	3.04E-02	5.65E-03
119	1.7	10.5	9.5	2	5000	4.35E-02	7.69E-03	4.01E-02	7.65E-03
120	1.7	5.75	8	2	5000	6.03E-02	8.32E-03	6.26E-02	8.42E-03
121	1.7	5.75	11	2	5000	3.01E-02	6.58E-03	2.77E-02	6.28E-03
122	1.7	5.75	9.5	1	5000	1.82E-02	5.27E-03	1.74E-02	5.21E-03
123	1.7	5.75	9.5	3	5000	8.69E-02	1.16E-02	9.08E-02	1.21E-02
124	1.7	5.75	9.5	2	2000	5.82E-02	1.07E-02	5.83E-02	1.09E-02
125	1.7	5.75	9.5	2	4000	4.44E-02	8.03E-03	4.44E-02	8.34E-03

Table A-2: Offset-Strip Fin Design Inputs & Outputs

DPs	MFS [mm]	PS [mm]	Fl [mm]	FIA [degree]	Re	f CFD	j CFD	f corr	j corr
1	0.9	1	2	30	1000	2.75E-02	9.77E-03	2.73E-02	8.68E-03
2	2.5	1	2	30	1000	2.92E-02	8.86E-03	2.74E-02	1.02E-02
3	0.9	5.4	2	30	1000	2.17E-02	1.01E-02	2.24E-02	1.30E-02
4	2.5	5.4	2	30	1000	2.56E-02	2.46E-02	2.78E-02	2.16E-02
5	0.9	1	7	30	1000	2.32E-02	6.26E-03	2.34E-02	5.92E-03
6	2.5	1	7	30	1000	2.52E-02	7.28E-03	2.53E-02	6.91E-03
7	0.9	5.4	7	30	1000	2.08E-02	5.55E-03	2.07E-02	5.41E-03
8	2.5	5.4	7	30	1000	2.59E-02	9.72E-03	2.54E-02	1.10E-02
9	0.9	1	2	90	1000	4.33E-02	9.66E-03	4.28E-02	1.01E-02
10	2.5	1	2	90	1000	3.11E-02	8.42E-03	3.33E-02	8.40E-03
11	0.9	5.4	2	90	1000	5.30E-02	1.57E-02	5.19E-02	1.46E-02
12	2.5	5.4	2	90	1000	5.72E-02	1.55E-02	5.46E-02	1.68E-02
13	0.9	1	7	90	1000	3.23E-02	7.67E-03	3.21E-02	8.49E-03
14	2.5	1	7	90	1000	2.62E-02	7.84E-03	2.64E-02	7.39E-03
15	0.9	5.4	7	90	1000	3.54E-02	1.13E-02	3.55E-02	1.10E-02
16	2.5	5.4	7	90	1000	3.91E-02	1.13E-02	3.95E-02	1.14E-02
17	0.9	1	2	30	5000	1.29E-02	4.89E-03	1.31E-02	5.51E-03
18	2.5	1	2	30	5000	1.32E-02	4.63E-03	1.32E-02	4.05E-03
19	0.9	5.4	2	30	5000	1.26E-02	8.87E-03	1.28E-02	8.49E-03
20	2.5	5.4	2	30	5000	1.46E-02	9.72E-03	1.44E-02	1.02E-02
21	0.9	1	7	30	5000	1.09E-02	3.76E-03	9.14E-03	3.91E-03
22	2.5	1	7	30	5000	1.14E-02	3.99E-03	1.07E-02	3.96E-03
23	0.9	5.4	7	30	5000	1.07E-02	4.14E-03	1.19E-02	4.57E-03
24	2.5	5.4	7	30	5000	1.27E-02	5.45E-03	1.24E-02	5.32E-03
25	0.9	1	2	90	5000	2.32E-02	5.04E-03	2.30E-02	5.37E-03
26	2.5	1	2	90	5000	1.48E-02	4.46E-03	1.49E-02	4.97E-03
27	0.9	5.4	2	90	5000	2.58E-02	7.39E-03	2.56E-02	7.36E-03
28	2.5	5.4	2	90	5000	2.58E-02	7.20E-03	2.60E-02	7.01E-03
29	0.9	1	7	90	5000	1.60E-02	4.17E-03	1.75E-02	2.97E-03
30	2.5	1	7	90	5000	1.20E-02	4.17E-03	1.27E-02	5.23E-03
31	0.9	5.4	7	90	5000	1.60E-02	5.12E-03	1.51E-02	5.50E-03
32	2.5	5.4	7	90	5000	1.65E-02	5.49E-03	1.63E-02	5.34E-03

Table A-2 Continued: Offset-Strip Fin Design Inputs & Outputs

33	0.9	3.2	4.5	60	3000	1.79E-02	6.86E-03	1.74E-02	6.94E-03
34	2.5	3.2	4.5	60	3000	1.90E-02	6.55E-03	1.90E-02	6.61E-03
35	1.7	1	4.5	60	3000	1.58E-02	5.23E-03	1.55E-02	5.26E-03
36	1.7	5.4	4.5	60	3000	1.99E-02	8.31E-03	1.94E-02	8.51E-03
37	1.7	3.2	2	60	3000	2.24E-02	8.67E-03	2.21E-02	8.96E-03
38	1.7	3.2	7	60	3000	1.74E-02	6.07E-03	1.73E-02	6.34E-03
39	1.7	3.2	4.5	30	3000	1.58E-02	6.62E-03	1.58E-02	6.55E-03
40	1.7	3.2	4.5	90	3000	2.10E-02	6.75E-03	2.12E-02	6.78E-03
41	1.7	3.2	4.5	60	1000	3.36E-02	1.16E-02	3.26E-02	1.15E-02
42	1.7	3.2	4.5	60	5000	1.49E-02	5.50E-03	1.46E-02	5.56E-03
43	1.7	3.2	4.5	60	3000	1.90E-02	6.81E-03	1.84E-02	7.09E-03
44	0.9	1	2	30	2000	1.94E-02	7.32E-03	1.97E-02	6.80E-03
45	2.5	1	2	30	2000	2.01E-02	6.68E-03	1.96E-02	7.24E-03
46	0.9	5.4	2	30	2000	1.65E-02	1.03E-02	1.54E-02	1.03E-02
47	2.5	5.4	2	30	2000	1.96E-02	1.71E-02	1.97E-02	1.68E-02
48	0.9	1	7	30	2000	1.61E-02	4.37E-03	1.62E-02	4.85E-03
49	2.5	1	7	30	2000	1.71E-02	5.58E-03	1.79E-02	5.23E-03
50	0.9	5.4	7	30	2000	1.49E-02	4.81E-03	1.44E-02	4.10E-03
51	2.5	5.4	7	30	2000	1.87E-02	7.92E-03	1.80E-02	8.10E-03
52	0.9	1	2	90	2000	3.12E-02	7.43E-03	3.15E-02	7.55E-03
53	2.5	1	2	90	2000	2.16E-02	6.40E-03	2.22E-02	5.82E-03
54	0.9	5.4	2	90	2000	3.67E-02	1.09E-02	3.85E-02	1.09E-02
55	2.5	5.4	2	90	2000	4.00E-02	1.15E-02	4.05E-02	1.21E-02
56	0.9	1	7	90	2000	2.27E-02	6.05E-03	2.27E-02	6.27E-03
57	2.5	1	7	90	2000	1.78E-02	5.92E-03	1.70E-02	5.65E-03
58	0.9	5.4	7	90	2000	2.36E-02	8.02E-03	2.41E-02	8.27E-03
59	2.5	5.4	7	90	2000	2.60E-02	8.32E-03	2.73E-02	8.15E-03
60	0.9	1	2	30	3000	1.61E-02	6.19E-03	1.65E-02	6.10E-03
61	2.5	1	2	30	3000	1.65E-02	5.73E-03	1.64E-02	5.66E-03
62	0.9	5.4	2	30	3000	1.46E-02	9.91E-03	1.33E-02	9.04E-03
63	2.5	5.4	2	30	3000	1.72E-02	1.28E-02	1.66E-02	1.37E-02
64	0.9	1	7	30	3000	1.34E-02	4.37E-03	1.32E-02	4.62E-03

Table A-2 Continued: Offset-Strip Fin Design Inputs & Outputs

65	2.5	1	7	30	3000	1.41E-02	4.85E-03	1.48E-02	4.64E-03
66	0.9	5.4	7	30	3000	1.27E-02	4.52E-03	1.27E-02	3.98E-03
67	2.5	5.4	7	30	3000	1.57E-02	6.83E-03	1.51E-02	6.65E-03
68	0.9	1	2	90	3000	2.70E-02	6.40E-03	2.62E-02	6.38E-03
69	2.5	1	2	90	3000	1.80E-02	5.51E-03	1.72E-02	4.84E-03
70	0.9	5.4	2	90	3000	3.08E-02	8.82E-03	3.15E-02	8.90E-03
71	2.5	5.4	2	90	3000	3.29E-02	9.62E-03	3.28E-02	9.37E-03
72	0.9	1	7	90	3000	1.92E-02	5.26E-03	1.88E-02	5.07E-03
73	2.5	1	7	90	3000	1.48E-02	5.12E-03	1.34E-02	5.16E-03
74	0.9	5.4	7	90	3000	1.95E-02	6.58E-03	1.88E-02	6.89E-03
75	2.5	5.4	7	90	3000	2.10E-02	6.91E-03	2.11E-02	6.51E-03
76	0.9	1	2	30	4000	1.42E-02	5.57E-03	1.52E-02	5.90E-03
77	2.5	1	2	30	4000	1.45E-02	5.15E-03	1.52E-02	4.83E-03
78	0.9	5.4	2	30	4000	1.35E-02	9.33E-03	1.33E-02	8.68E-03
79	2.5	5.4	2	30	4000	1.57E-02	1.08E-02	1.57E-02	1.17E-02
80	0.9	1	7	30	4000	1.19E-02	4.11E-03	1.18E-02	4.53E-03
81	2.5	1	7	30	4000	1.24E-02	4.42E-03	1.33E-02	4.44E-03
82	0.9	5.4	7	30	4000	1.15E-02	4.34E-03	1.27E-02	4.36E-03
83	2.5	5.4	7	30	4000	1.39E-02	6.12E-03	1.42E-02	5.94E-03
84	0.9	1	2	90	4000	2.48E-02	5.75E-03	2.43E-02	5.88E-03
85	2.5	1	2	90	4000	1.61E-02	4.97E-03	1.57E-02	4.79E-03
86	0.9	5.4	2	90	4000	2.78E-02	7.82E-03	2.81E-02	7.96E-03
87	2.5	5.4	2	90	4000	2.87E-02	8.44E-03	2.89E-02	7.89E-03
88	0.9	1	7	90	4000	1.73E-02	4.79E-03	1.80E-02	4.20E-03
89	2.5	1	7	90	4000	1.31E-02	4.65E-03	1.28E-02	5.25E-03
90	0.9	5.4	7	90	4000	1.74E-02	5.83E-03	1.66E-02	6.19E-03
91	2.5	5.4	7	90	4000	1.84E-02	6.11E-03	1.84E-02	5.80E-03
92	0.9	3.2	4.5	60	1000	3.01E-02	1.08E-02	3.10E-02	1.03E-02
93	2.5	3.2	4.5	60	1000	3.41E-02	1.11E-02	3.35E-02	1.14E-02
94	1.7	1	4.5	60	1000	2.79E-02	8.30E-03	2.81E-02	8.54E-03
95	1.7	5.4	4.5	60	1000	3.34E-02	1.44E-02	3.38E-02	1.38E-02
96	1.7	3.2	2	60	1000	3.74E-02	1.52E-02	3.77E-02	1.46E-02
97	1.7	3.2	7	60	1000	3.10E-02	1.02E-02	3.08E-02	1.00E-02
98	1.7	3.2	4.5	30	1000	2.63E-02	9.90E-03	2.66E-02	1.02E-02

Table A-2 Continued: Offset-Strip Fin Design Inputs & Outputs

99	1.7	3.2	4.5	90	1000	3.96E-02	1.16E-02	3.89E-02	1.13E-02
100	0.9	3.2	4.5	60	2000	2.14E-02	8.19E-03	2.16E-02	8.01E-03
101	2.5	3.2	4.5	60	2000	2.34E-02	8.05E-03	2.36E-02	8.25E-03
102	1.7	1	4.5	60	2000	1.90E-02	6.19E-03	1.93E-02	6.29E-03
103	1.7	5.4	4.5	60	2000	2.39E-02	1.02E-02	2.39E-02	1.04E-02
104	1.7	3.2	2	60	2000	2.69E-02	1.05E-02	2.71E-02	1.10E-02
105	1.7	3.2	7	60	2000	2.12E-02	7.43E-03	2.15E-02	7.57E-03
106	1.7	3.2	4.5	30	2000	1.89E-02	7.88E-03	1.89E-02	7.72E-03
107	1.7	3.2	4.5	90	2000	2.60E-02	8.16E-03	2.70E-02	8.28E-03
108	0.9	3.2	4.5	60	4000	1.58E-02	6.20E-03	1.58E-02	6.47E-03
109	2.5	3.2	4.5	60	4000	1.66E-02	6.06E-03	1.71E-02	5.82E-03
110	1.7	1	4.5	60	4000	1.40E-02	4.83E-03	1.43E-02	4.76E-03
111	1.7	5.4	4.5	60	4000	1.75E-02	7.37E-03	1.77E-02	7.53E-03
112	1.7	3.2	2	60	4000	1.96E-02	7.77E-03	1.98E-02	7.83E-03
113	1.7	3.2	7	60	4000	1.52E-02	5.63E-03	1.56E-02	5.65E-03
114	1.7	3.2	4.5	30	4000	1.41E-02	6.01E-03	1.45E-02	6.00E-03
115	1.7	3.2	4.5	90	4000	1.87E-02	6.01E-03	1.87E-02	6.08E-03
116	0.9	3.2	4.5	60	5000	1.44E-02	5.71E-03	1.41E-02	5.90E-03
117	2.5	3.2	4.5	60	5000	1.50E-02	5.57E-03	1.52E-02	5.17E-03
118	1.7	1	4.5	60	5000	1.28E-02	4.50E-03	1.28E-02	4.11E-03
119	1.7	5.4	4.5	60	5000	1.57E-02	6.73E-03	1.60E-02	6.77E-03
120	1.7	3.2	2	60	5000	1.77E-02	7.13E-03	1.77E-02	6.90E-03
121	1.7	3.2	7	60	5000	1.38E-02	5.19E-03	1.36E-02	4.82E-03
122	1.7	3.2	4.5	30	5000	1.28E-02	5.55E-03	1.25E-02	5.40E-03
123	1.7	3.2	4.5	90	5000	1.71E-02	5.48E-03	1.69E-02	5.51E-03
124	1.7	3.2	4.5	60	2000	2.32E-02	8.36E-03	2.29E-02	8.58E-03
125	1.7	3.2	4.5	60	4000	1.65E-02	6.23E-03	1.65E-02	6.31E-03

9.2. APPENDIX B

Table B-1: Correlation Coefficients from 43 Runs

Wavy Fin			Offset-Strip Fin		
Coefficients	f	j	Coefficients	f	j
1	-3.68E-03	4.07E-03	1	2.81E-02	7.57E-03
MFS	8.11E-02	2.55E-03	MFS	1.49E-03	4.02E-03
PS	7.82E-03	9.04E-04	PS	-6.45E-04	1.64E-03
Wl	-1.64E-02	9.41E-04	Fl	-1.65E-03	-1.33E-03
Amp	8.30E-02	2.58E-03	FIA	4.05E-04	7.33E-05
Re	-1.79E-05	-3.21E-06	Re	-1.03E-05	-2.96E-06
MFS^2	1.55E-03	-8.35E-04	MFS^2	-4.62E-04	-4.62E-04
MFS×PS	2.47E-03	2.21E-04	MFS×PS	8.48E-04	3.98E-04
PS^2	-3.04E-04	-5.20E-05	PS^2	-1.86E-04	-4.75E-05
MFS×Wl	-1.31E-02	-1.44E-04	MFS×Fl	1.94E-04	-7.41E-05
PS×Wl	-8.17E-04	-5.47E-05	PS×Fl	-1.21E-04	-1.72E-04
Wl^2	2.79E-03	-2.99E-05	Fl^2	1.84E-04	5.88E-05
MFS×Amp	3.01E-02	4.16E-04	MFS×FIA	-5.14E-05	-2.94E-05
PS×Amp	2.19E-03	1.71E-04	PS×FIA	3.73E-05	-4.85E-07
Wl×Amp	-1.55E-02	-4.59E-04	Fl×FIA	-2.67E-05	7.93E-06
Amp^2	1.47E-02	1.06E-03	FIA^2	-3.39E-07	-3.53E-07
MFS×Re	-1.06E-06	3.11E-08	MFS×Re	-1.84E-07	-3.09E-07
PS×Re	-7.44E-07	-6.03E-08	PS×Re	-1.45E-07	-1.40E-07
Wl×Re	1.18E-06	1.04E-07	Fl×Re	1.48E-07	1.23E-07
Amp×Re	-4.13E-06	-4.50E-07	FIA×Re	-3.51E-08	-4.04E-09
Re^2	2.04E-09	3.22E-10	Re^2	1.38E-09	3.90E-10

Table B-2: Correlation Coefficients from 125 Runs

Wavy Fin			Offset-Strip Fin		
Coefficients	f	j	Coefficients	f	j
1	4.32E-03	7.78E-04	1	1.45E-04	1.45E-04
MFS	2.41E-03	3.33E-04	MFS	2.82E-05	2.82E-05
PS	4.73E-03	8.85E-04	PS	-2.24E-05	-2.24E-05
Wl	1.33E-02	2.43E-03	Fl	5.98E-05	5.98E-05
Amp	3.63E-03	5.08E-04	FIA	2.37E-03	2.37E-03
Re	-5.00E-05	-1.00E-05	Re	-1.63E-05	-1.63E-05
MFS^2	3.48E-04	-5.71E-05	MFS^2	-9.50E-05	-9.50E-05
MFS×PS	9.82E-03	1.08E-03	MFS×PS	-2.96E-05	-2.96E-05
PS^2	5.86E-03	1.21E-03	PS^2	-3.28E-04	-3.28E-04
MFS×Wl	3.82E-04	-4.13E-04	MFS×Fl	-6.32E-05	-6.32E-05
PS×Wl	-1.00E-02	-1.74E-03	PS×Fl	-9.30E-05	-9.30E-05
Wl^2	-1.15E-03	1.10E-04	Fl^2	-4.31E-04	-4.31E-04
MFS×Amp	6.90E-03	1.36E-04	MFS×FIA	1.03E-04	1.03E-04
PS×Amp	1.49E-02	1.85E-03	PS×FIA	6.84E-05	6.84E-05
Wl×Amp	4.28E-03	7.85E-05	Fl×FIA	2.80E-06	2.80E-06
Amp^2	2.44E-03	1.86E-04	FIA^2	-4.13E-05	-4.13E-05
MFS×Re	5.06E-06	6.69E-07	MFS×Re	-7.27E-07	-7.27E-07
PS×Re	-2.70E-06	-1.81E-07	PS×Re	-7.50E-09	-7.50E-09
Wl×Re	5.56E-06	1.11E-06	Fl×Re	2.94E-07	2.94E-07
Amp×Re	-1.26E-05	-1.80E-06	FIA×Re	-9.79E-08	-9.79E-08
Re^2	9.27E-09	1.41E-09	Re^2	4.56E-09	4.56E-09
MFS^3	-1.02E-03	1.09E-05	MFS^3	-1.58E-04	-1.58E-04
MFS^2×PS	5.90E-04	-3.89E-05	MFS^2×PS	8.86E-05	8.86E-05
MFS×PS^2	-5.14E-04	-4.11E-05	MFS×PS^2	4.11E-05	4.11E-05
PS^3	-2.52E-04	-6.58E-05	PS^3	-7.13E-05	-7.13E-05
MFS^2×Wl	-2.65E-03	-4.09E-05	MFS^2×Fl	2.93E-05	2.93E-05
MFS×PS×Wl	-5.01E-04	-4.27E-05	MFS×PS×Fl	-7.03E-05	-7.03E-05
PS^2×Wl	-2.57E-05	7.29E-06	PS^2×Fl	5.23E-05	5.23E-05
MFS×Wl^2	1.16E-03	4.02E-05	MFS×Fl^2	1.70E-05	1.70E-05
PS×Wl^2	5.48E-04	8.88E-05	PS×Fl^2	1.07E-05	1.07E-05
Wl^3	-4.23E-05	-1.79E-05	Fl^3	3.54E-05	3.54E-05
MFS^2×Amp	1.54E-02	3.35E-05	MFS^2×FIA	-5.12E-06	-5.12E-06

Table B-2 Continued: Correlation Coefficients from 125 Runs

MFS×PS×Amp	1.65E-03	1.24E-04	MFS×PS×FIA	1.65E-05	1.65E-05
PS^2×Amp	-4.34E-04	-7.30E-05	PS^2×FIA	4.74E-06	4.74E-06
MFS×Wl×Amp	-1.16E-02	-6.44E-05	MFS×Fl×FIA	3.98E-06	3.98E-06
PS×Wl×Amp	-4.82E-04	-2.50E-05	PS×Fl×FIA	-6.05E-06	-6.05E-06
Wl^2×Amp	4.87E-04	-1.89E-05	Fl^2×FIA	2.83E-06	2.83E-06
MFS×Amp^2	1.82E-02	3.75E-05	MFS×FIA^2	-1.77E-06	-1.77E-06
PS×Amp^2	-1.03E-03	-1.76E-04	PS×FIA^2	-3.15E-07	-3.15E-07
Wl×Amp^2	-1.96E-03	-5.18E-06	Fl×FIA^2	-4.35E-07	-4.35E-07
Amp^3	6.02E-04	1.92E-04	FIA^3	2.63E-07	2.63E-07
MFS^2×Re	-7.00E-07	-7.61E-08	MFS^2×Re	1.70E-07	1.70E-07
MFS×PS×Re	-7.45E-07	-3.41E-08	MFS×PS×Re	-1.34E-07	-1.34E-07
PS^2×Re	5.46E-08	6.44E-09	PS^2×Re	7.55E-08	7.55E-08
MFS×Wl×Re	-4.64E-08	-1.48E-10	MFS×Fl×Re	-1.19E-08	-1.19E-08
PS×Wl×Re	3.54E-07	1.18E-08	PS×Fl×Re	8.78E-09	8.78E-09
Wl^2×Re	-2.93E-07	-5.10E-08	Fl^2×Re	-2.33E-08	-2.33E-08
MFS×Amp×Re	-5.59E-07	-2.17E-08	MFS×FIA×Re	3.49E-09	3.49E-09
PS×Amp×Re	-6.76E-07	-3.88E-08	PS×FIA×Re	-1.05E-08	-1.05E-08
Wl×Amp×Re	6.66E-07	4.48E-08	Fl×FIA×Re	4.20E-09	4.20E-09
Amp^2×Re	3.21E-07	1.44E-07	FIA^2×Re	-7.55E-13	-7.55E-13
MFS×Re^2	3.22E-10	-3.02E-11	MFS×Re^2	3.38E-11	3.38E-11
PS×Re^2	1.09E-10	1.22E-11	PS×Re^2	3.43E-11	3.43E-11
Wl×Re^2	-3.54E-10	-3.17E-11	Fl×Re^2	-3.43E-11	-3.43E-11
Amp×Re^2	9.82E-10	1.05E-10	FIA×Re^2	1.23E-11	1.23E-11
Re^3	-7.45E-13	-1.06E-13	Re^3	-4.45E-13	-4.45E-13